DYNAMICS OF THE HUMAN PELVIS

DYNAMICS OF THE HUMAN PELVIS

Identification methodology
for low back pain diagnosis

Proefschrift

ter verkrijging van de graad van doctor
aan de Technische Universiteit Delft,
op gezag van de Rector Magnificus prof. dr. ir. J.T. Fokkema,
voorzitter van het College voor Promoties,
in het openbaar te verdedigen op donderdag 7 december 2006 om 10:00 uur
door Nadine Eva CONZA
Diplomierte Maschineningenieurin
Eidgenössiche Technische Hochschule (ETH) Zurich, Zwitserland
geboren te Sorengo, Zwitserland.

Dit proefschrift is goedgekeurd door de promotor:
Prof. dr. ir. D.J. Rixen

Samenstelling promotiecommissie:
Rector Magnificus, voorzitter
Prof. dr. ir. D.J. Rixen, Technische Universiteit Delft, promotor
Prof. dr. ir. C.J. Snijders, Erasmus MC Universitair Medisch Centrum Rotterdam
Prof. Dr. -Ing. M. Link, Universität Kassel, Duitsland
Prof. dr. ir. A. de Boer, Universiteit Twente
Prof. dr. ir. N. de Jong, Erasmus MC Universitair Medisch Centrum Rotterdam
Prof. dr. ir. F.T.C. van der Helm, Technische Universiteit Delft
Dr. R.L.A.W. Bleys, Universitair Medisch Centrum Utrecht

To my grandfather Celestino and my godmother Trudy
beautiful angels
for that blessed sacred place in my soul
filled with enchanted memories and wonderful feelings.

Contents

The Beginning

אב

24 November 2002

It could have been a normal day, today.
Actually an unremarkable one. The clouds were hanging
low from the sky, attached by some irregular unquiet threads
to the invisible universe above, and they seemed painted by
Van Gogh in a moody day, when he had only black and
white on his palette.

An unremarkable day, if it wasn't for this mysterious script
that I have found while strolling undisturbed on the beach
in this November morning.
It looks very ancient, and it is written in some weird
characters that I've never seen before. It is beautiful.
And it really tickles my curiosity, with the same sense
of frustration and powerlessness that being tickled triggers.
I love reading, and it bothers me that such a wonderful
scroll holds secrets which I can't steal.
And beyond the mere fact that I don't like feeling like a
preschooler unable to read, I have the most definite
feeling that it treasures an important message.

Introduction

Introduction
Chapter 1

This chapter introduces the research frame, the gap which it intends to fill, and the objectives of this dissertation as part of the overall approach.

1.1 Background

N 1974 THE AMERICAN anthropologist Donald Johanson and his student Tom Gray made an incredible discovery. In a maze of ravines at Hadar in northern Ethiopia they found the bones of the first hominid science is aware of: Lucy. Based on the 47 recovered bones, and especially on the morphology of the pelvis and the knee, they concluded that, unlike chimps, 3.2 million years ago Lucy used to walk in upright position.

Bipedalism is certainly the most striking difference between apes and humans. But if we broaden our comparison including all the mammals, we realize even more what a huge impact this revolution in posture must have had. All of a sudden, in an evolutionary timescale, the spine ceased to be a horizontal link between front and rear limbs, and became the vertical structure transferring the load from the trunk to the locomotion system. With the pelvis as a fulcrum.

Can we flex a bit our perfectionistic idea of the human evolution and consider that our musculoskeletal apparatus might not be ready for this, yet? Maybe not. Well, let's blame it then to our way of living, where physical activities have fallen short in our quest for mental development. We do not train our muscles enough, we stay for long periods of time in the same positions, we weigh more, the cardiovascular system is overloaded. Moreover, we live too long. All this is way too far from the original functions we were built for. In a very simplistic line of thoughts, might that be why we have musculoskeletal disorders?

In a European Social Statistics publication over accidents at work and work-related health problems[20] it was estimated that in a one year period between 1998 and 1999 nearly eight million workers or retired workers in the European Union were diagnosed with health problems imputable to their employment. 53% of those cases fell in the category of musculoskeletal disorders. The same group of disorders was accountable for almost half of the absences from work which lasted more than three days, and also for almost half of the absences which lasted more than two weeks. According to this information, about 185 million working days were lost during that year in the European Union. On a global scale, if expressed in Disability Adjusted Life Years (DALYs[1]), musculoskeletal disorders rank as the ninth most frequent cause of health problems

---

[1]A measure used to express how a healthy life is affected by disease; it combines the years lost because of premature death and disability.

---

[20] European Commission. European social statistics, accidents at work and work-related health problems. Technical report, Office for Official Publications of the European Communities, 2003.

worldwide[53]. That makes it a relevant problem.

Elaborating more on the little provocation of a few lines ago, the problem has started precipitating, paradoxically enough, with the exorbitant achievements in medicine and technology, which have prolonged the lifespan and enabled a comfortable life style. Lack of physical activity and erroneous nutrition, coupled with the underestimation of their consequences and the failure to recognize the necessity for a dedicated education, have lead, in the developed countries, to a society for the majority populated by plump sedentary people. Progress in this case has translated into a reality where wondrous surgeries can be performed (let us think about Siamese twins separation), or where molecular medicine is about to defeat cancer, and where at the same time millions of workers are bound to bed for just a (provocatively said) simple back pain. If we attempted a speculation on the reasons for this imbalance we might wander involuntarily in the direction of politics: in a society which relies on the public sentiment to steer the research vessel (directly, or indirectly through the elected politicians), it becomes more than human that heartbreaking stories about children dying of leukemia attract more attention (emotional and financial) than the occasional non-lethal discomfort of back pain.

1.2   The missing tool

Low back pain refers to pain in the lumbosacral area of the spine between the first lumbar vertebra and the first sacral vertebra. It is a sore point in diagnostics, since its etiology is in many cases unclear, making the choice of a therapy difficult.

As the term suggests, the main characteristics of this disorder is the fact that it hurts: there are no earlier indicators that might help prevent the onset of the symptoms. Much can be said about the causes of pain. In many cases medical screening reveals pathological conditions for which a treatment can be designed. In other cases, however, no indications of an anatomical or physiological culprit can be found. Due to this frequent lack of evidence, many speculations leading to as many therapies can cost time and money to the society, and pain to the distressed patient. There is therefore a strong need in the medical world for a diagnostic tool able to identify in an objective way the pathology, if present, behind the disorder.

[53] World Health Organization Statistical Information System (WHOSIS). Global burden of disease estimates for the year 2001. Technical report, World Health Organization, 2001.

1.3 Objective and approach

Our research is based on the working assumption that the sacroiliac joints can initiate pain, should their biomechanical properties slide in abnormal ranges[49]. The ultimate objective of the project, which is a symbiotic effort of three students working each on a different task, is to develop a diagnostic tool to **predict or assess low back disorders of sacroiliac origin**.

The idea behind has been borrowed from the dynamic field, and is based on the fact that the properties of a system can be derived from its dynamic behaviour. Imparting an excitation to the system and measuring the provoked vibrations is routine in structural identification practice. The goal is to apply this technique on the human pelvis *in vivo*, with the purpose of deriving the biomechanical properties of the sacroiliac joints.

One of the elements which are absolutely necessary to achieve this objective is a medical apparatus, able to introduce a known excitation in the system and accurately measure the vibration of the bones *in vivo*. Such an apparatus, in turn, implicitly involves two aspects: the fact of existing, and the fact of being used. The development of the medical tool was the task of one of the involved students[51], while its operability in the clinical environment was to be demonstrated by the second student[29].

A first idea to objectively measure the vibration of the hip bone versus the vibration of the sacrum had already been investigated, and foresaw the use of a commercial Doppler ultrasound apparatus to pick-up the velocities of the bones[17,18]. A follow-up study however showed that the applied technology, based on the frequency shift of the reflecting waves, was not suitable for the actual range of velocities of vibrating bones[29]. A new measurement system has therefore been developed, still based on ultrasound technique. However in this alternative approach the motion of a target object is detected by considering the time of flight of echo waves, which can be translated in the distance of the object from the source. Its motion is then reflected in the variation

[49] C.J. Snijders, A. Vleeming, and R. Stoeckart. Transfer of lumbosacral load to iliac bones and legs : Part 1: Biomechanics of self-bracing of the sacroiliac joints and its significance for treatment and exercise. *Clinical Biomechanics*, 8(6):285–294, 1993.

[51] E. Vlaanderen, N.E. Conza, C.J. Snijders, A. Bouakaz, and N. Jong (de). Low back disorders; the stiffness of the sacro iliac joint: A new method using ultrasound. *Ultrasound in Medicine and Biology*, 31(1):39–44, 2005.

[29] M. Groot (de), C.W. Spoor, and C.J. Snijders. Critical notes on the technique of doppler imaging of vibrations (DIV). *Ultrasound in Medicine and Biology*, 30(3):363–367, 2004.

[17] L. Damen. *Laxity Measurements of the Sacroiliac Joints in Women with Pregnancy-related Pelvic Pain*. PhD thesis, Erasmus University Rotterdam, 2002.

[18] L. Damen, T. Stijnen, M.E. Roebroeck, C.J. Snijders, and H.J. Stam. Reliability of sacroiliac joint laxity measurement with doppler imaging of vibrations. *Ultrasound in Medicine and Biology*, 28(4):407–414, 2002.

of the times of flight. This technique, which is related to but not part of this work, is briefly described later on.

Another essential element is a way of interpreting the raw data obtained from *in vivo* experiments. To translate the vibration measurements extracted from the reality into estimations of the properties of the sacroiliac joints we need to devise a decoding tool.

The establishment of a methodology to objectively derive the biomechanical properties of the sacroiliac joints from raw vibration measurements in the low back region is the subject of this dissertation.

The first element in the methodology chain is a dynamic model of the pelvis, designed according to simplifying assumptions and verified, whenever possible, with experimental data.

In vivo measurements, though, will not reveal the pelvis in the same terms in which we define its model. They are merely a collection of responses at a discrete number of points, to a limited set of excitations. Moreover, polluted with noise. The next element in the chain is therefore the lecture key necessary to read, between the measured lines, what the underlying reality is. We need an identification algorithm.

Like civil engineers do when casting a bridge between two shores, we try to build our construct from two sides with the purpose of having them meet in the middle. On one side the model and the identification algorithms are built in a virtual environment, creating vibration measurements *ad hoc* via computer simulations and verifying the devised lecture key. At the same time, experiments are performed on systems which progressively approach the real one (an embalmed human specimen, a fresh-frozen one, a living one) to provide hard facts against which the theory has to prove itself. But we are not civil engineers, and this is nothing as solid as a bridge. It is a fascinating and sometimes frustrating attempt to observe, theorize, and tentatively scribble down plausible descriptions of reality.

This dissertation is a work log of raw research, a diary of a journey in unknown land. It is a journal written in pencil to be considered, mused upon, corrected, laid to rest, picked up again. And who knows? To be continued.

1.4 Reading guide of the book

The work in this dissertation is presented accompanied by a parallel tale, pages of a diary describing how an ancient scroll, written in an unknown alphabet, is found, and after lengthy research, translated. In this allegory the illegible ancient scroll is the human pelvis, the decryption code is the identification methodology, the unknown

characters are what we can observe and measure, and the interpretation our attempt to draw a meaning from the lines. Each of the mentioned element (the scroll, the lecture key, the hieroglyphics, the interpretation) is therefore addressed in a dedicated Part, plus an introductory and a conclusive Part.

PART I: The Beginning introduces the background and the objectives of this research (Chapter 1).

PART II: The Scroll introduces the object of our research, the human pelvis, and describes some anatomical (Chapter 2) and pathological (Chapter 3) aspects.

PART III: The Key contains the elements of the methodology for the identification of the mechanical properties of the sacroiliac joints. It first introduces some mathematical concepts needed to create a dynamic model (Chapter 4), and continues by presenting the reasoning and establishment of the model (Chapter 5), the identification algorithms (Chapter 6), the investigation on frequency dependent mechanical properties (Chapter 7) and the ultrasound measurement technique (Chapter 8).

PART IV: The Hieroglyphic briefly describes tools commonly used in experimental dynamics (Chapter 9), and then presents the experimental work on embalmed human specimens (Chapter 10), fresh-frozen human specimens (Chapter 11), ligaments of rabbit knee (Chapter 12), and human subjects *in vivo* (Chapter 13).

PART V: The Interpretation explains the process of correlating the established model to the measured responses (Chapter 14).

PART VI: The Closure brings conclusions and recommendations, the appendices, the bibliography, summaries in English and Dutch, the acknowledgements and a brief note about the author.

A schematic overview of the structure of this book is provided on the next page. Chapters placed at the same level provide independent information, while subordinate chapters lie underneath their parent.

In addition, to facilitate the navigation while reading, each Chapter opens with a survey, indicating its position in the content structure of the Part, reminding the reader of the accomplished journey and the path lying ahead.

PART II

THE SCROLL

אב

11 May 2003

I have taken a closer look at the scroll, today. It has been lying on my desk for some months now, and a layer of dust has settled on it, as if trying to make it look even more ancient. Totally unnecessary!

The cover looks like leather: it is worn, but still strong.

There is a sign in the middle, composed of two characters:

אב

Inside it is filled with characters obviously belonging to the same letter system. They are written in black ink on vellum: it smells of leather, dust and clove.

I did some research. It is ancient Hebrew, derived from the very first alphabetical system, the Phoenician. Most of the original Hebrew Bible (the Old Testament) is written in it. The symbol on the cover, from right to left, reads: AB, which is, in alphabetical order, the first word of the Old Testament.

Ab (or abba) means father in Aramaic, and is used in prayers to invoke God.

But this is not all. The name of the single letters is Alef and Bet, which, later taken over by the Greeks, became Alpha and Beta. The alphabet!

The word "ab" can be read as alphabet: the tool through which all the words are created. The book of Yochanan (John) in the New Testament starts with "In the beginning was the Word, and the Word was with God, and the Word was God".

The Word, the alphabet, the Father!

I also learned that the letter Alef is reserved for God's messages to us here on Earth. In sign of humbleness the Genesis (the first book of the Old Testament) begins with the letter Bet of the word "bereishit" (which means "in the beginning"). Accordingly, the Ten Commandments, allegedly

written by God and given to Moses on Mount Sinai, start with the letter Alef of the word "anochi" (which means "I"). His first statement is "I am God".

The form itself of the Alef is also intriguing: it is formed by twice the same sign (one to the upper right and one to the lower left) divided by a bar: these represent the higher and lower waters, and the sky between them. Just like described in the second day of the Creation, when God stretched the firmament between the two waters.

So, if we are not to start a book with the letter Alef, and if this symbol is so undeniably powerful, why is it so demonstratively placed on the cover of a forlorn scroll?

The human pelvis

In this chapter the main character of this dissertation, the pelvis, is briefly presented.

2.1   Once upon a time

HERE WAS just some sort of broth, sometime four billion years ago. Molecules drifted aimlessly in this prebiotic chemistry of activated nucleotides, bumping into one another, parting way again, as time passed. One fine day a chain of molecules, assembled by sheer chance, somehow managed to replicate itself, and the first "living" organism was born from non-living matter: abiogenesis [1].

Amazing things started happening from that moment, and in the evolutionary counterpart of a couple of years, organized multicellular organisms were merrily swimming around. The first animals inhabiting our blue marble, some 500 million years ago, were fishes. A couple of evolutionary months later they discovered that land was emerging from the primordial oceans, and that there was a new world to explore above the surface. In the Paleozoic era, about 400 million years ago, some of them developed legs and started exploring that unknown dry environment, even though returning to the water for procreation: amphibians. Reptiles followed from amphibians, and were the first animals not to resort to water for any of their functions. From the flourishing of one species to the extinction of another, Earth slowly transformed in a most celebrated environment: we are in the Mesozoic era. The very first mammals appeared in the Triassic period of that era (205 to 250 million years ago), but were kept in check by huge dinosaurs, which dominated in the Jurassic period (200 to 146 million years ago) and witnessed with a certain indifference the evolution of the first birds. But as oftentimes before, things came to an abrupt stop at the end of the Mesozoic era, some 65 million years ago: the terminal extinction swept away the legendary reptiles, changing forever the face of the planet and signposting the begin of the Cenozoic era. With the bullies no more around, the mammals could start their own evolution, and huge rhinoceros-like types were seen roaming around, sometimes absentmindedly observing a couple of silvery dolphins elegantly whirling in the deep blue.

Now imagine a fish and imagine a salamander, a bird and a chimp. Quite different... if it was not for a structure called a notochord, a sort of cartilaginous rod that extends most of the length of the body, present at least during some part of their development,

---

[1]This is the story we remember from our school time, but it is far from being established. Lacking any evidence, it is just an explanation, plausible according to the laws of nature. Just as plausible is the autocatalytic anabolist theory, which places the beginning of life in the inorganic volatiles in magmatic exhalations. The scientific debate can be appreciated in the following publications.[52,1]

[52] G. Waechtershaeuser. Origin of life: Life as we don't wkow it. *Science*, 289(5483):1307–1308, 2000.

[1]   J.L. Bada and A. Lazcano. Origin of life: some like it hot, but not the first biomolecules. *Science*, 296(5575):1982–1983, 2002.

and providing support and locomotion capability. That's what characterizes species belonging to the phylum chordata[2]. Some of them, classified in the subphylum vertebrata (fishes, reptiles, amphibians, birds, and mammals) go even one step further: the notochord present at embryonal level is replaced, during development, by an osseous vertebral column. The first tetrapods among them (creatures with four limbs) were amphibians: four legs connected to the vertebral column by means of pectoral and pelvic girdles. All tetrapods have those girdles, and all terrestrial vertebrates are tetrapods. Yes, human beings as well.

2.2 Anatomy

The pelvic girdle in the human body is a basin-like structure connecting the vertebral column to the legs. Its functions are protection of internal organs, such as the reproductive system and the gastrointestinal tract, and the transmission of loads from the upper body to the locomotion system. If we think 3.2 million years back about Lucy standing up for the first time, a sense of awesome appreciation overcomes us: the fore part became the upper part, and what the pelvis came to accomplish was not only to link the spine to the legs, but support the weight of head and trunc as well. All kind of forces began being transmitted through the pelvis, up and down. Osteology, which is the the study of the skeletal system, and syndesmology, which is the study of the ligamentous system, can help us have a better look at it.

Osteology

Even though it is often thought of as a single bone, the pelvis is in reality composed of three bones of complex geometry, the two hip bones and the sacrum, held in place by a massive ligamentous system.

The two **innominate** (or hip) bones are composed of three fused bones: the ilium, the ischium and the pubis (Fig. 2.1). The **ilia** are the relatively flat and thin wings spanning the width of the girdle and forming the walls of the basin. The **ischia** form the inferior posterior part of the pelvis, and are fused with the ilia just below the acetabula, the sockets where the femur heads are inserted. The ischial tuberosities are the points we painfully feel when we sit on a hard surface. The **pubic bones** constitute the infe-

---

[2]Phylum is the first taxonomic classification after the kingdom (e.g. animal), and is followed by class, order, family, genus and species, as introduced by Linnaeus in 1735.[34]

---

[34] C. Linnaeus. *Systema Naturae*. 1735.

rior anterior part of the girdle, and join at the front at the pubic symphysis, completing the pelvic loops.

The **sacrum** is a large triangular bone at the base of the vertebral column and is inserted as a wedge between the two hip bones, at the back of the pelvis. It is composed of four to five sacral vertebrae, still separated in a child, and fused together in adulthood. The coccyx, or tailbone, is the very last part of the spinal column, and is composed of three to five coccygeal vertebrae fused together. A fibrocartilaginous joint connects it to the sacrum, and allows for a very limited movement.

A number of concepts are of help when defining anatomical landmarks on a bone. The established terminology defines, among others:

Crest A prominent ridge.

Foramen An opening through a bone.

Fossa A broad, shallow depressed area.

Process A relatively large projection or prominent bump.

Spine A relatively long, thin projection or bump.

Tuberosity A projection or bump with a roughened surface.

Tubercle A projection or bump with a roughened surface, generally smaller than a tuberosity.

The main landmarks of the pelvic girdle are the iliac crest, the iliac fossa, the anterior superior iliac spine (Latin: *spina iliaca anterior superior*, shortcut to SIAS), the posterior superior iliac spine (Latin: *spina iliaca posterior superior*, SIPS), the posterior inferior iliac spine, the spine of the ischium, the tuberosity of the ischium, and the median sacral crest surmounted by three or four tubercles (the rudimentary spinous processes of the upper three or four sacral vertebrae). Some of these landmarks are shown in Fig. 2.1

Syndesmology

The pelvic ligaments can be divided in four groups, according to the bones they connect. They are the ligaments: (1) between the sacrum and the ilium, (2) between the sacrum and the ischium, (3) between the sacrum and the coccyx, and (4) between the two pubic bones. In addition, (5) there are the ligaments which connect the pelvis to the spine. For reference see Fig. 2.2[27].

---

[27] H. Gray. *Anatomy of the Human Body*. Lea & Febiger, Philadelphia, 20 edition, 1918.
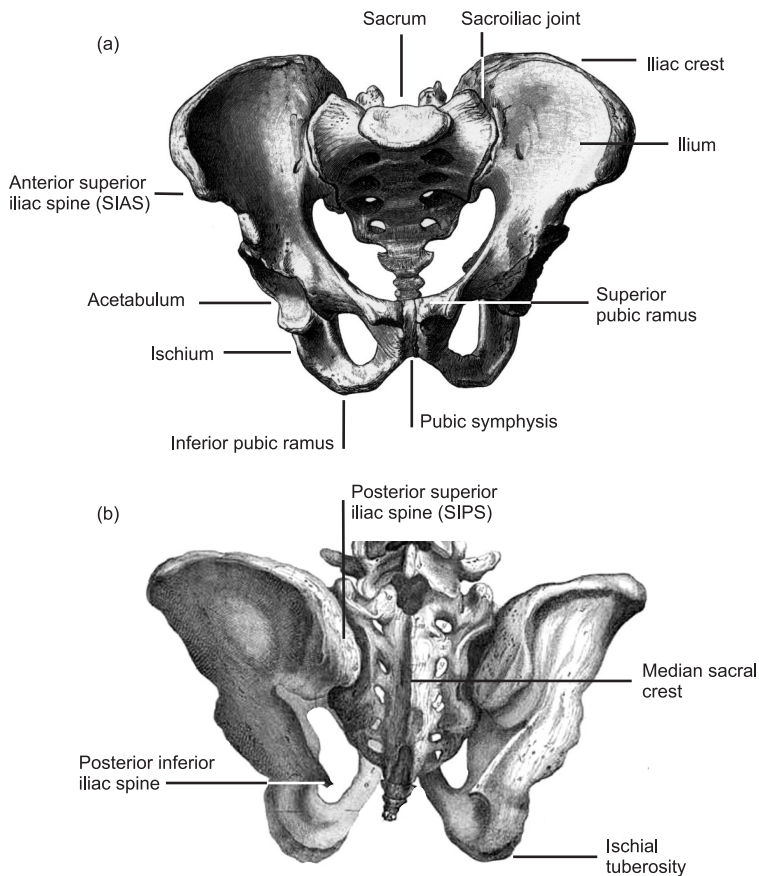
Figure 2.1: Bone anatomy of the pelvic girdle: (a) anterior view, (b) posterior view.

(1) The sacroiliac joint is an amphiarthrodial articulation[3] formed by the sacrum and the ilium. Cartilage not only lines the articular surface of the bones, but also forms patches where it actually unites the bones together, especially in young age. With aging, a gap forms between the inner surfaces of the joint and synovial fluid slowly fills it, giving the joint the characteristics of a diarthrosis[4].

The ligaments of the sacroiliac joints are the anterior sacroiliac, the posterior sacroiliac, and the interosseus.

---

[3]In an amphiarthrodial articulation the bones are connected by intervening substance (cartilage) admitting slight motion. Another word for it it symphysis.

[4]An articulation permitting free motion in the joint.

The anterior sacroiliac ligament is composed of numerous thin bands connecting the anterior surface of the sacrum to the anterior surface of the ilium.

The posterior sacroiliac ligament is a massive and very strong band inserted in a depression on the posterior side of the pelvis, between the sacrum and the ilium. The **short** posterior sacroiliac ligament is located in the upper part of the joint and runs almost horizontally between the bones, while the **long** posterior sacroiliac ligament passes in oblique direction from the posterior superior iliac spine to the lower part of the sacrum.

The interosseus ligament is the deepest band of the posterior sacroiliac ligament, and is made of a number of short strong fibers connecting the tuberosities of the two bones.

(2) The ligaments connecting the sacrum and the ischium are the sacrotuberous and the sacrospinous.

The sacrotuberous ligament is flat and triangular. It is attached by its broad base to the posterior inferior iliac spine, to the fourth and fifth transverse tubercles of the sacrum, and to the lower part of the lateral edge of the sacrum and the coccyx. From there it runs obliquely downwards, becoming narrow, and is attached to the inner edge of the tuberosity of the ischium.

The sacrospinous ligament is thin, and has a triangular shape narrower than the sacrotuberous. The base is attached to the lateral edge of the sacrum and the coccyx and its apex is attached to the spine of the ischium.

(3) The articulation between the sacrum and the coccyx is also amphiarthrodial, and it is similar to the intervertebral joints, with an interposed disc of fibrocartilage. Four ligaments hold the two bones together: the anterior, posterior and lateral sacrococcygeal, and the interarticular. Since modeling of this joint was not necessary, a more thorough description is not provided in this work.

(4) The pubic symphysis is the joint where the two oval articular surfaces of the pubic bones meet, interfaced by the interpubic fibrocartilaginous lamina. The pubic ligaments are the anterior, the posterior, the superior, and the arcuate pubic.

The anterior pubic ligament is formed by several layers which run on the anterior side of the joint: the superficial bands obliquely, and the deep bands horizontally, intertwining with the interpubic fibrocartilaginous lamina.

The posterior and superior pubic ligaments connect the two extremities of the pubic bones on the posterior and superior sides of the articulation.

The arcuate pubic ligament is located below the joint and forms the upper delimitation of the pubic arch. Above it blends with the interpubic fibrocartilaginous lamina, and laterally it is attached to the inferior rami of the pubic bones.

(5) The ligaments which connect the last lumbar vertebra to the sacrum are basically the same as the ligaments between the vertebrae. In addition, on both sides, the iliolumbar ligament connects the last lumbar vertebra to the ilia.

The iliolumbar ligament is attached above to the transverse process of the fifth lumbar vertebra and descends laterally towards the ilia. It splits in two main bands: a lower band runs downwards on the ventral side, intertwining with the anterior sacroiliac ligament, while the upper band is attached to the iliac crest just next to the sacroiliac articulation.
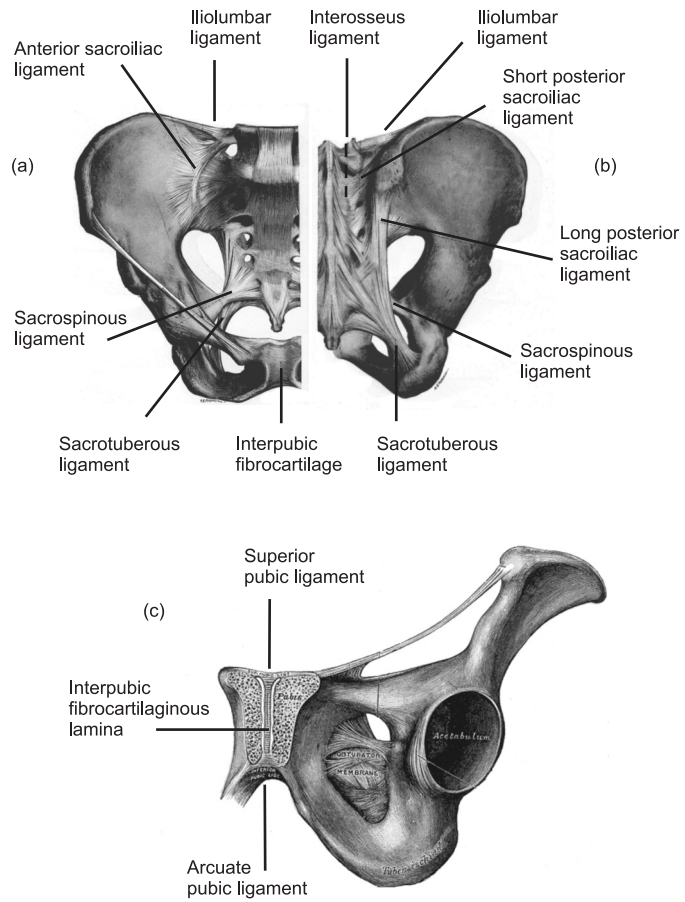
Figure 2.2: Ligamentous system of the pelvic girdle: (a) anterior view, (b) posterior view, (c) anterior close-up of the pubic symphysis.

Low back pain

This chapter describes in brief the problematic of low back pain. In the first section it will give a short introduction in the clinical concept of pain, followed by an overview of the common causes of the disorder, and its treatments. Main source of the information contained here is the internet site www.spine-health.com.

3.1 It hurts

T MIGHT BE FEASIBLE for Indian gurus to stand pain with apparent ease, but for most people physical pain is such a source of distress and distraction, when not of actual physical incapability, that working becomes impossible. Among the musculoskeletal disorders, which, as already mentioned, rank at the ninth position in the causes of health problems[53], low back pain is the most relevant. According to a study published in 2000, the one year prevalence of back pain lasting for at least 24 hours among the British population had increased from 36.4% to 49.1% over a ten-year interval (1987-1997)[41]. This fact emerges also in a social survey, indicating that about one third of the European workers consider their health at risk for back disorders[22]. Moreover, according to a forecast, the situation might deteriorate even further: lack of physical activity has been identified as the most emerging risk for musculoskeletal disorders in the work environment[21]. Unfortunately, physical activity can at the same time be a risk factor for the spine: up to 20% of all injuries that occur in sports involve the lower back or neck. Damage to the lower back region is commonly suffered during sports that involve repetitive impact (such as running or playing squash) or weight loading at the extremes of the articulation range of motion (such as weightlifting), while the upper part of the spine (neck) is more prone to be injured during sports that involve contact (such as rugby or martial art).

[53] World Health Organization Statistical Information System (WHOSIS). Global burden of disease estimates for the year 2001. Technical report, World Health Organization, 2001.

[41] K.T. Palmer, K. Walsh, H. Bendall H, C. Cooper C, and D. Coggon. Back pain in britain: comparison of two prevalence surveys at an interval of 10 years. *BMJ*, 320(7249):1577–1578, 2000.

[22] European Foundation for the Improvement of Living and Working Conditions. Third european survey on working conditions 2000. Technical report, Office for Official Publications of the European Communities, 2001.

[21] European Agency for Safety and Health at Work. Expert forecast on emerging physical risks related to occupational safety and health. Technical report, Office for Official Publications of the European Communities, 2005.

> *Pain is life - the sharper, the more*
> *evidence of life.*
>
> Charles Lamb

Although the insight of Mr Lamb[1] might bring some consolation, pain is and remains uncomfortable. Moreover, it is not that simple of a matter.

René Descartes, the French scientist and philosopher who lived in the seventeenth century, suggested that the human body is comparable to a machine and that it can be studied using a mechanistic approach. Regarding the reaction to pain, he theorized that a stimulus applied to the body would travel along a stimulus-specific neural pathway to a stimulus-specific center in the brain, which would allow for the perception of the pain. The experienced pain was then, according to him, directly proportional to the intensity of the stimulus. This theory of specificity lead to some extravagant experiments (e.g. resecting the responsible nerve to remove pain), and to the conclusion that there can be no pain in absence of an injury. Many people in pain were just dismissed as mentally ill.

This postulation was replaced in the mid 1960's by the gate control theory, developed by the Canadian psychologist Ronald Melzack and the British physiologist Patrick Wall[40], which sees the stimulus coming from the nerve terminations as being scrutinized in the spinal cord by "neural gates" and modulated before being allowed to proceed. The gates do not decide on their own to which stimulus to heed attention: they receive instructions from the peripheral nervous system as well as from the brain. Rubbing a toe after having hit it does bring some sort of relief: in fact the information of the loving massage is transmitted to the gates, which are then less prone to send a red alert message to the brain. Similarly, the mediating signal can come from the brain consequent on sensory, cognitive or emotional factors.

In medical practice, pain has been divided in three categories:

Acute pain is defined as lasting less than 3 to 6 months, or directly related to a tissue damage.

Chronic pain is a pain which lasts more than 6 months. The pain generator can be known (e.g. an injury) or unidentified, as after the healing of the tissue. In the latter case, the pain becomes the disease itself.

---

[1]Charles Lamb (1775 - 1834) was an English essayist, best known for his *Essays of Elia* and for the children's book *Tales from Shakespeare*, which he produced along with his sister, Mary Lamb (1764 - 1847).

---

[40] R. Melzack and P. Wall. Pain mechanisms: A new theory. *Science*, 150(3699):971–978, 1965.

Neuropathic pain is a pain which, similar to chronic pain, persists beyond the healing of the damaged tissue. It has however a different texture: unlike the dull persisting nature of chronic pain, it is sharp and lancinating, sometimes burning or cold, or it feels like a tingling or numbness sensation traveling along the pathways from the spine to the periphery. It is thought to be caused by a damage in the peripheral sensory or motor nerves.

3.2   Common causes

The causes to acute low back pain are easier to identify since they are very often directly related to an injury. The majority of episodes are due to muscular strains, and normally recede in time thanks to the efficient healing process of muscles. Nevertheless, research is ongoing focussing on the role of ligaments strain in the origin of acute low back pain. In recent studies a model has been proposed which relates slouching from an unconstrained erect position (flexing the spine with no compressive spinal load) to strain in the iliolumbar ligaments[48,47].

As for chronic low back pain, the commonest causes can be grouped according to the age span, and encompass lumbar disc herniation, degenerative disc disease and isthmic spondylolisthesis[2] for adults in the range 20 to 60 years old, and is more likely to be caused by the facet joints[3] or osteoarthritis in older adults (over 60 years old). Moreover a number of other factors can be named which can lead to low back pain, among which tumors, hip osteoarthritis, abdominal aortic aneurysm, sacroiliac joint dysfunction, pregnancy, and osteoporosis.

However, a diagnosis is not that straightforward.

---

[2]A spondylolysis is a fracture in part of a vertebra and may cause no problem at all. However, sometimes the cracked vertebra slips forward over the vertebra below it. This is known as adult isthmic spondylolisthesis.
[3]Facet joint is the joint between two adjacent vertebrae.

---

[48] C.J. Snijders, P.F.G. Hermans, R. Niesing, C.W. Spoor, and R. Stoeckart. The influence of slouching and lumbar support on iliolumbar ligaments, intervertebral discs and sacroiliac joints. *Clinical Biomechanics*, 19(4):323–329, 2004.

[47] C.J. Snijders, P.F.G. Hermans, R. Niesing, A.L. Pool-Goudzwaard, and G.J. Kleinrensink. New concepts and hypotheses; Sudden slouching in the upright posture is a possible cause of back sprain in view of a biomechanical model on sacroiliac joints and iliolumbar ligaments. *Accepted for publication Manual Therapy*, 2006.

3.3 Diagnostic methods

The physician usually makes a preliminary diagnosis based on factors such as the type of pain and its area of distribution. The hypermobility or hypomobility in the pelvic joints can be detected at this stage through function tests, pain provocation tests and palpation[28]. Function tests aim at assessing the functionality and range of motion of a joint to determine abnormal motions or positions. In pain provocation tests, the physician induces shearing or rotational forces in the structure in an attempt to stress inflamed tissues, thus provoking pain. Palpation consists in feeling the patient's body with the hands to examine the size, consistency, texture, location, and tenderness of an organ or body part.

Following this assessments the physician prescribes a period of conservative care[4], with the aim of reducing the pain, providing conditioning for the back and addressing the secondary effects of the distress, such as sleeplessness or depression.

Should a more thorough investigation be required, several diagnostic tools are at disposal, such as radiologic imaging (radiographs, computer tomographic scans), magnetic resonance imaging (MRI), electromyography, somatosensory evoked potentials (SSEP)[5], discogram injections[6], bone scans[7], bone densitometry (DEXA)[8].

Controversial and difficult to diagnose is the responsibility of the sacroiliac joints. That these joints play a significant role in low back pain patients has been attested[7,19,

---

[4]A treatment is considered conservative when it is non-invasive (e.g. physiotherapy, medication) or minimally invasive (e.g. injections).

[5]To assess the speed of electrical signals across the spinal cord.

[6]In this procedure, the discographer inserts a needle through the patients back into the center of the disc. Fluid is then injected into the disc to increase the pressure. If the provoked pain is the same as the normally felt back pain (concordant), the disc is considered the source of pain, otherwise (discordant pain) the hypothesis is dismissed.

[7]A damaged bone has a higher turnover (the replacement of old bone with new bone material). After injection of a radiogenic substance in the blood circulation, a scan can be performed to localize the areas of higher concentration.

[8]Low energy x-rays are passed through the bones to measure the mineral (calcium) content of the bones, which is a good indicator of osteoporosis.

---

[28] W.B. Greene and J.D. Heckman. *The Clinical Measurement of Joint Motion*. American Academy of Orthopedic Surgeons, Rosemont, 1 edition, 1994.

[7] Y.C. Chen, M. Fredericson, and M. Smuck. Sacroiliac joint pain syndrome in active patients. A look behind the pain. *The Physician and sportsmedicine*, 30(11):30–37, 2002.

[19] W.J. Daum. The sacroiliac joint: an underappreciated pain generator. *The American Journal of Orthopedics*, 24(6):475–478, 1995.

[46], and the prevalence of sacroiliac dysfunctions has been investigated[35,36]. However, low back pain originating in the sacroiliac area is still poorly understood.

3.4   Treatment

As mentioned in the previous section, conservative care is the first course of action when dealing with low back pain. Such an approach consists of one or more of the following treatments: medications; passive therapy such as heat or ice packs, iontophoresis[9], transcutaneous electrical nerve stimulator (TENS) and ultrasound; active physical therapy such as stretching and strengthening; chiropractic[10] and osteopathic[11] manipulations to mobilize the lumbar spine joints; braces to limit the movement of the low back to allow for healing; and injection of numbing substances.

When conservative treatments do not provide a satisfactory result, an invasive approach can be envisaged. There are several surgical interventions, from the replacement of a spinal disc to the fusion of the sacroiliac joint. Please refer to the field literature for a more comprehensive and detailed description.

---

[9]A means of delivering steroids through the skin, which produce an anti-inflammatory effect in the general area that is causing pain. This modality is especially effective in relieving acute episodes of pain.

[10]Chiropractice is the science of applied neurophysiologic diagnosis based on the theory that restoration of health and maintenance of good health depend on normal function of the nervous system (especially the spine, and the nerves extending from the spine to all parts of the body). Irritation of the nervous system by mechanical, chemical or psychological factors is thus the cause of disease. Diagnosis is the identification of these noxious irritants and treatment is their removal by the most conservative method.

[11]Osteopathy is a system of diagnosis and treatment which emphasizes methods of recognizing and alleviating structural and mechanical problems of the body.

[46] A.C. Schwarzer, C.N. Aprill, and N. Bogduk. The sacroiliac joint in chronic low back pain. *Spine*, 20(1):31–37, 1995.

[35] J.Y. Maigne, A. Aivaliklis, and F. Pfefer. Results of sacroiliac joint double block and value of sacroiliac pain provocation tests in 54 patients with low back pain. *Spine*, 21(16):1889–1892, 1996.

[36] J.Y. Maigne and C.A. Planchon. Sacroiliac joint pain after lumbar fusion. A study with anesthetic blocks. *European Spine Journal*, 14(7):654–658, 2005.

PART III

THE KEY

אב

7 December 2003

One year has passed by. Unsettling.
Life hasn't been easy for all sorts of personal battles.
I wonder whether I'll win the war, or succumb under
life's siege. I guess I'll have to see it to the end to know.

I have been studying the writing inside the scroll.
I can recognize most of the characters of the old Hebrew
alphabet now, but I can't identify any word they spell.
Anyway, I start now seeing patterns in the fabric of the
writing. There are words that are repeated more often than
others : modal verbs ? or nouns related to the subject of
this text ?

I have to catalogue the most recurrent words in this script,
and at the same time create a model of "educated guesses",
reflecting the use of the words nowadays. I won't pretend
that modern languages are good models for this mysterious
idiom, but maybe the frequency of certain words is similar.

It is very unfortunate that I don't even know in what language
it is written! In fact, if you think about it, sharing the
Roman alphabet is really not much of a help for a
German trying to read a book in French. The sounds just
don't bear a meaning.

In such case I have to skip the sounds, and look for the
meanings!

The mathematical bit

In this chapter we will provide the reader with the minimal set of tools to understand the mathematics behind the modeling process. Three methods for the derivation of the equations of motion are sketched, followed by their implementation in a mathematical symbolic environment. The basics of modal analysis are presented in simple words, as well as the description of the dynamics of a system in frequency domain. The last section gives a brief introduction on the experimental identification of modal parameters.

4.1 Equations of motion

HE EQUATIONS OF MOTION describe the mathematical relationship between the force applied to a system and its response to it. This is valid regardless of the complexity of the system: the response of a one degree of freedom system will be obtained by solving a scalar equation of motion, while the motion of a system having N degrees of freedom will be derived by a set of N equations of motion. This relationship can thus be expressed in matrix form

$$\boldsymbol{M}\ddot{\boldsymbol{q}}(t) + \boldsymbol{C}\dot{\boldsymbol{q}}(t) + \boldsymbol{K}\boldsymbol{q}(t) = \boldsymbol{f}(t), \tag{4.1}$$

where $\boldsymbol{M}$, $\boldsymbol{C}$ and $\boldsymbol{K}$ are the $(N \times N)$-dimensional mass, (viscous) damping and stiffness matrices, and $\boldsymbol{q}(t)$ and $\boldsymbol{f}(t)$ are the $(N \times 1)$-dimensional arrays of generalized coordinates and applied forces. Generalized coordinates are a set of independent variables sufficient to fully describe the system configuration.

There are several methods to obtain the equations of motion. The most direct way is to apply Newton's second law, which states that the acceleration $\ddot{\vec{u}}$ of an object of mass m depends on the vector sum of the forces (net force) $\vec{F}$ acting upon the object, as expressed in

$$\vec{F} = m\ddot{\vec{u}}, \tag{4.2}$$

where the resulting acceleration is in the direction of the net force. This relation has to be written for each mass point in a system and requires all the forces applied to each mass point to be expressed (e.g. by drawing a free body diagram showing the forces acting on it as if it were freely floating in space). This can make the derivation of the equations of motion a fairly complicated matter.

Another method uses the virtual work principle. To introduce this idea, a few concepts need reminding:

Constraint is a kinematical restriction on the possible configurations which a system can assume.

Virtual displacement is an infinitesimal configuration change that the system can undergo without breaking any constraint. It indicates the direction in which the motion is unknown and needs solving.

Principle of D'Alembert is derived from Newton's second law and enables the reduction of a dynamic problem into a static-like problem, by stating that a system is in (dynamic) equilibrium when subjected to a net external force and a net fictitious

(inertial) force, as expressed for each mass k as

$$\vec{F}_k - m_k \ddot{\vec{u}}_k = \mathbf{0}. \tag{4.3}$$

The virtual work is the work of the forces acting on a system while it undergoes a virtual displacement, or in other terms the projection of the forces on the virtual displacement. The principle states that for any arbitrary virtual displacement the combined virtual work of the external forces and the inertial forces must be equal to zero. This translates into the fact that the work is calculated only for those forces which act in the direction of allowed displacements. It would be an unnecessary effort indeed to consider the equilibrium for displacements which are inconsistent with the constraints, where in addition to the external forces and the inertial forces, also the unknown reaction forces need to be expressed.

If we consider a system with n masses m_k subjected to the forces $\vec{F}_k$, and whose positions in space are described by the vectors $\vec{u}_k$ as a function of the generalized coordinates q_s for $s = 1..N$, the principle of virtual work would look like

$$\sum_{k=1}^{n} (m_k \ddot{\vec{u}}_k(\boldsymbol{q}) - \vec{F}_k) \cdot \delta_{q_s} \vec{u}_k(\boldsymbol{q}) = 0, \qquad s = 1..N. \tag{4.4}$$

The only way to fulfill this equation for any virtual displacement is for the expression in brackets to be equal to zero, which leads us to the formulation of the equations of motion as a function of the generalized coordinates.

Even though at first sight it looks the same as Newton's second law, there is an important difference: needed are only those forces which produce work for the chosen virtual displacement, and thus not the unknown reaction forces related to the constraints.

A further step in this mathematical stillicide allows an even more sophisticated method, which employs scalar quantities (kinetic and potential energies) and avoids the vectorial formulation of the forces. The Lagrangian equations can be derived from the principle of virtual displacements or from the Hamilton's principle. We spare the reader with these tedious derivations at this time, and redirect him to Appendix A for details.

The Lagrange equations emerge after lengthy shuffling as

$$-\frac{d}{dt}\left(\frac{\partial \mathcal{T}}{\partial \dot{q}_s}\right) + \frac{\partial \mathcal{T}}{\partial q_s} - \frac{\partial \mathcal{V}}{\partial q_s} - \frac{\partial \mathcal{D}}{\partial \dot{q}_s} + Q_s = 0, \qquad s = 1..N, \tag{4.5}$$

where $\mathcal{T}$ and $\mathcal{V}$ are the kinetic and potential energies, $\mathcal{D}$ the dissipation function, and Q_s the remaining generalized non-conservative forces. The formulation of the Lagrange equations leads as well to the equations of motion.

4.2   Symbolic model step by step

In the frame of this research, the dynamic model of the human pelvis has been derived in symbolic form using the equations of Lagrange. It comprises three rigid bodies linked by springs and dampers, inspired by the anatomical description provided in Chapter 2.2.

The generalized coordinates q of the model have been defined by means of the symbolic position of the centers of mass of the rigid bodies $\vec{u}_b$ and the angles expressing their rotation in space $\boldsymbol{\theta}_b$. To be able to partially differentiate the kinetic energy $\mathcal{T}$ by $\dot{q}_s$, as shown in Eq. (4.5), the first time derivative of q_s needs to be maintained in the Lagrange expression as a variable on its own. These quantities $\dot{q}$ have been defined symbolically as well. No mathematical relation exists between the two sets of symbolic expressions.

The position of an external point belonging to the rigid body b has been computed by kinematic relationship of the generalized coordinates as follows:

$$\vec{u}_{ext} = \vec{u}_b + \boldsymbol{R}_b \vec{\rho}_{ext}, \tag{4.6}$$

where $\vec{u}_b$ is the position of the center of mass of body b, $\boldsymbol{R}_b$ is its rotation matrix, and $\vec{\rho}_{ext}$ the vector connecting the center of mass of body b to the external point expressed in the reference configuration.

The rotation matrix $\boldsymbol{R}_b$ for body b has been obtained by the definition of the Bryant angles[25] (sequence of three rotations about successive axes X-Y'-Z''), as expressed in

$$\boldsymbol{R} = \begin{bmatrix} c\theta_z c\theta_y & c\theta_z s\theta_y s\theta_x - s\theta_z c\theta_x & c\theta_z s\theta_y c\theta_x + s\theta_z s\theta_x \\ s\theta_z c\theta_y & s\theta_z s\theta_y s\theta_x + c\theta_z c\theta_x & s\theta_z s\theta_y c\theta_x - c\theta_z s\theta_x \\ -s\theta_y & c\theta_y s\theta_x & c\theta_y c\theta_x \end{bmatrix}, \tag{4.7}$$

where $c\theta$ and $s\theta$ are abbreviations for $\cos\theta$ and $\sin\theta$, and θ_i indicates the rotation angle around the axis $i = x, y, z$.

---

[25] M. Gérardin and A. Cardona. *Flexible multibody dynamics. A finite element approach.* John Wiley & Sons, Ltd, 2001.

Since we expected minimal deformations during the dynamic response of the system (in the order of micrometers and fractions of degrees), the following approximations were applied:

$$c\theta \simeq 1,$$
$$s\theta \simeq \theta,$$
$$O(\theta^2) \simeq 0,$$
$$O(\theta^3) \simeq 0,$$

which resulted in the approximation of the rotation matrix in (4.7) into

$$\boldsymbol{R}_b = \begin{bmatrix} 1 & -\theta_{bz} & \theta_{by} \\ \theta_{bz} & 1 & -\theta_{bx} \\ -\theta_{by} & \theta_{bx} & 1 \end{bmatrix}, \tag{4.8}$$

and further translated in the reformulation of Eq. (4.6) as

$$\vec{u}_{ext} = \vec{u}_b + \begin{pmatrix} \theta_{bx} \\ \theta_{by} \\ \theta_{bz} \end{pmatrix} \times \vec{\rho}_{ext} + \vec{\rho}_{ext}. \tag{4.9}$$

The velocity of an external point has been computed according to the general formula

$$\dot{\vec{u}}_{ext} = \dot{\vec{u}}_b + \vec{\omega}_b \times \vec{\rho}_{ext}, \tag{4.10}$$

with $\vec{\omega}_b$ being the angular velocity of body b, which, for small angles, can be defined as

$$\vec{\omega}_b = \begin{pmatrix} \dot{\theta}_{bx} \\ \dot{\theta}_{by} \\ \dot{\theta}_{bz} \end{pmatrix}.$$

With position and velocity of the centers of mass and of external points symbolically expressed, the energies contained in the system can be formulated.

The kinetic energy $\mathcal{T}$ has been expressed as

$$\mathcal{T} = \sum_{b=1}^{n_b} (\frac{1}{2} m_b \dot{\vec{u}}_b^T \dot{\vec{u}}_b + \frac{1}{2} \vec{\omega}_b^T \boldsymbol{I}_b \vec{\omega}_b), \tag{4.11}$$

with n_b the number of bodies (three in our model), m_b the mass of body b, $\dot{\vec{u}}_b$ the

velocity of its center of mass, $\vec{\boldsymbol{\omega}}_b$ its angular velocity, and $\boldsymbol{I}_b$ its rotational inertia matrix.

The potential energy $\mathcal{V}$ is produced in a system by conservative forces. In our model the only conservative forces are the elastic forces of springs, and the gravitational force. The part of the potential energy coming from the springs has been derived as

$$\mathcal{V}_{el} = \sum_{l=1}^{n_l} \frac{1}{2} k_l \Delta u_l^2, \tag{4.12}$$

with n_l the number of springs, k_l the stiffness coefficient of spring l, and Δu_l the elongation of spring l obtained by expressing the distance between the actual position of the two spring attachment points $\vec{\boldsymbol{u}}_l^{sx}$ and $\vec{\boldsymbol{u}}_l^{dx}$ minus their distance at rest L_l, according to

$$\Delta u_l = \sqrt{(\vec{\boldsymbol{u}}_l^{sx} - \vec{\boldsymbol{u}}_l^{dx})^T (\vec{\boldsymbol{u}}_l^{sx} - \vec{\boldsymbol{u}}_l^{dx})} - L_l. \tag{4.13}$$

The indices sx and dx (traditionally standing for left (*sinistrum*) and right (*dextrum*)) indicate here any pair of contiguous bodies on which the spring is attached. The effect of the gravity has been investigated by comparing to the quantity (4.12) the change in energy content due to the vertical change in position of the centers of mass:

$$\mathcal{V}_g = \sum_{b=1}^{n_b} m_b g \Delta u_{vert,b}, \tag{4.14}$$

where m_b is the mass of body b, g is the gravitational acceleration, and $\Delta u_{vert,b}$ the vertical upward displacement of its center of mass. The relative difference in both the resulting stiffness matrix $\boldsymbol{K}$ and in the eigenvalues showed the negligible influence of the gravitational pull.

The dissipation function $\mathcal{D}$ has been expressed as

$$\mathcal{D} = \sum_{d=1}^{n_d} \frac{1}{2} c_d \Delta \dot{u}_d^2, \tag{4.15}$$

with n_d the number of dashpots, c_d the damping coefficient of dashpot d, and $\Delta \dot{u}_d$ the difference in velocity of the attachment points of dashpot d, calculated with

$$\Delta \dot{u}_d = \sqrt{(\dot{\vec{\boldsymbol{u}}}_d^{sx} - \dot{\vec{\boldsymbol{u}}}_d^{dx})^T (\dot{\vec{\boldsymbol{u}}}_d^{sx} - \dot{\vec{\boldsymbol{u}}}_d^{dx})}. \tag{4.16}$$

By further development of the Lagrange formulation the system mass matrix $\boldsymbol{M}$

and the ensemble of the forces $\boldsymbol{f}$ can be obtained, here described for the general case:

$$\boldsymbol{M}(\boldsymbol{q})\ddot{\boldsymbol{q}} + \boldsymbol{f}(\boldsymbol{q}, \dot{\boldsymbol{q}}) = \boldsymbol{0}, \tag{4.17}$$

where the following equivalences are valid:

$$M_{sr} \equiv \frac{\partial^2 \mathcal{T}}{\partial \dot{q}_s \partial \dot{q}_r}, \tag{4.18}$$

$$f_s \equiv \frac{\partial^2 \mathcal{T}}{\partial t \partial \dot{q}_s} + \sum_r \frac{\partial^2 \mathcal{T}}{\partial \dot{q}_s \partial q_r} \dot{q}_r - \frac{\partial \mathcal{T}}{\partial q_s} + \frac{\partial \mathcal{V}}{\partial q_s} + \frac{\partial \mathcal{D}}{\partial \dot{q}_s} - Q_s. \tag{4.19}$$

In our case, the dependence of $\boldsymbol{M}$ on $\boldsymbol{q}$ does not apply, since the linearization has already been performed on the rotation components. Moreover the first three terms and the last term of Eq. (4.19) are zero, since in the expression of the kinetic energy $\mathcal{T}$ there is no dependence either on time or on $\boldsymbol{q}$, and we have no non-conservative forces beside the damping force provided by the dissipation function $\mathcal{D}$.

The linearized system matrices $\boldsymbol{C}$ and $\boldsymbol{K}$ can be obtained by partial differentiation of $\boldsymbol{f}$

$$C_{sr} \equiv \frac{\partial f_s}{\partial \dot{q}_r}, \quad K_{sr} \equiv \frac{\partial f_s}{\partial q_r}. \tag{4.20}$$

The system matrices have been evaluated at the equilibrium configuration, characterized by $\dot{\boldsymbol{q}}_{eq} = \boldsymbol{0}$ and $\boldsymbol{f}(\ddot{\boldsymbol{q}} = \boldsymbol{0}, \dot{\boldsymbol{q}} = \boldsymbol{0}, \boldsymbol{q}_{eq}) = \boldsymbol{0}$, as follows:

$$\begin{aligned}
\boldsymbol{M}_{eq} &= \boldsymbol{M}, \tag{4.21}\\
\boldsymbol{C}_{eq} &= \boldsymbol{C}(\boldsymbol{q}_{eq}, \dot{\boldsymbol{q}}_{eq} = \boldsymbol{0}),\\
\boldsymbol{K}_{eq} &= \boldsymbol{K}(\boldsymbol{q}_{eq}, \dot{\boldsymbol{q}}_{eq} = \boldsymbol{0}).
\end{aligned}$$

The linearized dynamic problem is now given by

$$\boldsymbol{M}_{eq}\Delta\ddot{\boldsymbol{q}}(t) + \boldsymbol{C}_{eq}\Delta\dot{\boldsymbol{q}}(t) + \boldsymbol{K}_{eq}\Delta\boldsymbol{q}(t) = \Delta\boldsymbol{f}(t), \tag{4.22}$$

where Δ indicates small perturbations around the equilibrium configuration. In the sequel $\Delta\boldsymbol{q}$ will be called $\boldsymbol{q}$, and the subscript eq for the matrices at equilibrium will be omitted to preserve legibility.

4.3 Modal Analysis in a nutshell

A mathematical model described as in Eq. (4.1) in the form

$$M\ddot{q}(t) + C\dot{q}(t) + Kq(t) = f(t),$$

can be transformed into a modal model.

In many textbooks at this point we would consider the undamped case ($C = 0$):

$$M\ddot{q}(t) + Kq(t) = f(t), \tag{4.23}$$

and propose a form for the solution of the homogeneous problem as in

$$q(t) = ze^{i\omega t}, \tag{4.24}$$

where $i^2 = -1$. A complex term at exponential indicates that there is a vibration involved with frequency ω, for that providential idea of using the complex plane to mathematically deal with harmonic functions, as elucidated in

$$\cos(\omega t) = Re(e^{i\omega t}). \tag{4.25}$$

We would then transform the problem into

$$(-\omega^2 M + K)z = 0, \tag{4.26}$$

and we would find ourselves facing a classical eigenproblem, whose non-trivial solution exists when the characteristic equation is equal to zero:

$$det(-\omega^2 M + K) = 0. \tag{4.27}$$

The solution of this problem is obtained by expanding the determinant, and by solving the resulting characteristic polynomial of order N in the variable ω^2. The N solutions are the eigenvalues, and represent the N squared **natural** (undamped) frequencies of the system ω_n^2. The associated eigenvectors, the solutions for z, represent the mode shapes (also called eigenmodes) of the system.

Some more mathematical cooking would then show that z in such a case is always real, and that a real z would be obtained also if we had a damping which is propor-

tional to the mass and stiffness matrices, as in

$$C = \alpha M + \beta K,\tag{4.28}$$

or for small damping associated to well separated resonance frequencies (in which case the real mode shapes would provide a satisfactory approximation[44]).

One of the characteristics of the real mode shapes z_j, $j = 1..N$, is that they are orthogonal to each other with respect to the mass and stiffness matrices, which in mathematical terms looks like

$$z_s^T M z_r = 0, \quad z_s^T K z_r = 0, \quad \forall s \neq r.\tag{4.29}$$

The set of orthogonal mode shapes can thus be used as a basis to express any vector in that space. This translates in the idea that the system response $q(t)$ can be seen as the superposition of all the mode shapes z_j modulated by a time-dependent amplitude $\eta_j(t)$, as shown in

$$q(t) = \sum_{s=1}^{N} \eta_s(t) z_s.\tag{4.30}$$

By substitution of Eq. (4.30) in Eq. (4.23) and premultiplication with each eigenmode z_j, and by remembering that the modes are orthogonal to one another with respect to the mass and stiffness matrices, we are left with uncoupled equations for the modal amplitudes $\eta_j(t)$:

$$\ddot{\eta}_j(t) + \omega_j^2 \eta_j(t) = \phi_j(t),\tag{4.31}$$

where $\phi_j(t)$ is the modal participation factor

$$\phi_j(t) = \frac{z_j^T f_j(t)}{\mu_j},\tag{4.32}$$

μ_j is the modal mass of mode j

$$\mu_j = z_j^T M z_j,\tag{4.33}$$

and

$$\omega_j = \frac{\gamma_j}{\mu_j} = \frac{z_j^T K z_j}{z_j^T M z_j}.\tag{4.34}$$

[44] J.S.W. Rayleigh. *The Theory of Sound*. Dover Publications, 1945.

Should we now substitute Eq. (4.30) in Eq. (4.1) we would obtain

$$\ddot{\eta}_j(t) + \frac{1}{\mu_j} \boldsymbol{z}_j^T \boldsymbol{C} \sum_{s=1}^{N} \eta_s(t) \boldsymbol{z}_s + \omega_j^2 \eta_j(t) = \phi_j(t), \tag{4.35}$$

where

$$\boldsymbol{z}_j^T \boldsymbol{C} \boldsymbol{z}_s \neq 0, \quad \forall j \neq s. \tag{4.36}$$

The system of equations (4.35) remains coupled unless $\boldsymbol{C}$ is proportional to $\boldsymbol{M}$ and $\boldsymbol{K}$, as shown in Eq. (4.28). In that case Eq. (4.35) would turn into

$$\ddot{\eta}_j(t) + \frac{c_j \dot{\eta}_j(t)}{\mu_j} + \omega_j^2 \eta_j(t) = \phi_j(t), \tag{4.37}$$

with

$$c_j = \boldsymbol{z}_j^T \boldsymbol{C} \boldsymbol{z}_j. \tag{4.38}$$

And one more treat! It can be shown that a system with non-proportional damping could still be decoupled in N equations, should the **damping be small**, and the **frequencies well separated**[44].

Unfortunately here we don't have the luxury of a small damping, and most probably not even the one of proportional damping, and thus the equations (4.35) are most certainly coupled. Therefore, if we want to interpret the system in terms of uncoupled modes, we have to go the hard way, in state space.

If we now take the matrix $\boldsymbol{C}$ in consideration, and we rearrange Eq. (4.1) a little, we obtain the following:

$$\begin{bmatrix} \boldsymbol{K} & \boldsymbol{0} \\ \boldsymbol{0} & -\boldsymbol{M} \end{bmatrix} \begin{pmatrix} \boldsymbol{q}(t) \\ \dot{\boldsymbol{q}}(t) \end{pmatrix} + \begin{bmatrix} \boldsymbol{C} & \boldsymbol{M} \\ \boldsymbol{M} & \boldsymbol{0} \end{bmatrix} \begin{pmatrix} \dot{\boldsymbol{q}}(t) \\ \ddot{\boldsymbol{q}}(t) \end{pmatrix} = \begin{pmatrix} \boldsymbol{f}(t) \\ \boldsymbol{0} \end{pmatrix}, \tag{4.39}$$

which is a differential equation of first order

$$\boldsymbol{A}\boldsymbol{r}(t) + \boldsymbol{B}\dot{\boldsymbol{r}}(t) = \boldsymbol{s}(t), \tag{4.40}$$

[44] J.S.W. Rayleigh. *The Theory of Sound*. Dover Publications, 1945.

where

$$A \equiv \begin{bmatrix} K & 0 \\ 0 & -M \end{bmatrix}, \tag{4.41}$$

$$B \equiv \begin{bmatrix} C & M \\ M & 0 \end{bmatrix}, \tag{4.42}$$

$$r(t) \equiv \begin{pmatrix} q(t) \\ \dot{q}(t) \end{pmatrix}, \tag{4.43}$$

$$s(t) \equiv \begin{pmatrix} f(t) \\ 0 \end{pmatrix}. \tag{4.44}$$

We are now pretty much where we were before, except for the fact that instead of proposing a solution like in Eq. (4.24), for the homogeneous problem we now propose the following:

$$q(t) = z e^{\lambda t}, \tag{4.45}$$

and, solving for λ, consider those solutions which are complex, as in

$$\lambda = -\sigma \pm i\omega. \tag{4.46}$$

It would look similar to the suggestion in Eq. (4.24) if it weren't for the real term σ, which takes care of the fact that the damping exists and that it dissipates energy causing the vibration to exponentially fade away in time.

We first solve the homogeneous problem and we obtain $2N$ eigensolutions, encompassing N eigenvalues $\lambda = -\sigma + i\omega_d$ and their N complex conjugates $\bar{\lambda} = -\sigma - i\omega_d$, and N eigenvectors y and their complex conjugates $\bar{y}$. An eigenvector can be written as

$$y = \begin{pmatrix} z \\ \lambda z \end{pmatrix}, \tag{4.47}$$

where z has to be thought of as the complex eigenmode of the damped system (in contraposition to z proposed in (4.24), which was the real eigenmode of the associated conservative (undamped) system). Please note the index d in ω_d, which indicates that this is the **damped** resonance frequency of the system, smaller than the natural resonance frequency ω_n defined a few lines ago. The relation between the two is

$$\omega_n = \sqrt{\sigma^2 + \omega_d^2}. \tag{4.48}$$

45

Details on the solution of Eq. (4.39) can be found in Appendix B.

An important tool frequently used in modal analysis is the Modal Assurance Criterion (MAC). It compares mode shapes between one another and evaluates their correlation with a value ranging from 0 (no correlation at all) to 1 (perfect matching). Mathematically, the MAC value between mode shape z_r and mode shape z_s is defined as

$$MAC(z_r, z_s) = \frac{(\bar{z}_r^T z_s)^2}{(\bar{z}_r^T z_r)(\bar{z}_s^T z_s)}, \tag{4.49}$$

where $\bar{z}_s$ is the complex conjugate of z_s.

4.4 Dynamic response in frequency domain

If we now return to the equation of motion Eq. (4.1) and assume a harmonic excitation with given frequency ω, expressed in the form

$$f(t) = p e^{i\omega t}, \tag{4.50}$$

and anticipate a solution such as

$$q(t) = z e^{i\omega t}, \tag{4.51}$$

we can rewrite the equation of motion as

$$(-\omega^2 M + i\omega C + K) z e^{i\omega t} = p e^{i\omega t}. \tag{4.52}$$

The quantity

$$\frac{z_j}{p_i} \tag{4.53}$$

is called Frequency Response Function (in short FRF) between the response of the degree of freedom j to a unit input at the degree of freedom i oscillating with frequency ω. For a system with N degrees of freedom, the ensemble of all the FRFs is contained in the $(N \times N)$-dimensional matrix

$$H(\omega) = (-\omega^2 M + i\omega C + K)^{-1}. \tag{4.54}$$

Very useful is the fact that this matrix of functions can be expressed in terms of

modes z_s:

$$H(\omega) = \sum_{s=1}^{N} \left(\frac{1}{\sigma_s + i(\omega - \omega_s)} \frac{z_s z_s^T}{\rho_s} + \frac{1}{\sigma_s + i(\omega + \omega_s)} \frac{\bar{z}_s \bar{z}_s^T}{\rho_s} \right), \qquad (4.55)$$

where σ_s and ω_s are the damping factor and the damped frequency for mode s, z_s is the complex mode with its complex conjugate $\bar{z}_s$, and ρ_s can be seen as a squared norm of the mode z_s, defined as

$$\rho_s = z_s^T C z_s + 2\lambda_s z_s^T M z_s. \qquad (4.56)$$

Details on the derivation of these expressions can be found in Appendix B.

The matrix

$$R_s = \frac{z_s z_s^T}{\rho_s} \qquad (4.57)$$

is the residue matrix for mode s, whose elements $R_{s,ij}$ can be obtained by performing a curve fitting on experimental Frequency Response Functions where a harmonic excitation is applied at the degree of freedom i and the displacement response measured at the degree of freedom j. This is actually the goal of the experimental modal analysis: to obtain the modal parameters (mode shapes, frequencies, damping) from measured Frequency Response Functions. But how are the FRFs obtained experimentally?

4.5 Experimental modal analysis

To make a long story very short and probably too simple, there are two ways of obtaining the Frequency Response Functions necessary to perform an experimental modal analysis: either you attach the structure to an actuator, or you don't.

If you don't, it means that you input the excitation through an impact, most commonly with a hammer, and measure the transient response[1] which follows. A hammer impact is a very short pulse, whose width determine the frequency content of the force spectrum, while its shape and amplitude result in the level of the spectrum.

On the other hand, if you do attach the structure to a shaker, you can apply a variety of signals, which can be subdivided in transient, periodic and non-periodic, and mea-

---

[1]Transient signals may be defined as signals starting and ending at zero within the observation time period[30].

---

[30] W. Heylen, S. Lammens, and P. Sas. Modal analysis theory and testing. Lecture notes Katholieke Universiteit Leuven, 1998.

sure the response of the system. All this is performed and recorded in time domain. So how do we get the response in frequency domain?

Monsieur Fourier, the French mathematician and physicist, while musing on music in the early 19th century, developed the very ingenious idea that each periodic signal $x(t)$ with period T can be seen as a superposition of harmonic signals with frequencies which are multiples of the basic frequency $\omega_o = \frac{2\pi}{T}$:

$$x(t) = \frac{a_0}{2} + \sum_{n=1}^{\infty} a_n \cos(n\omega_o t) + b_n \sin(n\omega_o t). \tag{4.58}$$

The coefficients can be calculated with

$$a_n = \frac{2}{T} \int_0^T x(t) \cos(n\omega_o t) dt,$$
$$b_n = \frac{2}{T} \int_0^T x(t) \sin(n\omega_o t) dt. \tag{4.59}$$

Another way of putting it makes use of the complex representation of harmonic functions, and results in the expression

$$x(t) = \sum_{n=-\infty}^{\infty} \alpha_n e^{in\omega_o t}, \tag{4.60}$$

where again $i^2 = -1$, and

$$\alpha_n = \frac{1}{T} \int_0^T x(t) e^{-in\omega_o t} dt. \tag{4.61}$$

To obtain something similar for any signal, which is what we actually want, we need to stretch the definitions a little and consider a "periodic" signal with an infinitely long period T. The basic frequency is then infinitely small, and the decomposition is expressed as

$$x(t) = \int_{-\infty}^{\infty} X(\omega) e^{i\omega t} d\omega \tag{4.62}$$

and

$$X(\omega) = \frac{1}{2\pi} \int_{-\infty}^{\infty} x(t) e^{-i\omega t} dt. \tag{4.63}$$

The transformation from $x(t)$ to $X(\omega)$ is called a Fourier transform, and changes the domain of the function from the time to the frequency domain. With this tool at disposal, the spectral content of the response of the system can be calculated.

Very often you will hear about the Fast Fourier Transform, or FFT. What is it? So far we have considered a continuous signal $x(t)$. Nowadays however most of the acquired signals are digitized, meaning that values of the function $x(t)$ are provided only at discrete points in time, $x(t_1), x(t_2), x(t_3)$ and so on. The Discrete Fourier Transform (DFT) has been developed from the continuous Fourier transform to deal with these cases, and is formulated as

$$x(t_n) \equiv x_n = \frac{1}{N} \sum_{k=0}^{N-1} X_k e^{in\omega kt}, \tag{4.64}$$

where

$$X_k = \sum_{n=0}^{N-1} x_n e^{-in\omega kt}. \tag{4.65}$$

The FFT is just a fast algorithm to calculate the DFT, which requires N to be a power of 2.

Thinking the model

In this chapter the creation of the dynamic model of the human pelvis is presented. The final version has been achieved based on reasoning, trial and error and educated guesses, following a learning curve which is described here.

5.1 Mumble mumble...

E HAVE LEARNED in Chapter 2.2 that the human pelvis is composed of three separate bones interfacing at three articulations: the sacroiliac joints between the ilia and the sacrum on either side, and the pubic symphysis at the front. When having to decide on the topology of a dynamic model of the pelvis, this observation provides a justification for choosing the same number of bodies.

Organs and soft tissues surrounding the pelvic girdle in vivo are not included in the model to keep it as simple as possible. Of course the option of implementing them, should they result necessary, is always open. The ligaments on the contrary, which in our vision are the elements which introduce the stiffness, are to be included in the model. The rationale for choosing to favor the ligaments over the other soft tissues and organs lies in the intention of investigating those cases of low back pain which are caused by abnormalities in the sacroiliac joints (thus interfaces of bones held together by ligaments), and not by muscle strains or spine injuries.

Regarding the modeling of the bones, since in the proposed methodology we expect the eigenfrequencies related to bone deformation to lie well above the frequency range of excitation, they will be implemented as lumped masses with rotational inertia properties, thus representing rigid bodies. This assumption dispenses with the use of finite elements in the modeling phase.

The following sections will discuss the modeling of inertia, stiffness and damping properties.

5.2 Mass properties

The model consists of three rigid bodies representing the two innominate bones and the sacrum, each with a given mass and a given mass distribution, and each defined in a three-dimensional space. Since the motion of each body in a three-dimensional space is determined by six parameters (three translations and three rotations), **the number of degrees of freedom of the model sums up to 18**.

The frame of reference is defined by three bony landmarks on the pelvic girdle (Fig. 5.1): the two anterior superior iliac spines (SIAS), and the outer margin of the upper ridge of the pubic symphysis. These three points define the plane y-z, with the y axis passing through the two SIAS and the z axis intersecting the y axis at the mid point between them. The plane x-z divides the pelvic girdle sagittally in the middle, and the plane x-y is the plane perpendicular to the previous two.
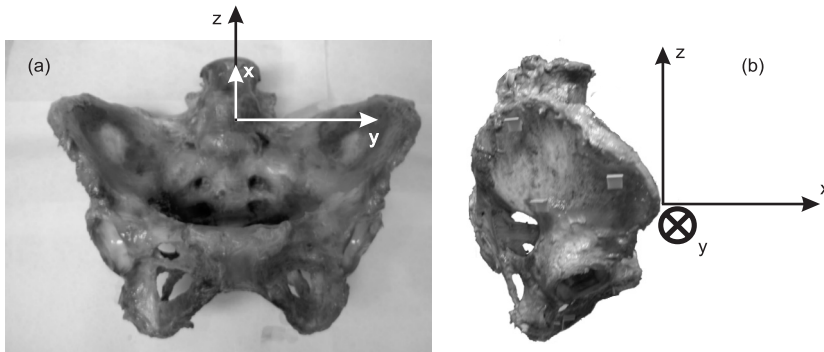
Figure 5.1: Frame of reference defined by bony landmarks on the pelvis.

An indication of the mass of the human pelvic skeletal structure has been obtained in the early phase of the project by weighing an embalmed specimen (1.64 kg), and has been taken as a reference for the sum of the mass of the three rigid bodies in the model. Their individual mass has been assigned by estimating the relative size of the three bones in a human pelvis and by assuming a uniform mass density (innominate bone: 0.64 kg each, sacrum: 0.36 kg).

Typical inertia properties have been estimated by means of a geometric model of a human pelvis in Pro/ENGINEER (PTC, Needham, USA), as depicted in Fig. 5.2. The contours of a set of computer tomographical (CAT) scans of a human pelvis[1], spanning the pelvic ring in vertical direction, have been imported in the software and post-processed to build a solid geometry. The material of the model has been chosen to be homogeneously distributed with a density of 1.99 kg/m^{3}[16]. The rotational inertia matrix expressed in the above mentioned frame of reference has been calculated by Pro/ENGINEER, and divided by the mass value. This mass scaling was performed to retain the geometric factor in the expression of the moments of inertia (thus assuming constant geometry), while removing the mass factor, with the objective to enable the modulation of the rotational inertia matrix with different mass values. The actual mass of the model in Pro/ENGINEER has therefore been uncoupled and discarded.

Whether the mass of the three rigid bodies was used as a parameter of the model or was taken as a constant depended on several factors, and was decided upon on a

---

[1]The CAT scan data have been provided by Dr. Niels Moes of the Faculty of Industrial Design of the Delft University of Technology.

[16] J.D. Currey. *Handbook of Biomaterial Properties*, chapter A1-Cortical bone, pages 3–14. Chapman & Hall, 1998.
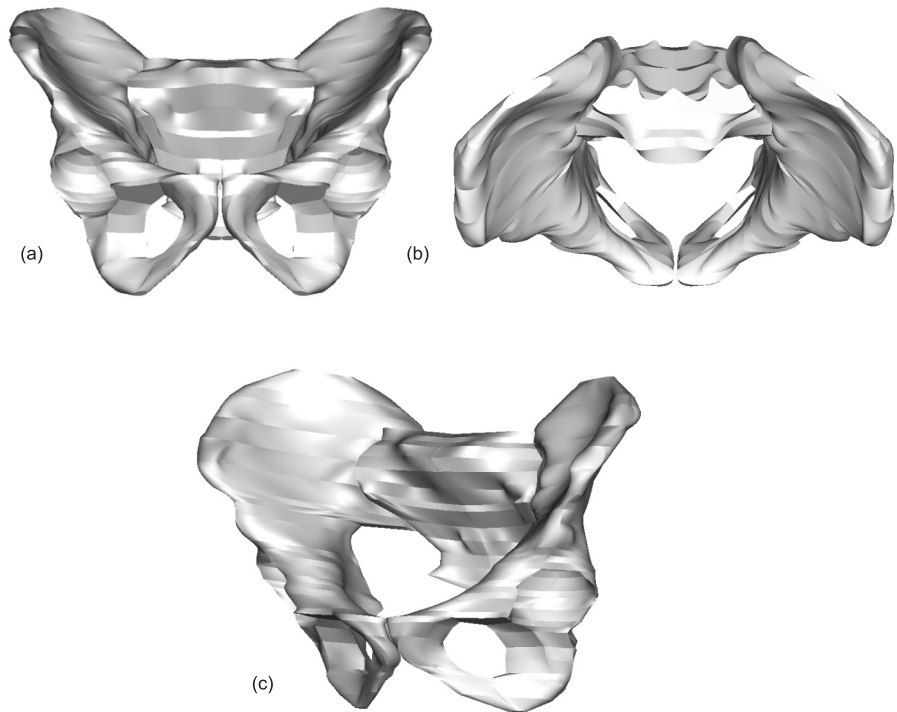
Figure 5.2: Geometric model of a pelvis in Pro/ENGINEER. (a) Front view, (b) top view, (c) general view.

case by case basis throughout the research phases. Details on the single studies will be presented in the corresponding Chapters.

Interindividual variations of geometry

As mentioned in the introduction the aim of this research is to devise a procedure for the identification of the mechanical properties of the sacroiliac joints *in vivo* **for each individual subject**.

Unfortunately there is no way to measure *in vivo* the mass and mass distribution of the individual pelvises. What is usually available in form of specifications or of direct measurements, is in our case denied, and has to be estimated.

One possible way to attain such an estimation is by measuring the position of bony landmarks which can be felt under the skin. From palpation, information can be gath-

ered such as the distance between the two anterior superior iliac spines (SIAS), the depth of the structure from the anterior superior iliac spines (SIAS) to the posterior superior iliac spines (SIPS), the height from the ischial tuberosity to the upper most point of the iliac crest. These data could be fed into a parametric geometric model to accordingly stretch in all directions a preset standard geometry (such as the one described above). The density of the material could also be chosen from a range of values, depending on data such as the age and gender of the subject and the general calcification conditions of the bones. From the adjusted geometric model and with the estimated bone density, the mass of the individual bones and the moments of inertia could be derived.

During this research no indications have been found that such a fine tuning of the rotational inertia matrix was necessary. It could however be an interesting subject for a future study.

5.3   Springs configuration

The stiffness is implemented in the model in form of linear springs, whose configuration is inspired by the anatomy of the pelvic ligamentous system. Note that this does not imply that we assume that the joint properties are linear, rather we assume that, during vibration, only linearized properties are relevant. The topology of the springs has undergone modifications throughout the phases of this project according to experimental indications.

The number of springs is not arbitrary, as we candidly thought in the very early phase of the research while setting up the first model. In fact it is determined by the number of degrees of freedom of the model. With 18 degrees of freedom, the modal representation of the system foresees 18 eigenvectors (see Chapter 4.3). In absence of any connection to the environment, the structure can freely and rigidly move in the six global degrees of freedom (three translations and three rotations), using 6 of the 18 eigenvectors at disposal. The remaining 12 eigenvectors could then represent the 12 vibration modes of the structure. However, in order to ensure an eigensolution with 12 non-zero eigenfrequencies, elastic energy has to be involved in all these vibration shapes (in absence of elastic energy we would obtain a mechanism, which is a mode shape devoid of any energy build-up, thus with frequency zero). A configuration of 12 independent springs is therefore necessary to ensure elastic energy in all 12 eigenmodes. Any additional spring would increase the intricacy of the problem, possibly impairing the identifiability of parameters.

This realization reminded us of the concept of tensegrity. Tensegrity is derived from

the combination of the words "tensional integrity", and refers to the integrity of structures which draw their stability and strength from the synergy between elements able to bear tension and compression, and purely tension elements. These tension-bearing elements position themselves in a geodesic manner, thus mapping the shortest path between two points in space. A simple example is shown in Fig. 5.3. An interesting
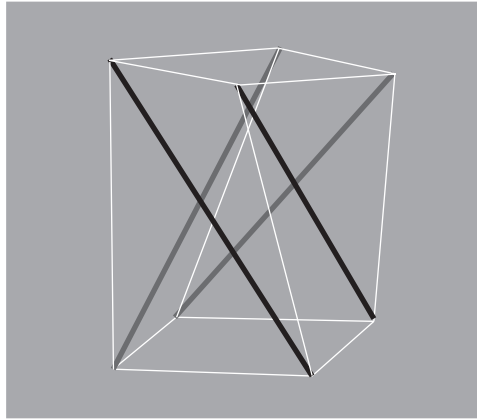

Figure 5.3: A tensegrity tetrahedron. The black and gray bars are the compression (rigid) elements, while the white lines are strings under tension.

domain for the observation of this principle is nature: biotensegrity is used to explain many biological structures, for example the cytoskeleton of a cell, viruses, the vertebral column and birds lungs[4,24,31,37].

The final version of the spring topology foresees one horizontal spring in y direction and a spring in the sagittal plane in direction $(1, 0, 1)^T$ at the pubic symphysis, three springs per side representing the interosseous, the long sacroiliac and the short sacroiliac ligaments on the posterior side of the sacroiliac joints, and two springs representing the anterior sacroiliac ligaments (one ascending from the sacrum across to the

[4]   P. Canadas, S. Wendling-Mansuy, and D. Isabey. Frequency response of a viscoelastic tensegrity model: structural rearrangement contribution to cell dynamics. *Journal of Biomechanical Engineering*, 128(4):487–495, 2006.

[24] C. Galli, S. Guizzardi, G. Passeri, G.M. Macaluso, and R. Scandroglio. Life on the wire: on tensegrity and force balance in cells. *Acta Biomedica Ateneo Parmense*, 76(1):5–12, 2005.

[31] D.E. Ingber. Cellular mechanotransduction: Putting all the pieces together again. *The FASEB Journal*, 20(7):811–827, 2006.

[37] J.N. Maina. Spectacularly robust! Tensegrity principle explains the mechanical strength of the avian lung. *Respiratory Physiology and Neurobiology*, Epub ahead of print, 2006.

ilium, and one descending), as shown in Fig. 5.4. The apparently scandalous omission of springs representing the sacrospinous, the sacrotuberous and the iliolumbar ligaments is actually the result of an experiment session, whose findings are presented in Chapter 11.
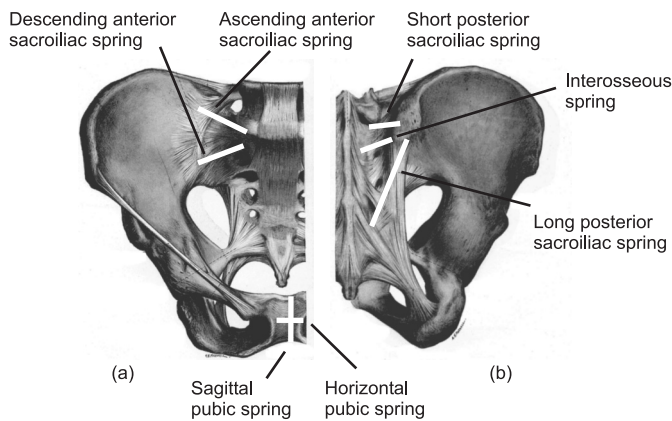
Figure 5.4: The springs in the model represented by the white lines: (a) anterior view, (b) posterior view. The five springs around the sacroiliac joint are present on both sides.

The spring attachment points have been defined as actually belonging to the two contiguous bodies as explained in Chapter 4.2, and do not lie at the same spatial coordinates at rest. This introduces a length of the springs at rest with no elongation, thus no energy storage, involved. Each spring has been assigned its dedicated stiffness coefficient. However in all the studies performed in this research the number of parameters has been reduced by assuming model symmetry between left and right, thus by forcing the homologous springs on the left and right side to have the same coefficient value. **The number of stiffness parameters can thus range from seven to twelve**.

In some studies, presented later in this work but performed earlier in the timeline of this research, the spring configuration had not reached this stage yet, and differ therefore from the model presented here. In case of deviations, the corresponding Chapters will explicitly describe the used model.

5.4 Modeling of damping

The damping is thought to originate mainly in the cartilage within the joints. The studies performed in the frame of this research have assumed that a viscous damping is present between each joint of the pelvis for all motions except those parallel to the joint inner surfaces. The idea behind is that the sliding of the two surfaces against each other is undamped (friction-free) due to the intra-articular synovial fluid.

At first, the implementation of such damping characteristics had been achieved by introducing three linear dashpots per joint, disposed within the joint in a parallel but non-coplanar manner (Fig. 5.5), and each of them designed to react to the projection of the velocity difference of the two attachment points onto the normal to the surface, as illustrated in Fig. 5.6. It has to be mentioned that the surface plane for the pubic symphysis is vertical and coincides with the sagittal plane x-z, while the planes of the two sacroiliac joints are not parallel to any reference plane.
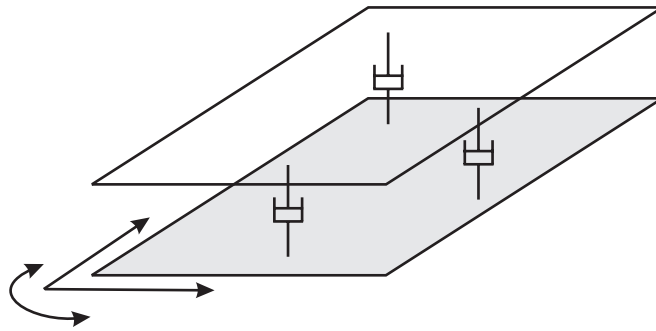
Figure 5.5: The three parallel non-coplanar dashpots spanned between the two joint inner surfaces. The arrows indicate the motions which leave the dashpots undisturbed.

If we take a poetic license, and express the eigenproblem in terms of velocity instead of displacement and ignore for a moment the stiffness in the structure, we can define a similar concept of "mechanism" as a (velocity) mode shape in which no energy is dissipated. With nine dampers in the system, we would expect the eigenproblem:

$$(\omega M + C)z = 0, \tag{5.1}$$

to result in nine eigenvectors z_j with non-zero eigenvalues, which can be seen as dissipative mode shapes. In reality, the resulting dissipative mode shapes were just eight, meaning that one "mechanism", as just defined, existed in which energy was not dissipated.
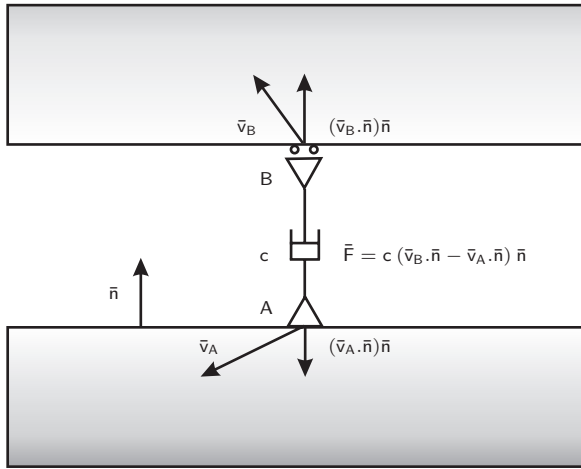
Figure 5.6: Schematic depiction of one dashpot between two cartilage surfaces. Points A and B belong to the two opposing surfaces, and move with velocities $\bar{v}_A$ and $\bar{v}_B$. The dashpot (with coefficient c) remains aligned with the normal vector $\bar{n}$ (with $|\bar{n}| = 1$) and reacts with a force $\bar{F}$ to the difference between the projections of the velocities along $\bar{n}$.

To help understand the nature of this mechanism we can think in terms of planes in which each joint is able to move without activating the dashpots, and in terms of intersections of these planes. Let's make the preliminary observation that, per definition, the dashpots of one single joint won't react to motions which happen within the plane of that joint, as depicted in Fig. 5.5.

If we now imagine the pelvis, and imagine one if its bones moving against the other two virtually fixed in space, we picture in our mind that its two articular surfaces lie in two non-parallel planes. Considering Fig. 5.5 and mentally expanding it to two joints (Fig. 5.7), we also see that if the body translates in the direction of the intersection line between those two planes, the dashpots of both articulations won't notice anything: we have a "mechanism". This is valid for each of the three bodies taken singularly while the others are fixed.

If we now allow two bodies to move against the third one fixed, we have three planes involved. As your intuition might already suggest, the only possibility for the "mechanism" to exist is when the three planes intersect exactly on the same line (this is a special case: if you look at the room you're in right now and consider the two horizontal lines where the floor hits the walls, and the vertical line between the two
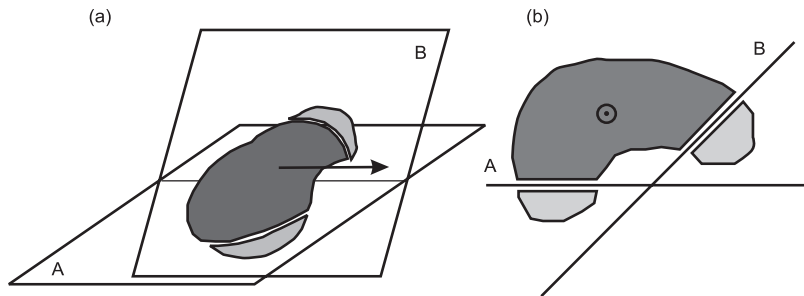
Figure 5.7: The darker body interfaces with the two lighter bodies in the planes A and B, where also the dashpots are located (three per interface) as shown in Fig. 5.5. (a) General view, (b) view in direction of the arrow. The arrow indicates the only motion (translation) that the darker body can perform without activating the dashpots of either interface. This translation is parallel to the intersection line of the two planes.

walls, you realize that usually three planes intersect on three different lines). Well, in fact, by symmetry, the planes defining the sacroiliac joints intersect on a line, which even though not being vertical, is contained in the vertical sagittal x-z plane. The plane of the pubic symphysis is the vertical sagittal plane itself, and therefore goes right through that intersection line: the mechanism! Considering all this, we decided to avoid the redundancy and remove one dashpot from the pubic symphysis.
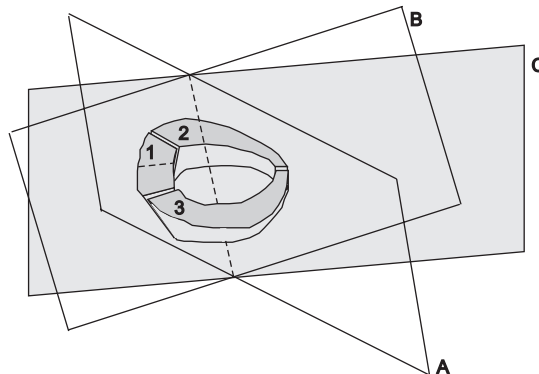
Figure 5.8: Schematic representation of the pelvis (1: sacrum, 2: left innominate bone, 3: right innominate bone) and the planes of interface of the joints (A, B and C). Planes A and B go through the sacroiliac joints and intersect on an oblique line contained in plane C, which is also the plane of the pubic symphysis.

The last established model consists therefore of three parallel non-coplanar dash-pots implemented in each sacroiliac joint and two in the pubic symphysis. The dash-pots belonging to the same articulation were assigned one and the same damping co-efficient, for a total of **three damping parameters in the model**.

An example of the parameter values can be found in Appendix E.

Identification algorithms

This chapter presents the two identification algorithms developed to post-process the raw data and obtain the mechanical properties of the sacroiliac joints. The first section describes the algorithm devised in modal domain, while the second section explains the algorithm created in frequency domain.

6.1   Sensitivity-based algorithm in modal domain

HE IDENTIFICATION ALGORITHM in modal domain has been our first idea to obtain the mechanical properties of the pelvis. We are in summer 2003. At this time a pilot experiment on an embalmed human pelvis (see Chapter 10) has revealed a first vibration mode at a frequency of 187 Hz. Based on the fact that only one resonance has been detected, we decide to **design an identification algorithm based on the first mode shape of the system**, and test it in simulations. In fact, only in a virtual environment the identification efficacy can be assessed by comparing the identified properties to the system known ones.

This application has been described in a conference paper[10].

The model

The model in this study has a spring configuration different from the one presented in Chapter 5.3, in two ways. The first difference lies in the modeled ligaments. The ones considered here are (on both sides): the sacrospinous ligaments, the sacrotuberous ligaments, the iliolumbar ligaments, the anterior sacroiliac ligaments, the posterior sacroiliac ligaments, and all the pubic ligaments grouped as one, for a total of eleven springs, as illustrated in Fig. 6.1.
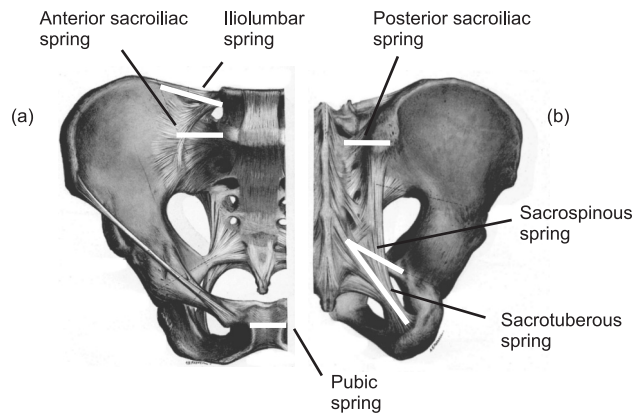
Figure 6.1: The spring configuration as used in the development of the identification algorithm in modal domain: (a) anterior, and (b) posterior views.

[10] N.E. Conza and D.J. Rixen. Dynamic model of the human pelvis - parameter identification. In *22nd International Modal Analysis Conference (IMAC XXII)*, Dearborn, Michigan, USA, January 26-29 2004. Society for Experimental Mechanics.

This last remark should immediately provoke an objection in the reader's mind, who has just been told that the springs need to be at least twelve to ensure twelve elastic modes. However, and here comes the second difference, in this early version the points used to determine the ligament elongation have not been chosen as the actual attachment points, residing at two separate locations, but as the mid-point between the mentioned spring extremities at rest. When the two bodies undergo certain relative position changes, the two points, which had been residing at the same spatial coordinates, split, each of them loyally following the body it belongs to, and introducing an elongation in the spring, as illustrated in Fig. 6.2. There are however configuration changes which do not result in the splitting of the mid-point, for instance all rotations for which the rotation axes pass through the mid-point, or also translations and rotations (with the axes somewhere else) which combine in such a way that the point remains at the same coordinates.

(a)

(b)

$A \equiv B$

B

k

A

$\bar{F} = (\bar{B} - \bar{A}) \, k$
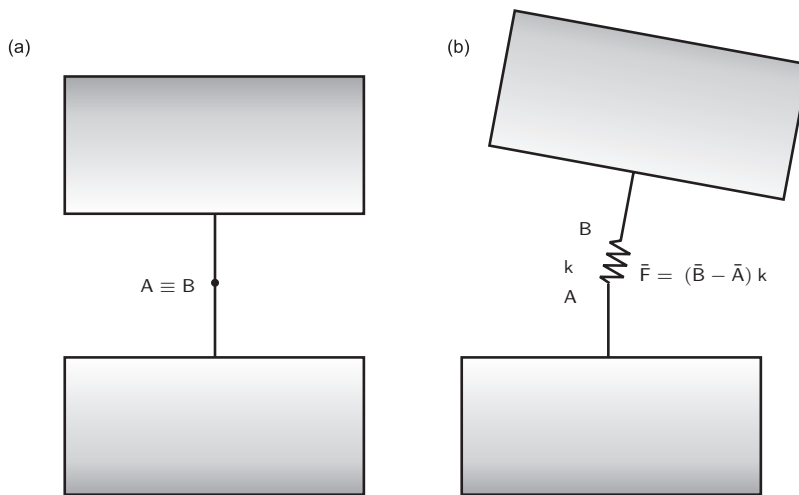
Figure 6.2: Schematic illustration of the elongation in each spring of the model: (a) in equilibrium configuration, (b) after relative motion of the two bodies. The line connecting the two bodies represent the ligament. Point A belongs to the lower body and moves rigidly with it, point B belongs to the upper body. At equilibrium the two points coincide. After relative motion of the bodies, points A and B do not lie at the same coordinates in space any more, and the difference between their new coordinates determines the direction and amplitude of the resulting elastic force $\bar{F}$.

When considering this apparently minor difference we realize that in such a model all mid-points of all springs have to remain coincident in order to have a mechanism

(a motion with no energy build-up). Since the sacrum is connected with five springs to each innominate bone, and due to the fact that three points of a rigid body are already enough to unequivocally determine its position and orientation in space, we see that an energy-free change in spatial configuration of the sacrum implies rigidly dragging the two innominate bones with it. The only energy-free motions possible in this model are the six global rigid body modes (in fact no connections to the environment preventing them has been implemented). Therefore, even with eleven springs, there is no mechanism.

Since the identification necessitates only the first mode shape assumed real (thus not affected by damping, as seen in Chapter 4.3), we choose not to implement any damping model.

The mass of the three bones are approximated starting from the total mass of the embalmed pelvis, and correspond to the values provided in Chapter 5.2 (0.64 kg per innominate bone, and 0.36 kg for the sacrum). The moments of inertia are estimated by comparison to similar geometric solids and to indications found in literature[39], with their principal axes corresponding to the global system of reference (at this stage the model in Pro/ENGINEER mentioned in Chapter 5.2 has not been created yet). The stiffness coefficients of the springs are estimated following mechanical considerations and indications found in the literature[16,23,26,27]. The positions of the attachment points are obtained by direct measurement on a plastic model, while the positions of the centers of mass are derived by geometric considerations. The values assigned to the model mass and stiffness coefficients are shown in Table 6.1, and serve as a testbench to assess the identification efficacy of the algorithm.

Sensitivity-based model updating

The procedure of adjusting the parameters of a model so that its response matches a certain target response is called model updating. One way to update a model is to define a function which reflects the difference between the actual model response

[39] J.T. McConville, T.D. Churchill, I. Kaleps, C.E. Clauser, and J. Cuzzi. Anthropometric relationships of body and body segment moment of inertia. Technical Report AFAMRL-TR-80-119, Wright-Patterson Air Force Base, 1980.

[16] J.D. Currey. *Handbook of Biomaterial Properties*, chapter A1-Cortical bone, pages 3–14. Chapman & Hall, 1998.

[23] Y.C. Fung. *Biomechanics. Mechanical Properties of Living Tissues*. Springer-Verlag, New York, 2 edition, 1993.

[26] U.J. Gerlach and W. Lierse. Functional construction of the sacroiliac ligamentous apparatus. *Acta Anatomica*, 144(2):97–102, 1992.

[27] H. Gray. *Anatomy of the Human Body*. Lea & Febiger, Philadelphia, 20 edition, 1918.

Table 6.1: Values of some of the parameters of the model. m_{in} and m_{sacrum} are the mass of the innominate bones and the sacrum respectively. The indices of the stiffness coefficients k refer to the springs: ss: sacrospinous, st: sacrotuberous, il: iliolumbar, as: anterior sacroiliac, ps: posterior sacroiliac, pub: pubic.

Parameter	Value	
m_{in}	0.64	kg
m_{sacrum}	0.36	kg
k_{ss}	$12 \cdot 10^4$	N/m
k_{st}	$8 \cdot 10^4$	N/m
k_{il}	$12 \cdot 10^4$	N/m
k_{as}	$1.5 \cdot 10^4$	N/m
k_{ps}	$20 \cdot 10^4$	N/m
k_{pub}	$1.5 \cdot 10^4$	N/m

and the target response. The set of model parameters is then searched, at which the function becomes zero (no difference, thus perfect match).

The iteration method called Newton-Raphson is able to do just that: identify the zero-crossing of a function. The basic idea of this method is elucidated in Fig. 6.3. The coordinate on the abscissa at which the function crosses over can be iteratively found by constructing the tangent at a start point on the curve $y(x_o)$ (which should not be too far away from the zero-crossing), "slide down" along this tangent onto the abscissa to find x_1, resume position on the curve at that coordinate $y(x_1)$, recalculate the tangent and "climb up" to find x_2. Again resume position on the function at $y(x_2)$ and "slide down". When this is repeated enough times, a good approximation of the zero-crossing can be found.

Since our model is defined by many parameters p and not just one, the function representing the difference between model and target response will be expressed in terms of system matrices $\boldsymbol{M}(p)$, $\boldsymbol{C}(p)$ and $\boldsymbol{K}(p)$ dependent on all the parameters p. In order to use the Newton-Raphson iteration method we need to calculate the multivariable tangent of the function, thus we need to differentiate the system matrices with respect to the parameter set p. Since in this study we are considering the difference in the first elastic mode shape, we need the sensitivity of that eigenmode.

Starting point to calculate the sensitivity of the eigenmodes (and before that of the eigenfrequencies) is the eigenproblem expressed for mode s:

$$(-\omega_s^2 \boldsymbol{M} + \boldsymbol{K})\boldsymbol{z}_s = \boldsymbol{0}. \tag{6.1}$$

Explicit writing of the dependence $\boldsymbol{M}(p)$, $\boldsymbol{K}(p)$, $\omega(p)$ and $\boldsymbol{z}(p)$ is omitted to improve ligibility.
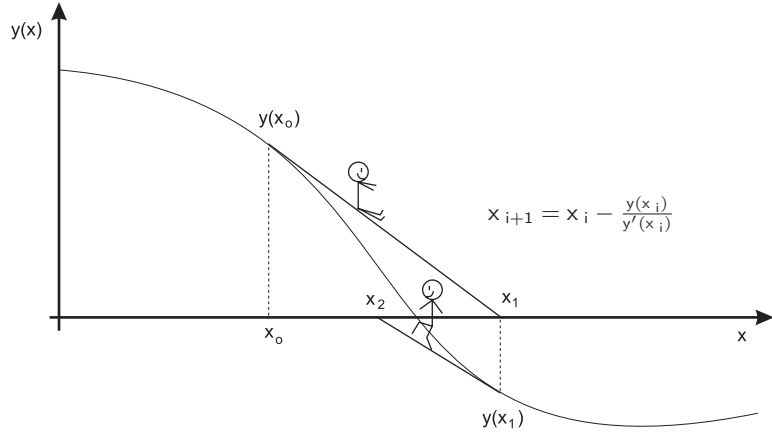
Figure 6.3: Representation of the Newton-Raphson iteration for a one-dimensional function.

The expression (6.1) is differentiated with respect to the model parameters p, and solved first for $\frac{\partial \omega_s^2}{\partial p}$ and then for $\frac{\partial z_s}{\partial p}$. The detailed derivation of these expressions is found in Appendix C.

The first elastic mode shape z_1 is expressed at the 18 degrees of freedom of the model, which we remind are the three translations and three rotations of the center of mass of each body. In practice however what we will measure are the displacements on the surface of the bones. Therefore the sensitivity of the mode shape has been transformed in the sensitivity of displacements on the bone surfaces, according to the kinematic relationship (4.8):

$$\frac{\partial \vec{u}_{ext}}{\partial p} = \frac{\partial \vec{u}_b}{\partial p} + \frac{\partial \vec{\theta}_b}{\partial p} \times \vec{\rho}_{ext}, \tag{6.2}$$

where $\frac{\partial \vec{u}_{ext}}{\partial p}$ is the displacement sensitivity at the measurement point on body b, $\frac{\partial \vec{u}_b}{\partial p}$ the translation sensitivity at its center of mass, $\frac{\partial \vec{\theta}_b}{\partial p}$ its rotation sensitivity, and $\vec{\rho}_{ext}$ the connecting vector from the center of mass to the measurement point.

The idea is thus to build a sensitivity matrix S, whose columns contain the sensitivity of the displacements to the different parameters. In the following formulae the vector sign is omitted, since the given quantities $u_{ext,i}$ represent one-dimensional displacement measurements at different points on the bone surface, and are not meant as

68

components of a vector. The matrix $\boldsymbol{S}$ writes

$$\boldsymbol{S} = \begin{bmatrix} \dfrac{\partial u_{ext,1}}{\partial p_1} & \dfrac{\partial u_{ext,1}}{\partial p_2} & \dots & \dfrac{\partial u_{ext,1}}{\partial p_n} \\ \dfrac{\partial u_{ext,2}}{\partial p_1} & \dfrac{\partial u_{ext,2}}{\partial p_2} & \dots & \dfrac{\partial u_{ext,2}}{\partial p_n} \\ \vdots & \vdots & \vdots & \vdots \\ \dfrac{\partial u_{ext,m}}{\partial p_1} & \dfrac{\partial u_{ext,m}}{\partial p_2} & \dots & \dfrac{\partial u_{ext,m}}{\partial p_n} \end{bmatrix}, \tag{6.3}$$

where $\frac{\partial u_{ext,i}}{\partial p_j}$ is the sensitivity of the displacement at the point i to parameter j. The choice of parameters is discussed in a moment.

With the Newton-Raphson iteration method, the parameters correction vector $\Delta \boldsymbol{p}$ is obtained at each iteration step from the updated difference in displacements $\Delta \boldsymbol{u}_{ext}$, as in

$$\Delta \boldsymbol{p} = \boldsymbol{S}^{-1} \Delta \boldsymbol{u}_{ext}, \tag{6.4}$$

where

$$\Delta \boldsymbol{p} = (\Delta p_1 \ \Delta p_2 \ \dots \Delta p_n)^T \tag{6.5}$$

and

$$\Delta \boldsymbol{u}_{ext} = (\Delta u_{ext,1} \ \Delta u_{ext,2} \ \dots \ \Delta u_{ext,m})^T. \tag{6.6}$$

The vector $\Delta \boldsymbol{u}_{ext}$ is built as the difference between the (simulated) displacement measurements $\tilde{\boldsymbol{u}}_{ext}$ and the displacements provided by the model at each iteration step. Also, at each iteration step the sensitivity matrix $\boldsymbol{S}$, which is as well dependent on the parameters, has to be updated.

We still have to determine the set of displacements $\boldsymbol{u}_{ext}$ to use in this algorithm. Since this exercise should set the path for dealing with real measurements in the future, the main requirements on the measurement points on the bones is for them to be unequivocally recognizable on the subjects, and just under the skin (as it will be explained in Chapter 8, the measurement technique relies on the ultrasound reflection of bones which lie not far beneath the skin). Good candidates are the anterior superior iliac spines (SIAS), the posterior superior iliac spines (SIPS), the highest points on both iliac crests, and the median sacral crest at the level of the third and at the level of the last sacral vertebra on the sacrum (Fig. 6.4).

From first manipulations of matrix $\boldsymbol{S}$ we realize that the sensitivity of the displacements to the stiffness coefficient of the spring at the pubic symphysis (parameter k_{pub}) can be expressed as a linear combination of the sensitivity of the displacements to the other stiffness coefficients, creating one dependence in the matrix.
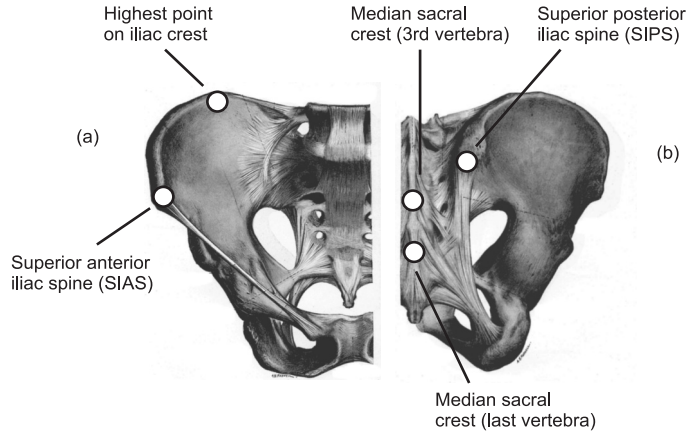
Figure 6.4: Candidate measurement points on the pelvis: (a) anterior view, (b) posterior view.

Reflecting on this finding we realize that the influence of k_{pub} on the first mode shape is already reflected in all other stiffness coefficients' sensitivities. In fact multiplying k_{pub} by a factor α is equivalent to dividing all other stiffness coefficients by α and multiplying the entire stiffness matrix by α. However multiplying $\boldsymbol{K}$ by α has no effect on the mode shape since the same mode $\boldsymbol{z}_1$ is solution of

$$(\boldsymbol{K} - \omega_1^2 \boldsymbol{M})\boldsymbol{z}_1 = 0 \tag{6.7}$$

and of

$$(\alpha \boldsymbol{K} - (\alpha \omega_1^2)\boldsymbol{M})\boldsymbol{z}_1 = 0. \tag{6.8}$$

Here only the associated frequency is modified, but frequencies are not considered in this preliminary updating process. This means that the identification method in this form is able to identify all eleven coefficients only down to a multiplication factor. The addition of the sensitivity of the natural frequency in the equation system would enable the detection of this factor as well. However we decide not to use the frequency sensitivity, since it wouldn't add any conceptual advance in this feasibility study, but to reduce the **parameters used for model updating** to **thirteen**: the three masses and the stiffness coefficients of all ligaments, except the one at the pubic symphysis.

To identify all thirteen parameters, **thirteen independent measurements are sufficient**. Due to the rigidity of the bones, three points on the same body cannot move independently from one another, but dispose of only six independent displacements

(dictated by the fact that the projection of the displacements along each connecting line must have the same direction and magnitude to maintain equidistance, a fact reflected also in the six degrees of freedom of a rigid body in space). Therefore a regular (13×13) matrix S contains sufficient information, if it is formed by the sensitivity of six independent measurements for each innominate (x-, y- and z-components for the two SIAS, y- and z-components for the two SIPS and z-component for the two highest points on the iliac crests), and one measurement for the sacrum (z-component for the median sacral crest at the level of the third vertebra), reducing the number of points from the original eight to the selected seven.

These displacement measurements have been generated, according to Eq. (6.2) and for the first mode shape, based on a model with perturbed parameters. They simulate experimental measurements taken on an unknown *in vivo* system. The model is updated with the Newton-Raphson iteration method, and finds the optimal set of parameters p which can be compared to the initial parameters used to generate the simulated measurements.

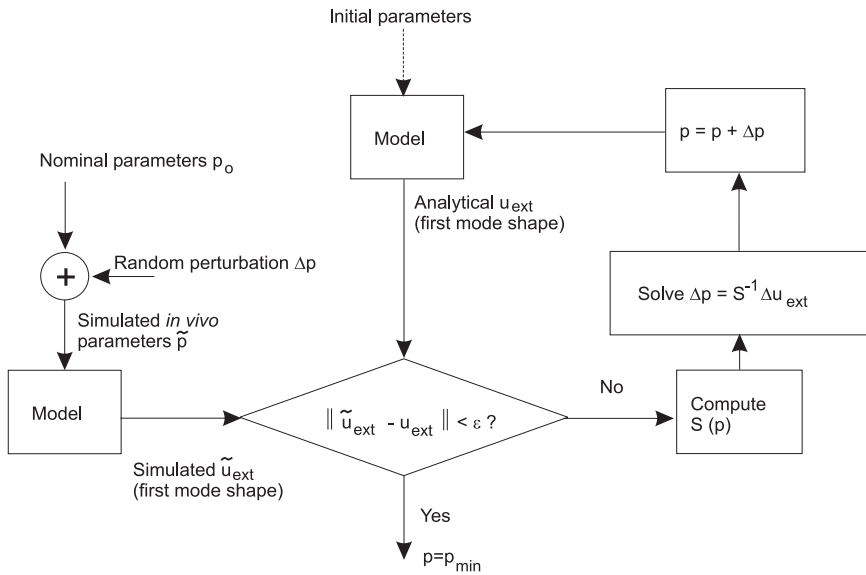A schematic representation of the identification procedure is given in Fig. 6.5.

Figure 6.5: Schematic overview of the identification procedure. The displacements $\tilde{u}_{ext}$ belonging to the first mode shape are simulated and used as target data for the iteration procedure.

Results

Convergence is achieved after eight iterations for perturbations of -30% up to 250% of the nominal parameters over all 13 parameters. At convergence, the difference in experimental and simulated displacements is in the order of magnitude of 10^{-11}% of the actual displacements. The identification of the parameters is successful with an error in the order of 10^{-6}% of the nominal values. However, the identification is only effective for noise-free measurements.

Discussion

In at least two aspects this study deviates substantially from reality. The first is the fact that the simulated measurements are noise-free, and the second is a damping-free modeling of the system.

Regarding the effect of noise on the displacement measurements, it has been assessed that the addition of a relative constant error to each measurement, which could represent systematic error in the measurement technique, leads to the convergence of the parameter identification towards the correct stiffness coefficients, but lower mass[10]. In fact this is equivalent to multiplying the mode shape by a constant factor, which would not influence the eigenproblem. However since the solution to the eigenproblem is computed while keeping the modal mass constant, a multiplication factor α in the mode shape results in the multiplication of the mass matrix $\boldsymbol{M}$ by the inverse of its square, as follows:

$$\boldsymbol{z}^T \boldsymbol{M} \boldsymbol{z} = 1 = \alpha \boldsymbol{z}^T \left(\frac{1}{\alpha^2} \boldsymbol{M} \right) \alpha \boldsymbol{z}. \tag{6.9}$$

Moreover it has been assessed that the addition of a random error on the displacement measurements, either relative or absolute, results in the loss of convergence, very likely due to a lack of solution, even for perturbations in the order of 10^{-4}% of the nominal values[10]. In fact, the identification procedure is based on the assumption that the measured displacements are a manifestation of the first vibration mode. If the measurements are noisy, they fail to represent in any way the assumed mode shape. One way to overcome this problem would be to add equations while keeping the number of unknowns constant. Such an overdetermined system could provide a mean to average out the noise, and can be achieved either by considering more measurement points,

[10] N.E. Conza and D.J. Rixen. Dynamic model of the human pelvis - parameter identification. In *22nd International Modal Analysis Conference (IMAC XXII)*, Dearborn, Michigan, USA, January 26-29 2004. Society for Experimental Mechanics.

or by introducing in the system the sensitivity of the frequency, or of more modes. However, experimental data gathered so far seem to indicate that there will be just one mode at disposal. A reduction in the number of unknowns, meaning a simplification of the model, is not advisable, since it could compromise its representativeness.

Concerning the lack of damping, this is accepted bearing in mind that this study is conceived as a feasibility analysis for an identification algorithm. However, since the level of damping of 3% observed for the first eigenmode in the pilot experiment (see Chapter 10) cannot be regarded as low, we foresee difficulties in the extraction of modal parameters.

All this, together with the fact that we don't expect to be able to identify modes and frequencies with the required accuracy, suggests the development of a new strategy, in which more information than the modal parameters is exploited. An algorithm in frequency domain, where the whole FRF is considered, seems the next logic choice.

6.2 Cost-function optimization in frequency domain

As it has been explained in the previous section, the sensitivity-based algorithm in modal domain, verified with simulated measurements, has proven the feasibility of the identification of the stiffness coefficients of the sacroiliac joints and of the mass of the bones. However the problem was oversimplified by assuming noise-free measurements and a negligible effect of the damping.

A second approach has thus been devised, in which the information not only at the resonance frequencies, but also between them is exploited, allowing for noise-polluted measurements and damping effects in the system. In this approach, a cost function is formulated which expresses the difference between the model FRFs $s(\omega)$ and the (simulated) target FRFs $\tilde{s}(\omega)$ in the considered frequency range. The model updating is then performed with the objective to minimize this cost function.

This section is based on a conference paper[11].

The model

The model used in this study is already a couple of steps further than the model used to establish the described algorithm in modal domain. Between summer 2003 and now (October 2004), different models of damping have been introduced and evaluated:

---

[11]   N.E. Conza and D.J. Rixen.   Biodynamical parameter estimation using frequency domain updating.   In *23rd International Modal Analysis Conference (IMAC XXIII)*, Orlando, Florida, USA, January 31 - February 3 2005. Society for Experimental Mechanics.

a general damping matrix, a modal damping matrix starting from modal damping values, a proportional damping matrix. All of them were as good as any, but lacked that physical meaning which we would like our model to have. At this point we have already formulated the idea that damping is generated in the cartilage lining the inner articular surfaces, and only by the velocity which is perpendicular to the surfaces (as explained in Chapter 5.4), and we have implemented three linear dashpots per joint, for a total of nine. It has not occurred to us yet that one of them is redundant. The coefficients of the three dashpots belonging to a joint are equal, and chosen so that the amount of damping per unit of cartilage surface is constant in all three joints. It is estimated that the interface surface in the pubic symphysis is four times smaller than in the sacroiliac joints.

Moreover we have perfected the modeling of the springs by considering the distance between the physical points of attachments, instead of the virtual mid-point between them, as implemented in the previous model. By doing this we have introduced the concept of a length at equilibrium, as seen in Eq. (4.13), and we have come to realize that a configuration of eleven springs modeled like this introduced a mechanism in the system. Therefore a spring has been added to the pool described in the earlier Chapter in the sagittal plane at the pubic symphysis (thus named k_{pubs}), in direction $(1, 0, 1)^T$, to achieve the target number of twelve.

The inertia properties are still introduced by three rigid bodies representing the three bones of the pelvic girdle. This time however the estimation of the rotational inertia properties, up to now rudimentarily estimated by comparing the bones to simple geometric solids coinciding with the reference axes, have been calculated by a more sophisticated geometric model in Pro/ENGINEER, as presented in Chapter 5.2.

The values of mass, stiffness coefficients and damping coefficients used in this study are given in Table 6.2.

The mass of the innominate bones has been adjusted to the weight of fresh-frozen bones. The estimation of the damping coefficients is obtained by qualitative comparison of a Frequency Response Function measured on a fresh-frozen specimen and a simulated Frequency Response Function. The values of the dashpot coefficients have been modified until the resonance peaks of the constructed FRF had approximately the same "sharpness" as the measured ones, as shown in Fig. 6.6. No comparison has been attempted at this point on the magnitude of the FRF.

Table 6.2: Values of some of the parameters of the model used in this study. m_{in} and m_{sacrum} are the mass of the innominate bones and the sacrum respectively. The indices of the stiffness coefficients k refer to the springs: ss: sacrospinous, st: sacrotuberous, il: iliolumbar, as: anterior sacroiliac, ps: posterior sacroiliac, $pubh$: horizontal pubic, $pubs$: sagittal pubic. c_{sij} and c_{pub} are the damping coefficients for the sacroiliac joints, and the pubic symphysis.

Parameter	Value	
m_{in}	0.61	Kg
m_{sacrum}	0.36	Kg
k_{ss}	$12 \cdot 10^4$	N/m
k_{st}	$8 \cdot 10^4$	N/m
k_{il}	$12 \cdot 10^4$	N/m
k_{as}	$1.5 \cdot 10^4$	N/m
k_{ps}	$20 \cdot 10^4$	N/m
k_{pubh}	$1.5 \cdot 10^4$	N/m
k_{pubs}	$0.5 \cdot 10^4$	N/m
c_{sij}	$16 \cdot 10^2$	Ns/m
c_{pub}	$4 \cdot 10^2$	Ns/m
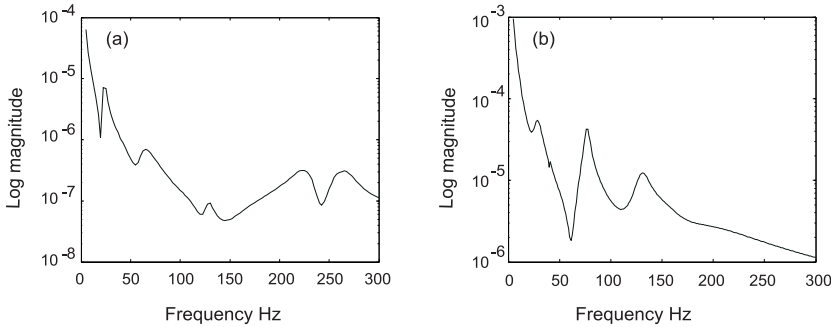
Figure 6.6: Measured (a) and simulated (b) Frequency Response Functions.

The study design

Performing a simulation study offers the possibility to individually investigate all the elements affecting the outcome. These elements can be inherent to the algorithm itself or to the virtual experimental protocol. Important indications can therefore be obtained at this investigative level on how the experimental set-up and protocol should be like.

In order to illustrate the identification process a flow diagram of the algorithm is presented in Fig. 6.7. The design elements mentioned above are highlighted through

numbering and will be discussed in the following paragraphs.
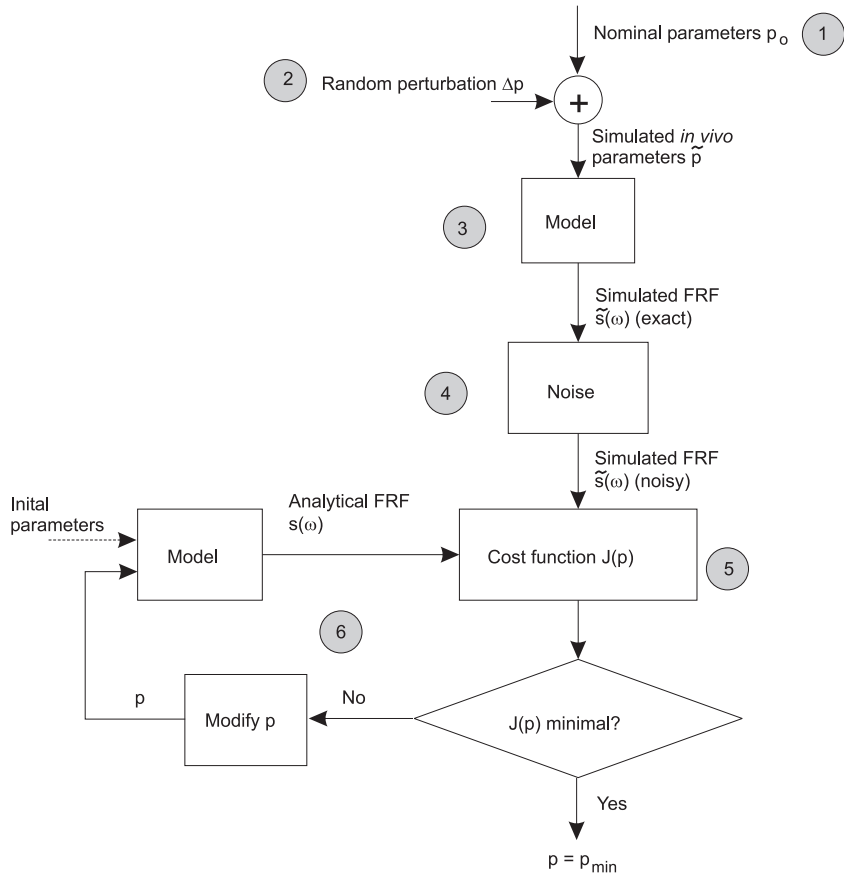
Figure 6.7: Schematic representation of the identification procedure. The Frequency Response Functions $\tilde{s}(\omega)$ are simulated and used to formulate the cost function. The points in the balloons are addressed in the text.

1. As mentioned earlier, the **nominal values** assigned to the parameters are the result of indicative measurements or rough estimations. Even though they serve as initial values and are updated during the procedure, they nevertheless are the baseline around which the simulated measurements are constructed. Important differences with respect to their physical meaning can lead to false conclusions.

2. The nominal parameters are randomly perturbed and used to generate simulated measurements. The **perturbation** is generated by multiplying a given amplitude

Δp (in percentage of the nominal values) with a random value between -1 and 1, and then added to the nominal value. A new set of parameters is thus obtained, whose maximal difference from the nominal parameter set is plus or minus the given percentage. This is performed ten times per value of Δp, creating perturbation level bins. The influence of the perturbation level is investigated for percentages of $\Delta p = 10, 20, 30$ and 40%.

3. The model is used to simulate experimental FRFs (indicated with $\tilde{s}(\omega)$ in the scheme), and then to generate updated FRFs as a function of the parameter set in the attempt to match them (indicated with $s(\omega)$). A pilot experiment performed on a fresh-frozen specimen indicated that the bones can be considered rigid bodies when subjected to vibrations below 300 Hz (absence of major resonance peaks). The shaker used to vibrate the system is able to provide a clean sinus excitation down to 5 Hz. For these reasons the **frequency range** for the identification has been fixed in the interval 5 to 300 Hz. In an experimental setting, the **frequency increment** influences directly the duration of the sine-sweep. When measuring *in vivo*, the duration of the measurement sequence has to be limited in order to minimize the amount of changes in the system itself (e.g. movements of the patient, tension in the muscles). If we assume to acquire 10 sine periods per frequency value and we allow for a delay of 50 milliseconds between frequency steps, we can calculate that about 12 seconds are necessary to complete one sine-sweep with a frequency increment of 5 Hz, 23 seconds with an increment of 2.5 Hz, and 45 seconds with an increment of 1.25 Hz (which could be the maximum duration in which a patient can try to remain perfectly still). The influence of these three frequency increment levels is investigated in this study. The **number, position and orientation of the measurements** depend greatly on the experimental set-up. For model updating it is essential that the points in the model and in the real structure correspond. This is achievable *in vivo* only for a limited set of locations, where the underlying bony structure can be accurately assessed by palpation. The points and orientations selected on the pelvis are depicted in Fig. 6.8. The probable scenario *in vivo* is that for each excitation point the vibration is measured at two other points in addition to the drive point.

4. Modeling **noise** is an art on its own. Nevertheless, even when roughly modeled, important indications can be achieved. Considering a real experimental set-up, two types of noise have been defined:

   a) Error in the *positioning* of the sensor (in our case an ultrasound transducer,
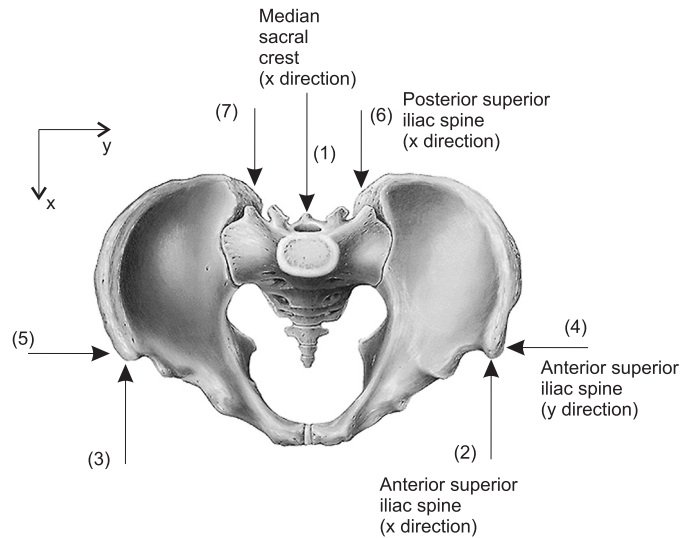
Figure 6.8: The locations of excitation and vibration pick-up on the pelvis: (1) on the median sacral crest at the level of the fourth sacral vertebra (in x direction), (2-3) on both the anterior superior iliac spine (SIAS) in x direction, (4-5) externally below both the anterior superior iliac spine (SIAS) in y direction, (6-7) on both the posterior superior iliac spine (SIPS) in x direction.

as will be explained in Chapter 8). It is modeled by adding or subtracting randomly between 0 and 2 mm from the coordinates of the points where the measurement is taken. This error affects the two directions perpendicular to the ultrasound transducer, since the third coordinate (the distance to the bone) is given by skin contact.

b) Error in the *orientation* of the transducer, not perfectly positioned perpendicular to the bone surface. The measured displacements are then higher, inversely proportional to the cosine of the angle offset (see Fig. 6.9). The angle is taken randomly between 0 and $10°$.

Noise originating from the measurement apparatus, which delivers amplitude and phase of the vibration, is not modeled, since the apparatus itself is still under development at this time.
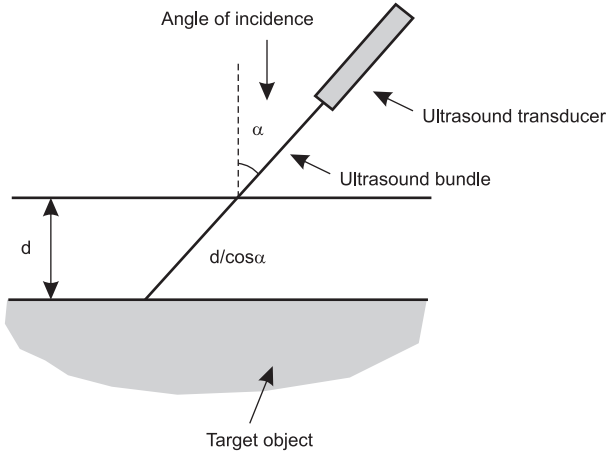
Figure 6.9: Schematic depiction of the effect of error in transducer orientation. The target object vibrates in vertical direction at an amplitude d. The ultrasound waves hit the target with an angle of incidence α. The measured distance is then $\frac{d}{\cos \alpha}$.

5. The **cost function** to minimize is defined as:

$$J(p) = \sum_{k} \sum_{e=1}^{7} \sum_{d=e}^{7} a \ Re \left(s_{ed}(\omega_k, p) - \tilde{s}_{ed}(\omega_k) \right)^2 + b \ Im \left(s_{ed}(\omega_k, p) - \tilde{s}_{ed}(\omega_k) \right)^2$$

(6.10)

where e is the point of excitation, d is the point of vibration detection, a and b are factors multiplying the real and the imaginary parts, s_{ed} is the analytical displacement measured at point d following an excitation at point e at frequency ω_k, and $\tilde{s}_{ed}$ is the (simulated) displacement measured at point d following an excitation at point e at frequency ω_k. The seven mentioned points and directions (see Fig. 6.8) are used as excitation and detection degrees of freedom. The total number of frequency response measurements would be 49, but since the reciprocals are not considered (in linear systems reciprocal FRFs are identical), the number of measurements is reduced to 28. The influence of the factors a and b, giving the ratio between real and imaginary part, is investigated. Per definition, at resonance there is a phase difference of 90° between the excitation and the response, which in the complex domain means a multiplication with i. At resonance, the FRF is therefore imaginary. A ratio $\frac{a}{b} < 1$ (higher weighting of the imaginary part of the FRF difference with respect to its real part) means magnifying the difference near the resonances, while a ratio $\frac{a}{b} > 1$ means magnifying the difference

away from the resonances.

6. Pilot simulations with different standard **optimization** tools provided by the simulation environment lead to different results. A robust optimization is however necessary, and the adopted solution will be briefly discussed.

The strategy

A strategic approach is needed to systematically address the mentioned issues: the effects on the identification procedure of the perturbation level, of the factors a and b in Eq. (6.10), of the increment level and of the two sources of noise. This is the sequence of steps:

1. **Influence of the factors a and b, and of the frequency increment level**. Starting from a pool of arbitrary parameter sets (10 for each bin, randomly generated with Δp = 10, 20, 30 and 40%), noise-polluted measurements have been generated and used for identification, with different ratios $\frac{a}{b}$ = 0.01, 0.1, 1, 10, 100 and different frequency increment levels. The combination of a and b and the frequency increment level allowing for the best outcome is then adopted throughout the rest of the study. The simulated measurements are affected by both types of noise at the same time.

2. **Influence of the noise types**. Here the influence of the individual noise sources is investigated for the bins Δp = 10, 20, 30%, starting from the same arbitrary parameter sets used in step 1. It has to be anticipated that the bin Δp = 40% has been removed from the investigation already in step 1 since it proved to completely impair the identification.

3. **Experimental scenarios** In practice there might be limitations in the patient positioning. In fact a plausible *in vivo* measurement set-up could encompass an examination bed on which the subject lies, face-up or face-down, with an accessible part of the pelvis supported by a shaker platform. The shaker is positioned under the bed and reaches the subject through a hole in the bed. The ultrasound measurement system would be fixed above the subject. With the subject lying face-up, three points would be accessible on his dorsal side for the excitation (points 1, 6 and 7 in Fig. 6.8) and four for the measurement (points 2 through 5): this results in twelve FRFs, plus the three drive point FRFs. On a face-down scenario, only points 2 and 3 are accessible from below for the excitation, and three for the measurement, for a total of 8 FRFs (including the two drive point FRFs). These two experimental scenarios are summarized in Tables 6.3 and 6.4.

The feasibility within these constraints has been further investigated for the bins Δp = 10, 20, 30%.

Table 6.3: Experimental face-up scenario. The superscripts R and L mean right and left, the subscripts x and y indicate the direction.

Face-up scenario			
Excitation	Sacrum_x	SIPS_x^R	SIPS_x^L
Pick-up	Sacrum_x	SIPS_x^R	SIPS_x^L
	SIAS_x^R	SIAS_x^R	SIAS_x^R
	SIAS_x^L	SIAS_x^L	SIAS_x^L
	SIAS_y^R	SIAS_y^R	SIAS_y^R
	SIAS_y^L	SIAS_y^L	SIAS_y^L
Number of measurements	5	5	5

Table 6.4: Experimental face-down scenario. The superscripts R and L mean right and left, the subscripts x and y indicate the direction.

Face-down scenario		
Excitation	SIAS_x^R	SIAS_x^L
Pick-up	SIAS_x^R	SIAS_x^L
	Sacrum_x	Sacrum_x
	SIPS_x^R	SIPS_x^R
	SIPS_x^L	SIPS_x^L
Number of measurements	4	4

The optimization

Fig. 6.10 shows the course of the cost function (ordinate) when one single parameter is varied (abscissa), while the others are kept at their nominal values.

Two groups of functions can be recognized: the ones that drastically change in value when approaching or outstripping the nominal value, and the ones which seem not to change at all (the very flat lines near the abscissa). In this example the curves with the largest value change are functions of the masses of the sacrum and of one innominate bone, and of the stiffness coefficients of the sagittal pubic, of the sacrotuberous and of the anterior sacroiliac springs, while the flatter curves are functions of the other stiffness coefficients and the damping coefficients. Still thinking in one-dimensional
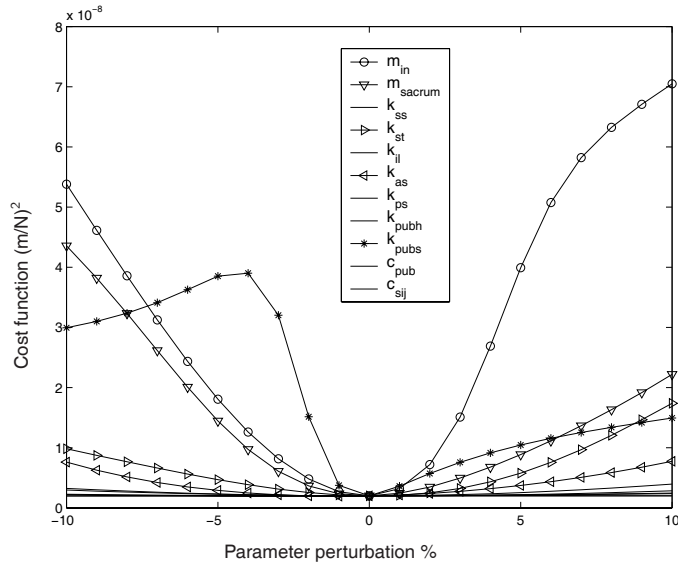
Figure 6.10: Value of the cost function as a function of the parameter deviation (one parameter at a time). In this example the curves with the largest value change are functions of the masses of the sacrum and of one innominate bone, and of the stiffness coefficients of the sagittal pubic, of the sacrotuberous and of the anterior sacroiliac springs. $\frac{a}{b} = 1$.

terms, there are therefore parameters which, taken individually, have a great influence on the cost function, and parameters whose influence is almost nihil. In such a case a single minimization routine considering all 18 parameters together might have difficulties discerning the minimal influence of the second group of parameters. To overcome this difficulty a minimization procedure has been developed, where the most influent set of parameters are optimized at first, while assigning nominal values to the other set. When they have converged to their optima, the second set of parameters is minimized. A series of simulation has shown that this method provides fast and satisfactory results, and that an iteration of this two-step optimization does not provide better results.

The optimization is based on the standard non-linear least-square algorithm implemented in the mathematical environment[1].

---

[1]Matlab, function *lsqnonlin*.

Results

Optimizations are performed per perturbation bin (Δp = 10, 20, 30, 40%), per combination of a and b ($\frac{a}{b}$ = 0.01, 0.1, 1, 10, 100), and per frequency increment level (df = 1.25, 2.5, 5 Hz).

The first immediate finding is that a parameter perturbation of 40% impairs the identification, and is therefore discarded from the study.

A second observation is that the ratio $\frac{a}{b}$ seems to have a different influence on the different parameters. The error in the identification of the mass of the bones is generally small (error of $<$ 2.5% for $\Delta p = 10\%$, $<$ 5% for $\Delta p = 20\%$ and $<$ 7% for $\Delta p = 30\%$), and in almost all the cases decreases with increasing ratio $\frac{a}{b}$. On the contrary, the identification of the stiffness and damping coefficients is less successful (the error climbs easily in the range 30-60%), and in general better with smaller ratios $\frac{a}{b}$ (0.01 and 0.1). Considering these two tendencies, the algorithm has been set to use the ratio $\frac{a}{b}$ = 0.1.

A third point is that the results of the identifications for df = 1.25 Hz are comparable to the results obtained for df = 2.5 Hz. In the case of df = 5 Hz however, the results show much greater errors.

The influence of the separate noise sources is therefore investigated for parameter perturbations of Δp = 10, 20, 30%, for a frequency increment of df = 2.5 Hz and for the ratio $\frac{a}{b}$ = 0.1. The results indicate that the two sources of noise, when applied separately, contribute equally to the identification error.

The investigation on the possible impairment due to a decrease in measurement numbers (face-up and face-down scenarios), performed for Δp =10, 20, 30% and df = 2.5 Hz, seems to indicate that this limitation is not necessarily a penalizing factor for the identification. For all combinations of $\frac{a}{b}$, the results of both scenarios are comparable with each other and only slightly worse than the results obtained with the full complement of measurements.

Discussion

As we have seen, surprising phenomena can be observed. Even though the measurements for lower frequency resolutions have been obtained by resampling the data generated with the highest resolution, they sometimes produce better results. Moreover, it is peculiar that in the face-down scenario, with just 8 measurement combinations out of 28, the algorithm performs not differently than when using 15 measurement combinations, as in the face-up scenario, and in general no much worse than when using the full complement.

A suspect arises on the reliability of the optimization algorithm. Could it be that our investigation has tumbled in some local minima? Improvements on this aspect will be embedded in the next simulation study, whose purpose is to address another intriguing question.

Frequency dependence of stiffness and damping

This chapter describes a simulation study performed to investigate the effect that frequency dependent mechanical properties of the system (damping and stiffness) might have on the system identification. Two commercially available modal analysis tools have been used to perform a standard modal identification, in addition to the in-house identification algorithm presented in Chapter 6.2.

7.1 What if?

S O FAR THE SYSTEM matrices M, C and K have been assumed constant. However tensile tests on tendons or ligaments reported in the literature have shown that the mechanical properties depend also on the rate at which the force or elongation is imparted to the structure[43]. This might suggest the possibility that the mechanical properties depend also on the excitation frequency when subjected to dynamic testing.

If so, what happens when we take experimental data and use them to perform a modal analysis? And what if we feed them directly into an optimization algorithm, which has never heard of such a thing as a system whose properties change with the frequency? Would the results be just a little bit off, or would we be completely mislead?

How nice that we have a computer model. We can generate the experimental data of such a weird system, try all this out, and compare the obtained results to the known properties. The findings have been summarized in a journal article[13]. Let's see them.

7.2 Simulation study

The spring configuration in this model is the same as in the previous Chapter, with two springs representing the ligaments of the pubic symphysis, and on each side springs representing the iliolumbar, the anterior sacroiliac, the posterior sacroiliac, the sacro-tuberous and the sacrospinous ligaments (see Fig. 2.2). However, in this end 2005, we have already realized that nine dampers show one redundancy, and we have now three dampers per sacroiliac joint, and two in the pubic joint. The stiffness coefficients have been estimated using the geometry of the pelvic girdle and published ligament properties[16,23,26,27], while the three damping coefficients have been set in order to ensure a subcritical damping throughout the frequency range. The parameters of the model used in this study are shown in Table 7.1.

[43] P.P. Provenzano, R.S. Lakes, D.T. Corr, and R. Vanderby. Application of nonlinear viscoelastic models to describe ligament behavior. *Biomechanics and Modeling in Mechanobiology*, 1(1):45–57, 2002.

[13] N.E. Conza and D.J. Rixen. Influence of frequency dependent properties on system identification: simulation study on a human pelvis model. *Submitted to Journal of Sound and Vibration*, 2006.

[16] J.D. Currey. *Handbook of Biomaterial Properties*, chapter A1-Cortical bone, pages 3–14. Chapman & Hall, 1998.

[23] Y.C. Fung. *Biomechanics. Mechanical Properties of Living Tissues*. Springer-Verlag, New York, 2 edition, 1993.

[26] U.J. Gerlach and W. Lierse. Functional construction of the sacroiliac ligamentous apparatus. *Acta Anatomica*, 144(2):97–102, 1992.

[27] H. Gray. *Anatomy of the Human Body*. Lea & Febiger, Philadelphia, 20 edition, 1918.

Table 7.1: Values of some of the parameters of the model. m_{in} and m_{sacrum} are the mass of the innominate bones and the sacrum respectively. The indices of the stiffness coefficients k refer to the springs: ss: sacrospinous, st: sacrotuberous, il: iliolumbar, as: anterior sacroiliac, ps: posterior sacroiliac, $pubh$: horizontal pubic, $pubs$: sagittal pubic. c_{sij} and c_{pub} are the damping coefficients for the sacroiliac joints, and the pubic symphysis.

Parameter	Value	
m_{in}	0.61	Kg
m_{sacrum}	0.36	Kg
k_{ss}	$12 \cdot 10^4$	N/m
k_{st}	$8 \cdot 10^4$	N/m
k_{il}	$12 \cdot 10^4$	N/m
k_{as}	$1.5 \cdot 10^4$	N/m
k_{ps}	$20 \cdot 10^4$	N/m
k_{pubh}	$1.5 \cdot 10^4$	N/m
k_{pubs}	$0.5 \cdot 10^4$	N/m
c_{sij}	0.8	Ns/m
c_{pub}	0.8	Ns/m

To create our weird system, different levels of linear frequency dependence has been implemented in the stiffness matrix K, while hysteretic damping D has been implemented next to the viscous damping provided by C. The harmonic equation of motion in complex form becomes:

$$(-\omega^2 M + j\omega C + jD + K + \omega K')\, z = F \;, \tag{7.1}$$

where ω is the frequency variable, M, K and C are the original system mass, stiffness and (viscous) damping matrices, z is the system response harmonic amplitude and F is the amplitude of the applied harmonic force. D and K' are defined as:

$$D = f_c\, C\, \frac{\omega_{max}}{4} \;, \tag{7.2}$$

$$K' = f_k\, K\, \frac{1}{4\,\omega_{max}} \;. \tag{7.3}$$

Here ω_{max} represents the maximal frequency in the range of interest, and the factors f_c and f_k allow for a modulation, for investigation purposes, of the linearity slope of the stiffness and of the hysteretic damping level, and will be chosen between 0 and 1. At maximal frequency the elastic and the dissipative forces in the case $f_c = f_k = 1$ are 25% bigger than in the case $f_c = f_k = 0$. This frequency dependence has been chosen mild enough to avoid drastic changes in the response of the system.

Since we are simulating measurements *in vivo*, the generated response has been

87

translated at nine points on the virtual surface of the bones, as indicated in Fig. 7.1.
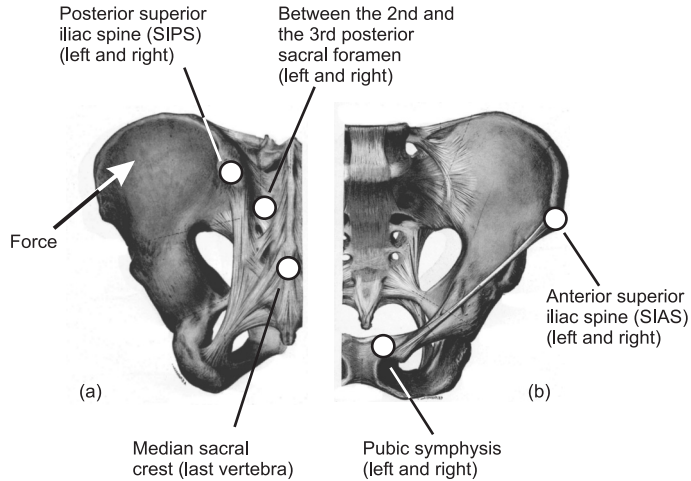
Figure 7.1: Points on the pelvis where the response has been simulated: (a) posterior view, (b) anterior view. Three points have been assigned per innominate bone, three on the sacrum. The force has been imparted in the upper external part of the left iliac fossa.

Identification tools

To answer our *what if's* we have selected two commercially available standard modal analysis tools, and the in-house updating algorithm in frequency domain presented in Chapter 6.2.

The first commercial tool is **ME'scope**VES 4.0 (Vibrant Technologies, Inc., USA, Visual Modal Pro Package), which is an ensemble of software packages for the post-test analysis of structures' dynamic behaviour. For this study we have estimated the modal parameters using the polynomial curve-fitting method, which utilizes the real and imaginary parts of the FRFs for a two-step identification in frequency domain[45].

The second commercial tool is **SDT** Structural Dynamics Toolbox (Structural Dynamics Tools, France), a software for the fitting of a parametric model to measured

[45] M.H. Richardson and D.L. Formenti. Global curve fitting of frequency response measurements using the rational fraction polynomial method. In *3rd International Modal Analysis Conference (IMAC III)*, Orlando, Florida, USA, January 28 - 31 1985. Society for Experimental Mechanics.

FRFs through the error minimization of a cost function in frequency domain[2].

And the third tool, this time not conceived to perform experimental modal analysis but model updating, is the **identification algorithm in frequency domain** presented in Chapter 6.2 and based on the cost-function in Eq. (6.10). Following the outcome of the first identification study (Chapter 6.2), the ratio $\frac{a}{b}$ has been chosen to be 0.1. The parameters tuned during updating are the three masses, the twelve stiffness and the three damping coefficients.

To provide an indication on the effectiveness of this in-house identification and the optimization routines, a **version B of the updating algorithm** has been created, where the frequency dependence as in Eq. (7.1) is included in the parametric model used for updating. In this second version, the factors f_k and f_c become parameters to be identified, in addition to the already considered 18 physical parameters. Version A remains the one with just the matrices C and K. Results from both versions are presented in this study.

Since we are still having doubts about the **optimization routine** used in the previous study to minimize $J(p)$, an automatic routine has been created to avoid local minima. The idea is the following: the routine randomly generates one start parameter set at a time within a range of $\pm$ 10% of the nominal parameters. Starting from this set, a non-linear least-squared minimum search[1] with fewer frequency points (to keep it computationally cheap) is performed to determine whether the optimization is converging towards the global minimum. If not, a new set is generated and the optimization attempted again. The indicator for the global minimum is a cost function descending to values smaller than 10^{-13} (the value for the cost function for a perturbed set of parameters is in the order of magnitude of 10^{-7}). This is however only valid in version B, where the model in the algorithm corresponds to the model used to generate the FRFs, and a zero-value optimum exists. In version A, the cost function will not assume zero value at optimum. Therefore an effective indication of the global minimum is a cost function descending below the value at nominal parameters. The code will keep generating start parameter sets and performing the cheaper minimization mentioned above (with fewer frequency points) until this condition is satisfied.

At this point, the optimization with the complete frequency set is started. Convergence is achieved with a termination tolerance on the cost function of 10^{-17}, approximating the zero slope of the minimum. This termination tolerance was established

---

[1]Matlab, function *lsqnonlin*.

---

[2]   E. Balmès. Frequency domain identification of structural dynamics using the pole/residue parametrization. In *14th International Modal Analysis Conference (IMAC XIV)*, Dearborn, Michigan, USA, February 12-15 1996. Society for Experimental Mechanics.

at the beginning by performing an optimization on one set of FRFs generated with no frequency dependence but polluted with noise. Different termination tolerances were tried out until all 18 parameters showed an error $< 1\%$. The noise added to the FRFs was Gaussian additive white noise in frequency domain[50]:

$$\tilde{s}_{d,noise}(\omega_k, p) = \tilde{s}_d(\omega_k, p) + g \, n_n e^{j2\pi n_u} \, , \tag{7.4}$$

where $\tilde{s}_{d,noise}(\omega_k, p)$ is the polluted FRF measured at point d at frequency ω_k, $\tilde{s}_d(\omega_k, p)$ the FRF measured at point d at frequency ω_k, g a constant, n_n a normally distributed random number with mean value 0 and standard deviation 1, and n_u a random number uniformly distributed between 0 and 1. The value of g was set as $5 \, 10^{-6}$ times the maximal amplitude present in all FRFs. The noise-polluted drive point FRF is shown in Fig. 7.2.
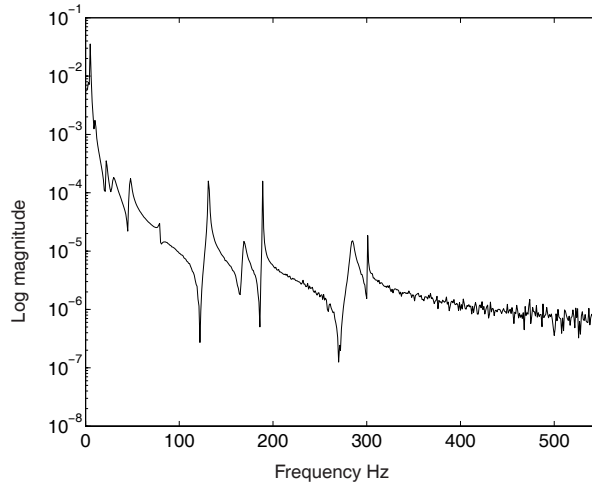
Figure 7.2: Magnitude of the simulated drive point FRF between 0 and 550 Hz with additive Gaussian white noise.

Data generation

To avoid problems arising from modes with zero frequency (rigid body modes), the diagonal terms of the stiffness matrix corresponding to the six degrees of freedom of

[50] A.N. Thite and D.J. Thompson. The quantification of structure-borne transmission paths by inverse methods. Part 1: Improved singular value rejection methods. *Journal of Sound and Vibration*, 264(2):411–431, 2003.

the sacrum are increased by 1%, which corresponds to attaching the sacrum to the environment with springs 100 times less stiff than the joints. In fact, the FRF of a system having rigid body modes shows an asymptotic increase in amplitude towards infinity when the frequency approaches zero. In addition to causing bad numerical conditioning, this would impair the analysis capability of the two commercial tools.

The system response is synthesized by solving the equation of motion in the frequency range 0 to 550 Hz (encompassing all the resonances) for a harmonic force applied on the left ilium, and transformed in displacements at nine points on the pelvis (three per bone), plus the drive point, for a total of 28 measurements, as shown in Fig. 7.1.

For both modal analysis tools a frequency increment of 0.05 Hz is chosen to maximize the information content. For the in-house updating algorithm a much coarser increment level has to be chosen for computational cost reasons. For the optimization screening, data points are generated every 50 Hz (for a total of 12 points), while for the actual optimization the frequency increment is of 10 Hz (for a total of 56 data points).

The investigation on the effects of frequency dependence is modulated with the factors f_k and f_c, as presented in Eqs. (7.2) and (7.3). Seven combinations of f_k and f_c are considered, as indicated in Table 7.2.

Table 7.2: Cases considered for the study.

Case	1	2	3	4	5	6	7
f_k	0	0	0	0.5	1	0.5	1
f_c	0	0.5	1	0	0	0.5	1

Determination of the theoretical values

The theoretical modal parameters are obtained by solving the eigenproblem in state space. In the case of constant system matrices ($f_c = f_k = 0$) a numerical solution is directly obtained (see Appendix B). In the case of frequency dependent system matrices the eigenproblem is solved for each mode by a fixed point iteration scheme (for a detailed derivation see Appendix D).

Solutions of the problem are the poles $\lambda_r = -\sigma_r \pm i\omega_r$ and the complex mode shapes z_r. The damping ratio is calculated from λ_r for each mode r:

$$\zeta_r = \frac{\sigma_r}{\sqrt{\omega_r^2 + \sigma_r^2}} \; . \tag{7.5}$$

91

The theoretical resonance frequencies and damping ratios are given in Tables 7.3 and 7.4.

Table 7.3: Theoretical resonance frequencies in Hz for the different cases. The rows contain the data for the 18 modes.

Mode	$f_k = 0$ $f_c = 0$	$f_k = 0$ $f_c = 0.5$	$f_k = 0$ $f_c = 1$	$f_k = 0.5$ $f_c = 0$	$f_k = 1$ $f_c = 0$	$f_k = 0.5$ $f_c = 0.5$	$f_k = 1$ $f_c = 1$
1	2.96	2.96	2.96	2.96	2.96	2.96	2.97
2	3.77	3.77	3.77	3.77	3.77	3.77	3.77
3	4.71	4.71	4.73	4.71	4.71	4.72	4.73
4	6.90	6.90	6.90	6.90	6.91	6.90	6.91
5	8.86	8.86	8.86	8.87	8.88	8.87	8.88
6	9.45	9.45	9.47	9.46	9.47	9.46	9.49
7	20.88	20.87	20.87	20.93	20.98	20.92	20.97
8	27.82	27.83	27.87	27.90	27.99	27.92	28.04
9	43.20	43.20	43.21	43.41	43.62	43.41	43.63
10	46.16	46.12	46.04	46.40	46.64	46.36	46.53
11	76.91	76.91	76.91	77.59	78.27	77.59	78.26
12	126.69	126.69	126.69	128.53	130.39	128.53	130.39
13	161.69	161.69	161.70	164.69	167.74	164.69	167.75
14	180.55	180.55	180.55	184.29	188.11	184.29	188.11
15	264.18	264.18	264.18	272.23	280.52	272.23	280.51
16	266.80	266.79	266.78	275.01	283.47	275.00	283.45
17	281.27	281.26	281.26	290.40	299.82	290.40	299.81
18	393.30	393.30	393.30	411.27	430.02	411.27	430.02

The modal parameters identified by the modal analysis tools are compared to the theoretical parameters: directly in the case of the frequencies and damping ratios, and with the aid of the Modal Assurance Criterion (MAC, Eq. (4.49)) for the mode shapes. In the case of the in-house updating algorithm, comparison is performed between the physical parameters. In addition the model, updated with the identified parameters, is used to compute the frequencies and modes, allowing for a comparison in modal space.

Identification results

ME'scope is able to identify the frequencies very well, with errors ranging between -0.4% and +0.6% (Fig. 7.3a). The damping ratio proves to be more challenging, with mode 2 showing the maximal error of +13% (Fig. 7.3b). Note that for the case $f_k = f_c = 0$ (case 1) the identification is not perfect. The mode shapes are generally very

Table 7.4: Theoretical damping ratios in % for the different cases. The rows contain the data for the 18 modes.

Mode	$f_k = 0$ $f_c = 0$	$f_k = 0$ $f_c = 0.5$	$f_k = 0$ $f_c = 1$	$f_k = 0.5$ $f_c = 0$	$f_k = 1$ $f_c = 0$	$f_k = 0.5$ $f_c = 0.5$	$f_k = 1$ $f_c = 1$
1	0.02	0.38	0.73	0.02	0.02	0.37	0.73
2	0.01	0.19	0.38	0.01	0.01	0.19	0.38
3	0.08	1.17	2.19	0.08	0.08	1.17	2.18
4	0.00	0.03	0.06	0.00	0.00	0.03	0.06
5	0.04	0.34	0.63	0.04	0.04	0.34	0.63
6	0.09	0.72	1.33	0.09	0.09	0.72	1.33
7	0.43	1.83	3.23	0.42	0.42	1.82	3.20
8	1.27	4.42	7.60	1.27	1.26	4.40	7.51
9	0.41	1.08	1.74	0.41	0.41	1.07	1.71
10	0.63	1.57	2.51	0.63	0.62	1.56	2.46
11	0.32	0.60	0.89	0.32	0.31	0.60	0.86
12	0.03	0.04	0.06	0.03	0.03	0.04	0.06
13	0.48	0.68	0.89	0.47	0.46	0.67	0.84
14	0.01	0.01	0.01	0.01	0.01	0.01	0.01
15	0.51	0.65	0.78	0.50	0.48	0.63	0.72
16	0.46	0.58	0.70	0.45	0.44	0.56	0.65
17	0.03	0.04	0.05	0.03	0.03	0.04	0.05
18	0.07	0.08	0.10	0.07	0.07	0.08	0.09

well identified (MAC > 0.95) with the exceptions of modes 15 and 18, which were increasingly difficult with increasing f_c (Fig. 7.4).

SDT performs comparably well in the estimation of the frequencies (Fig. 7.5a). The errors for modes 6, 7, 8, 9 and 10 increase with increasing f_c, independently from the value of f_k. The maximal error, for mode 8, reaches 0.75% for $f_c = 1$. The errors in damping ratio seem to be dependent mostly on the factor f_k (Fig. 7.5b). Modes 8 through 18 show an error which increased in sequence with the mode number. The maximal error is seen for mode 18 at $f_k = 1$, and it reaches 9%. Here the modal identification is nearly perfect for $f_k = f_c = 0$ (case 1). The mode shapes are very well identified. The MAC values for the worst case scenario $f_c = 1$ and $f_k = 1$ are all > 0.99 except mode 10, for which the value is 0.94. The MAC tables are therefore not shown.

With the **updating algorithm version A** the frequency estimation error grows from zero at $f_k = 0, f_c = 0$ to $\pm$ 3% at $f_k = 0, f_c = 1$, with the exception of mode 9, which reaches already 5% at $f_k = 0, f_c = 0.5$ (Fig. 7.6a). The results get generally worse with increasing f_k, with mode 9 remaining around +5% and mode 10 peaking to 35% at $f_k = 1, f_c = 1$. The damping ratio estimation is badly performed (Fig.

Figure 7.3: ME'scope: Relative estimation error in %: (a) in frequency, (b) in damping ratio. Each line connects the error related to the same mode throughout the cases, for the 18 modes. Numbered from 1 to 7 in the x-axis are the considered cases: (1) $f_k = 0, f_c = 0$, (2) $f_k = 0, f_c = 0.5$, (3) $f_k = 0, f_c = 1$, (4) $f_k = 0.5, f_c = 0$, (5) $f_k = 1, f_c = 0$, (6) $f_k = 0.5, f_c = 0.5$, (7) $f_k = 1, f_c = 1$.

7.6b). Errors are distributed in the range -100% to +400%. The identification of the physical parameters explains the poor identification of the damping: the errors in the two damping coefficients of the sacroiliac joints reach values between +300 and +500%

(a)

(b)

(c)
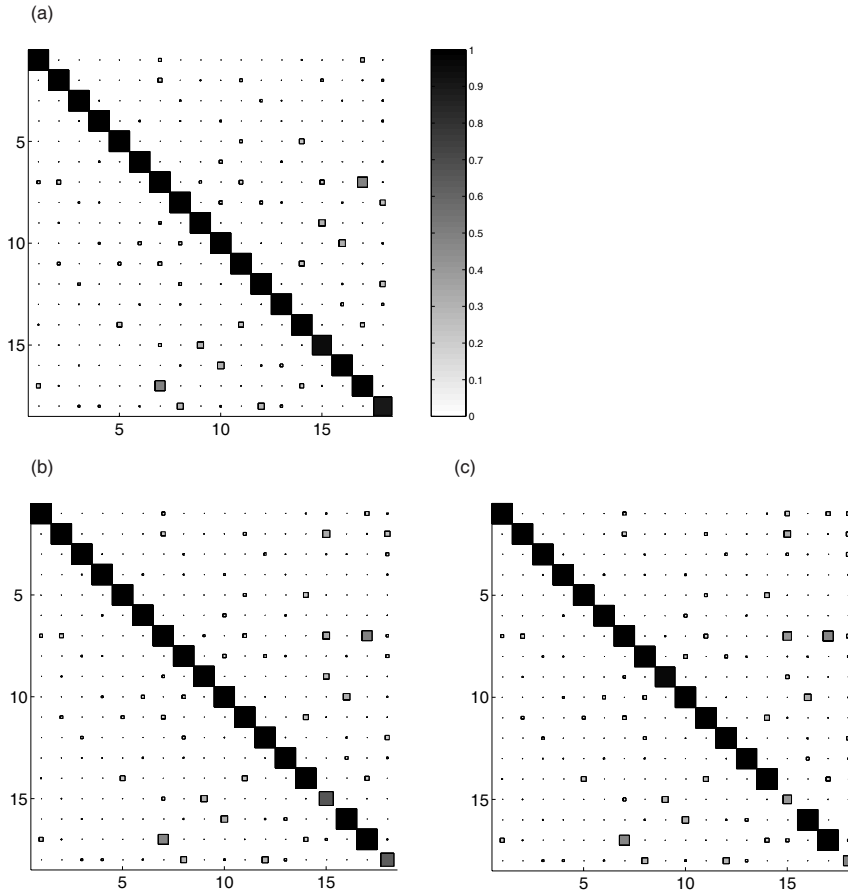
Figure 7.4: ME'scope: MAC values between the theoretical and the identified mode shapes for three of the seven considered cases. (a) Case 1: $f_k = 0, f_c = 0$, (b) case 2: $f_k = 0, f_c = 0.5$, (c) case 3: $f_k = 0, f_c = 1$. To be noted is the decrease in value for modes 15 and 18.

for $f_c = 0.5$ and $f_c = 1$, independently from f_k. The other model parameters show errors distributed in the range $\pm$ 30% (Fig. 7.7). The mode shape estimation shows switching between modes 9 and 10, and 15 and 16 (Fig. 7.8). No direct relation is seen between the occurrence of the switching and the factors f_k and f_c.

Even though a successful identification is expected in all cases for the **updating algorithm version B**, the routine cannot find the global minimum for cases 5 and 7 (characterized by $f_k = 1$): the optimization screening is interrupted after 2000 unsuccessful trials. In all other cases the algorithm performs perfectly. The relative error
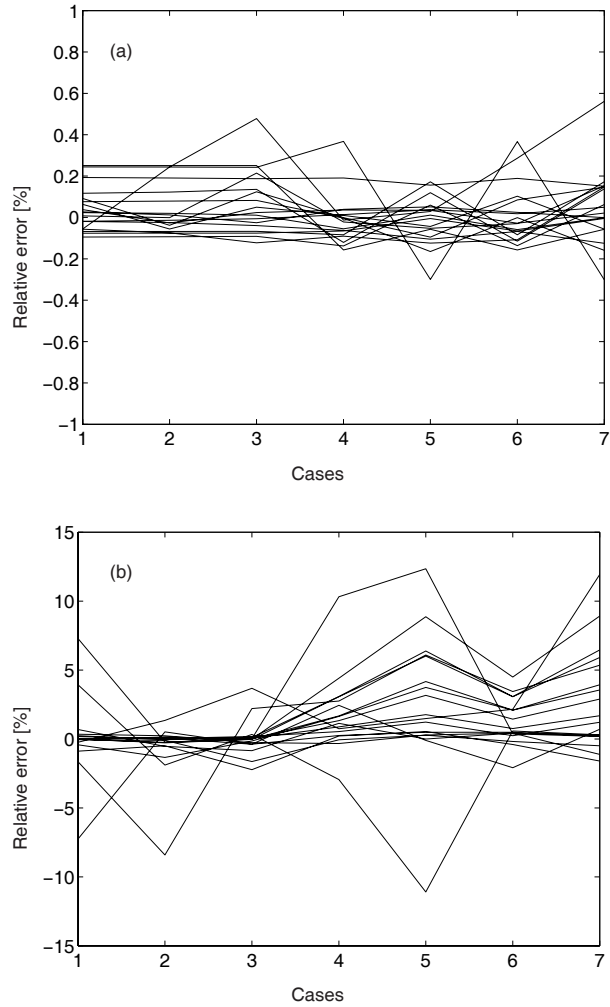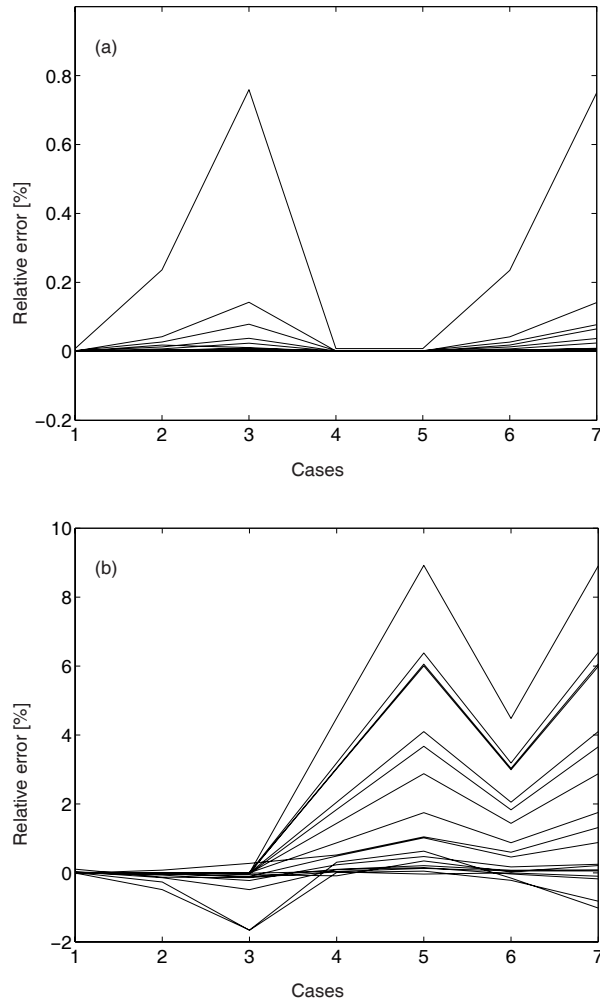
Figure 7.5: SDT: Relative estimation error in %: (a) in frequency, (b) in damping ratio. Each line connects the error related to the same mode throughout the cases, for the 18 modes. Numbered from 1 to 7 in the x-axis are the considered cases: (1) $f_k = 0$, $f_c = 0$, (2) $f_k = 0$, $f_c = 0.5$, (3) $f_k = 0$, $f_c = 1$, (4) $f_k = 0.5$, $f_c = 0$, (5) $f_k = 1$, $f_c = 0$, (6) $f_k = 0.5$, $f_c = 0.5$, (7) $f_k = 1$, $f_c = 1$.

in resonance frequency does not exceed $\pm\,0.01\%$, the error in damping ratio does not exceed $\pm\,0.5\%$, and the error in the physical parameters does not exceed $\pm\,0.5\%$. The MAC values reflect the quality of the identification and show perfect mode shapes
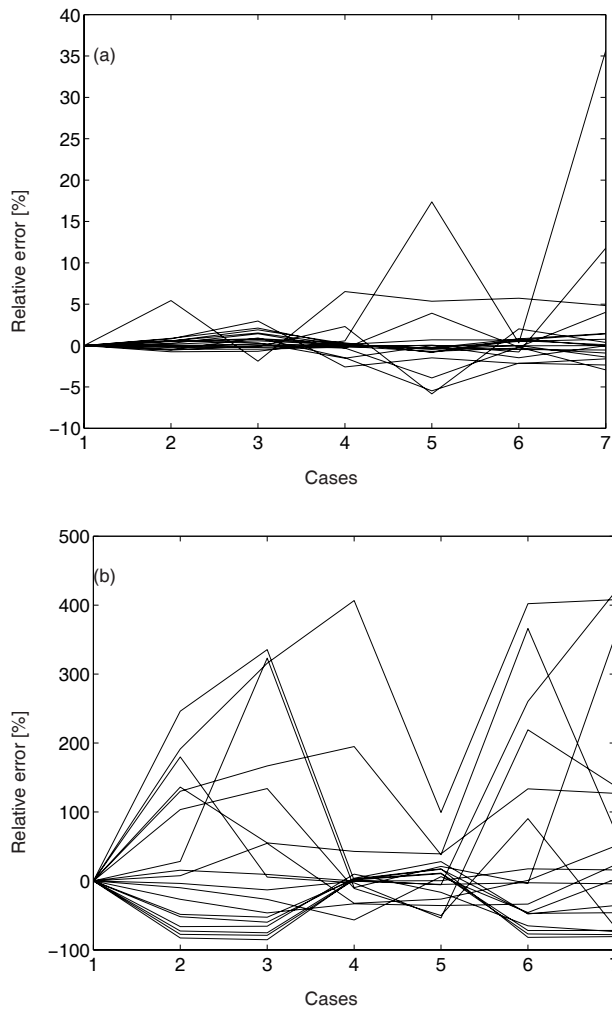
Figure 7.6: Updating algorithm A: Relative estimation error in %: (a) in frequency, (b) in damping ratio. Each line in figures (a) and (b) connects the error related to the same mode throughout the cases, for the 18 modes. Numbered from 1 to 7 in the x-axis are the considered cases: (1) $f_k = 0, f_c = 0$, (2) $f_k = 0, f_c = 0.5$, (3) $f_k = 0, f_c = 1$, (4) $f_k = 0.5, f_c = 0$, (5) $f_k = 1, f_c = 0$, (6) $f_k = 0.5, f_c = 0.5$, (7) $f_k = 1, f_c = 1$.

correlation. The provision of the individual results is deemed unnecessary due to the clarity of such results.
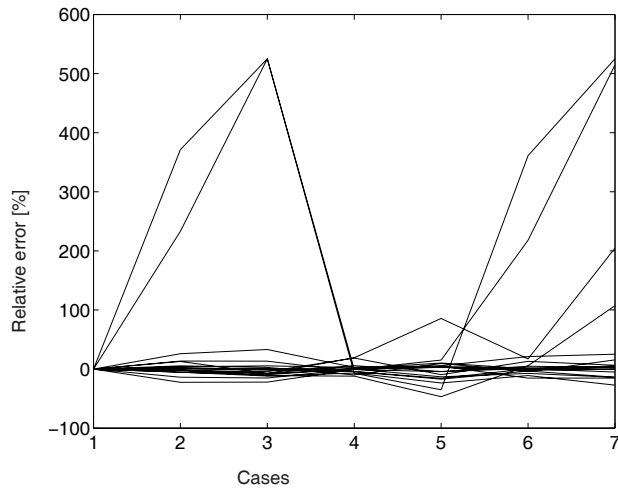
97

Figure 7.7: Updating algorithm A: Relative estimation error in % in the system parameters. The lines connect the 18 parameters of the model as defined in section 6.2. The two parameters showing the highest errors in cases (2), (3), (6) and (7) are the left and right c_{sij}. Numbered from 1 to 7 in the x-axis are the considered cases: (1) $f_k = 0, f_c = 0$, (2) $f_k = 0, f_c = 0.5$, (3) $f_k = 0, f_c = 1$, (4) $f_k = 0.5, f_c = 0$, (5) $f_k = 1, f_c = 0$, (6) $f_k = 0.5, f_c = 0.5$, (7) $f_k = 1, f_c = 1$.

Discussion

Both standard modal analysis tools perform well in estimating the resonance frequencies. The pattern in the damping estimation errors visible in the **SDT** results is remarkable when considering the high level of user interaction allowed during the analysis. The tendency seems to indicate that the higher the frequency of the mode, the more difficult the estimation of its damping. A possible explanation for this is that for a given damping ratio the peak is broader for modes at higher frequency. A frequency dependent damping has therefore a more important impact on the immediate surroundings of the peak, influencing its identification.

The difficulties of **ME'scope** in identifying mode shapes 15 and 18 could lie in their visibility on the FRFs. Mode 15 is often shadowed by mode 16, which lies a few Hz higher, while mode 18 is clearly visible only on few of the 28 FRFs, and in some it is not visible at all.

The **updating algorithm version A** shows a high sensitivity to frequency dependencies. The damping ratios suffers the most from the uncorrect estimation of the physical parameter, and reflects the large errors in the damping coefficients identifica-
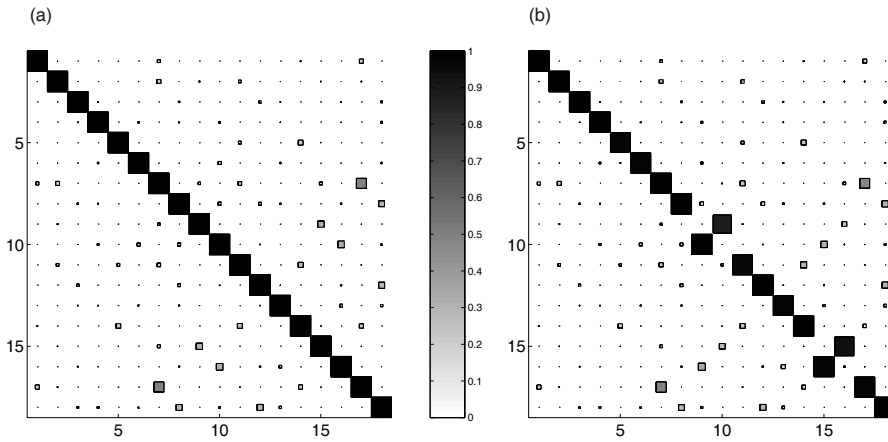
Figure 7.8: MAC values between the theoretical and the mode shapes estimated with the updating algorithm A for two of the seven considered cases: (a) Case 1: $f_k = 0, f_c = 0$, (b) Case 5: $f_k = 1, f_c = 0$.

tion. The frequency estimation is less dramatic, even though poor. The mode switching occurring between modes 9 and 10 and modes 15 and 16 can be explained by their respective proximity. Both pairs lie within few Hz from each other, as shown in Table 7.3. In fact in cases 2 and 4, corresponding to $f_k = 0, f_c = 0.5$ and $f_k = 0.5, f_c = 0$, the estimated parameters produced modes 9 and 10 with very close frequencies (45.549 Hz and 45.772 Hz in case 2, and 46.242 Hz and 46.661 Hz in case 4). A "numerical" switching can not be ruled out. The difficulties encountered by this method can be interpreted by considering the absence of user interaction: in its present form it does not allow for a preliminary localization of the peaks, and it is therefore less able to compensate for peak shifts.

The **updating algorithm version B**, however, even though theoretically provided with all the information to perform a perfect estimation, cannot always overcome the problem of the local minima. The two failed optimizations are tried again by reducing the range where the start parameter sets are randomly picked, from $\pm 10\%$ to $\pm 1\%$. In the case of $f_k = 1, f_c = 0$, the initial screening provides a valid start set after 7 trials, while in the case of $f_k = 1, f_c = 1$ it costs 366 trials. One more simulation shows that the algorithm is able to perform the identification under normal circumstances with $f_k = 0.9, f_c = 0$. All identifications are perfect. These results suggest that there are local minima very close to the global minimum. One-dimensional visualization of the cost function is obtained by fixing all parameters but one at their nominal values, and

sweeping the variable parameter from -20% to +20% of its nominal value. The presence of local minima is confirmed at $f_k = 1$ and $f_c = 1$ for the parameters m_{in}, m_{sacrum}, k_{il}, and k_{ps} (as shown in Fig. 7.9 for m_{sacrum}). The other parameters induce a concave cost function. The shape of the cost function remains very similar also when changing the ratio between a and b. Again it seems that the optimization algorithm is actually the sore link in the method, and not the definition of the cost function.
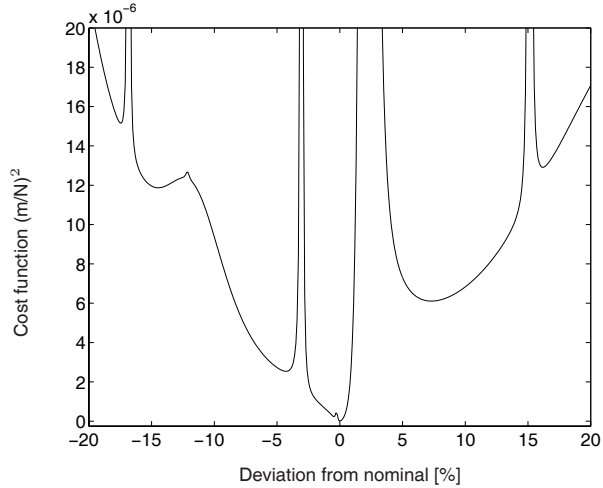
Figure 7.9: Example of cost function value (version B) calculated with the mass of the sacrum as variable, while all other parameters are kept fixed at the nominal values. The mass of the sacrum is in this case swept from -20 % to +20 % (x-axis). The factors of dependence are $f_k = 1$ and $f_c = 1$.

CHAPTER 8

Ultrasound technique

In this section the apparatus for the vibration measurement in vivo is presented. First the principle underlying the ultrasound detection of motion is elucidated, and then the apparatus is introduced, with results of the performed validation studies.

8.1 Background

A S WE HAVE SEEN in Chapter 3.3 there are means, such as function tests, pain provocation tests and palpation, to assess some important characteristics of the sacroiliac joints. However the reduced range of motion and the limited accessibility of these joints impair the diagnosis. Moreover, since there is no objective measure either of the applied force or of the felt response, the diagnosis risks being a question of subjective interpretation. There is therefore a need for an objective diagnostic tool.

As we have seen so far, the main idea at the base of this research is the use of vibration analysis to assess the mechanical properties of the sacroiliac joints. We have learned about the model and the kind of tools that can be developed to transform raw *in vivo* vibration measurements into stiffness and damping properties. What we are still missing is the technique to obtain those raw data in the first place.

As briefly mentioned in Chapter 1.3, this project has been carried out by three PhD students. One of them, Miss Ester Vlaanderen, was asked to refine the existing ultrasound Doppler Imaging of Vibration (DIV) technique applied in earlier studies[17,18]. However, at about the time when she started her research, the first PhD student, Miss Mirthe de Groot, responsible for the application and clinical testing of the apparatus, confuted the suitability of the DIV technique for bone vibration measurement[29]. The challenge changed drastically for Miss Vlaanderen.

8.2 Measurement principle

The idea underlying the new measurement technique is based on the time of flight of ultrasound waves instead of their frequency shift, as in the Doppler technique.

The principle is quite simple. An ultrasound transducer sends short pulses towards a structure, whose acoustic impedance ensures their (partial) reflection, and detects the reflected echoes together with their time of incidence. Should we now multiply the time of flight (between the moment a pulse is sent, to the moment its echo has returned) by the speed of sound in the surrounding medium (soft tissue in this case),

[17] L. Damen. *Laxity Measurements of the Sacroiliac Joints in Women with Pregnancy-related Pelvic Pain.* PhD thesis, Erasmus University Rotterdam, 2002.

[18] L. Damen, T. Stijnen, M.E. Roebroeck, C.J. Snijders, and H.J. Stam. Reliability of sacroiliac joint laxity measurement with doppler imaging of vibrations. *Ultrasound in Medicine and Biology*, 28(4):407–414, 2002.

[29] M. Groot (de), C.W. Spoor, and C.J. Snijders. Critical notes on the technique of doppler imaging of vibrations (DIV). *Ultrasound in Medicine and Biology*, 30(3):363–367, 2004.

we would obtain an estimation of the double of the distance of the object from the transducer. But this is not exactly what we are interested in, is it?

When the object is moving, the subsequent echoes returning to the transducer will be characterized by different times of flight: shorter when the object is nearer, and longer when the object is farther away. If we now consider the **difference** in times of flight of the pulses, let's say with respect to the very first pulse, we can obtain the displacement of the object with respect to its original position at the time when the first pulse hit it. Thus we can construct a displacement-time plot, from which the properties of the motion can be derived.

The phase shift information between two objects vibrating at the same frequency can be obtained by extending the system to two transducers, and having them take synchronous measurements on each object.

8.3 The apparatus

The schematic of the ultrasound measurement set-up is shown in Fig. 8.1. Two single element ultrasound transducers (Panametrics, 5 MHz, Model A326S-SU-F25mm, R/D Tech Instruments Inc., USA) with amplifiers (Panametrics, Model 5077 PR) are used to send and receive a number of subsequent ultrasound pulses. The amplifiers are externally triggered by a pulse generator (Agilent, Arbitrary Waveform Generator, Model 33220 A, USA) and the measured analog signals are digitized by means of a digitizer (Acqiris, Model DP235, USA). Pulser and digitizer are phase-synchronized by a 10 MHz clock provided by the digitizer.

Here is how it works. Each transducer sends a great number of subsequent echoes (e.g. 2000) with a pulse repetition frequency of 5 kHz (according to the example, it would send ultrasound pulses for 0.4 seconds). The digitizer samples a certain number of points (e.g. 500) of each echo signal with a sampling frequency of 500 MHz. The acquired echoes are then correlated with the first received echo to determine by how many points they are shifted. Extra points are added between each data point on the correlation curves, and the maximum of each interpolated correlation curve is detected. The maximum gives the distance in points, converted in time, of each echo from the first detected echo. The shifts in time of all echo signals with respect to the first echo are translated in position differences, which are then plotted against time with a position point each 0.2 ms. This results in the displacement-time plot.

This working principle has been validated on a one-channel set up by measuring
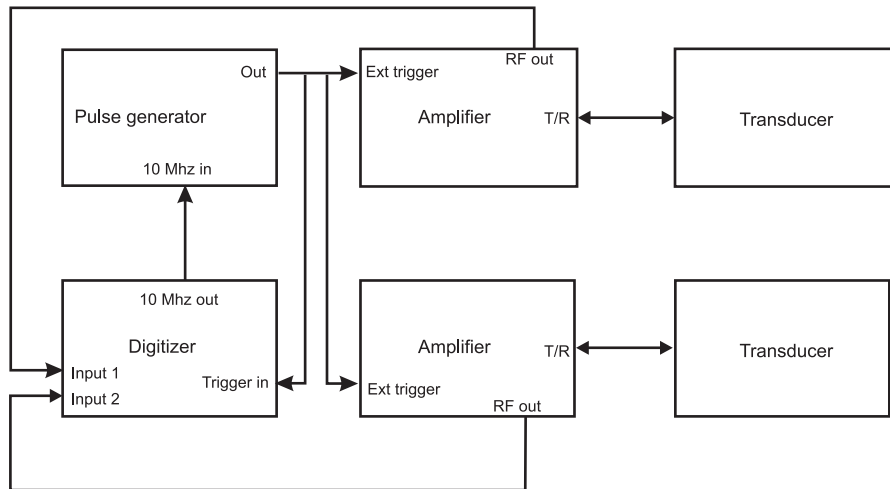
Figure 8.1: Schematic of the two-channel ultrasound measurement system.

the known vibration of a calibrated piezoshaker[51]. In that study 62 pulses (and not 2000) were sent and then detected: the limitation was due to the use of a less capable oscilloscope to digitize the pulses, instead of the digitizer mentioned above. Details on the technical specifications can be found in the article, and will be omitted at this point. The piezoshaker was set to vibrate at 80, 180 and 280 Hz, with amplitudes ranging from 0.25 to 3 μm. Results showed a mean error in amplitude estimation of -0.1%, normally distributed with a standard deviation of 3.65%. For the investigated range of amplitude it was concluded that 95% of the measured amplitudes differed by less than $\pm 7\%$ from the actual amplitude, with the percentage error increasing with decreasing amplitude. The maximum difference between frequencies measured by the ultrasound system and the reference values was 4.4%.

When two displacement-time plots are obtained synchronously for the two transducers, the phase shift between the two signals can be computed. The phase shift can be obtained by performing a clean Fast Fourier Transform (FFT) of the measured harmonic motions (with the sampling frequency of the signal and the lines used for the FFT resulting in a frequency resolution fitting an integer number of times in the frequency of the signal itself) and by calculating the difference between the phase content

[51] E. Vlaanderen, N.E. Conza, C.J. Snijders, A. Bouakaz, and N. Jong (de). Low back disorders; the stiffness of the sacro iliac joint: A new method using ultrasound. *Ultrasound in Medicine and Biology*, 31(1):39–44, 2005.

in the two signals. Alternatively, the phase shift could be computed by correlation of the measured displacements.

The validation of the phase shift estimation has been obtained in a second study[15], by measuring the vibration of two rigid bodies interfaced by a viscoelastic layer. The advantage of viscoelastic material is that it encompasses the elastic and dissipative elements in one homogeneous component and bypasses the need to build in and characterize separate springs and dashpots elements. The requirements on the material foresaw for the damping to allow for a smooth slow passage from a phase shift of $0°$ to a phase shift of $180°$ as a function of the excitation frequency, so that the validation of the system could be performed for different phase shift values. Moreover, this frequency span should lie in the range where the bones are expected to behave rigidly (between 5 and 300 Hz, according to the experiments performed on human specimens). Again we refer to the publication for more technical details. The test object was vibrated at five frequencies (80, 125, 156.25, 200 and 250 Hz) with an amplitude in the order of μm. The phase shift has been calculated by means of the FFT of the signals, as explained above. Table 8.1 gives the frequencies, the number of measurements per frequency, and the mean value and standard deviation of the phase shift resulting from the measurements in degrees. For one frequency (250 Hz) the vibration of the two objects was

Table 8.1: Phase shift values as assessed by the ultrasound system for different frequencies.

Frequency	No. of measurements	Mean phase shift	Standard deviation phase shift
80 Hz	5	-1° 55″	0° 9″
125 Hz	6	-7° 28″	0° 9″
156.25 Hz	4	-21° 5″	0° 42″
200 Hz	6	-80° 53″	0° 33″
250 Hz	6	-156° 3″	0° 8″

measured by a laser vibrometer as well and the phase shift was extracted by FFT in the same manner as with the ultrasound measurements. The phase shift obtained with the laser signals was of -155° 13″, with a mean difference to the shift obtained from the ultrasound measurements of -0° 50″.

This technique is promising, and even though still at a functional prototype level, ready for the first trials *in vivo*. We wonder.

---

[15] N.E. Conza, A. Soethoudt, E. Vlaanderen, and D.J. Rixen. In vivo bone vibration measurement by ultrasound. In *24th International Modal Analysis Conference (IMAC XXIV)*, St. Louis, Missouri, USA, January 30 - February 2 2006. Society for Experimental Mechanics.

THE HIEROGLYPHIC

אב

9 January 2005

It is now two years that I live in this country, and
honestly I still feel like a raft lost in the ocean.
Will I find land? I wouldn't even mind finding the
wrong land as Columbus did. Anything, as long as it is
land and it has a more sophisticated horizon than this
endless line dividing two shades of blue.

This project is becoming very intricate and interesting. I am
glad that I have this to hold on to, a little compass to show
the way.

While still trying to define and attribute meanings in my
semantic model, I noticed that the characters are not
consistent. Letters look alike at first sight, but at a closer
look differ in small details. Is it to be attributed to the
normal variance in handwriting? Or do the single letters
contribute to the logical function of the word by assuming
alternate forms?

I have armed myself with a magnifying glass. I am going
to analyze every letter, every line, every difference. And most
probably even every mood of the scribe, every tension after
a long day of work, every meaningless jerk of the hand.
Suppositions and assumptions are dangerous shortcuts in an
unexplored domain: they might lead me astray.
No, I really have to see it through. One hieroglyph after
the other, scrutinizing the whole text.

This is going to be painstaking.

CHAPTER 9

The tools

The tools
Chapter 9

	In vitro	*In vivo*
Human	Impact test on an embalmed pelvis Chapter 10	*In vivo* ultrasound measurements Chapter 13
	Sine-sweep test on a fresh-frozen pelvis Chapter 11	
Animal	Dynamic test on rabbit ligaments Chapter 12	

A brief description of the basic tools necessary to perform dynamic testing is provided in this chapter. These are standard tools used to obtain information on the system in vitro and in vivo, and are not meant as part of the identification methodology.

111

S WE HAVE LEARNED so far there are two important aspects of performing a system identification by means of dynamic testing: the introduction of an excitation in the system, and the detection of its response. In the next sections we will provide a brief introduction on the technology at disposal for both tasks.

9.1 Excitation

In Chapter 4.5 two ways were mentioned to excite a system: through an impact, or with a shaker. It the first case the system receives a shock of very short duration which contains enough energy to excite the whole structure in a certain frequency range. In the second case the system is connected to an actuator which inputs a preset excitation. How are these two scenarios commonly (and sometimes less commonly) set up?

Impact testing

The easiest way to trigger a transient response in a system is by hitting it with an object, like a hammer. Usually the hammers used for this purpose are equipped with a force sensor to measure the applied excitation necessary for the computation of the Frequency Response Function, being the complex ratio between the response and the imparted force. Fig. 9.1 depicts the hammer available in our lab (PCB Piezotronics, Model 086C03).
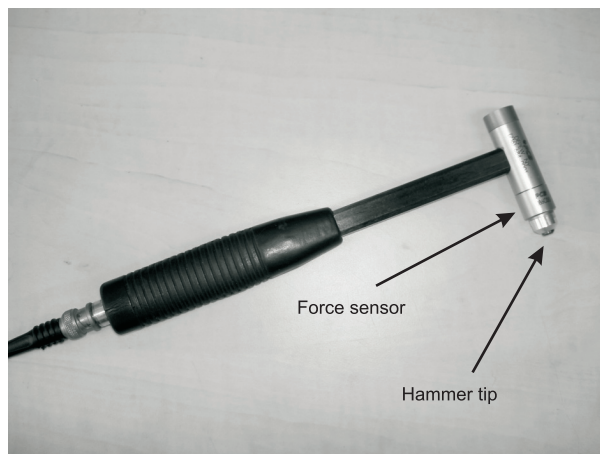

Figure 9.1: Impact hammer with calibrated force sensor.

Occasionally the standard ways of impacting a structure are not applicable, and problem-inspired solutions are implemented. In one very enlightening tutorial given on experimental modal analysis[5], Mr Carne presented a situation in which he and his team had to perform a modal analysis on a huge wind turbine, and there was no hammer sufficiently big to input that much energy (and to be handled, that is). They ended up with a wonderfully creative solution, in which they attached a rope to the top of the wind turbine and pulled it down towards the ground, like a giant catapult. Foreseeing the amount if energy release at the moment of cutting the tie, they decided to do it remotely through a little explosive charge mounted on the rope, and went for cover. They obtained beautiful recordings of the transient response.

Like this one, there are many other tricks and tips known to the structural dynamics community. In fact it seems to be an art on its own to design and perform flawless (or almost) impact testing. An interesting presentation with the provocative title "*Hit me baby one more time*"[6] described the lessons learned in years of experience, unfortunately immortalized only in form of an abstract.

Shaker testing

In this type of testing the system is connected to a shaker which is instructed to perform a specific action. The shaker can be driven by voltage or current: in the first case the action of the shaker is regulated on the velocity of the armature, while in the second case on the force. In fact motion and force are not equivalent. This notion is not that obvious, so let me give some examples: imagine placing your hand against the wall of your office, and start pushing. Most probably, unless you're Superman, the wall won't budge. Nevertheless, it will feel the force that you're applying and will react to it: maybe a frame hanging there might fall off, to your utter surprise. Now picture yourself in a playground with children happily swinging on a swing. Now go behind one child who is periodically moving towards you and then away from you. Should you want to push him, and should you decide to do it at exactly the same frequency and amplitude at which he's swinging, your hands might very well touch his back and move with it, but you won't be able to impart any force, because his body is as fast as your hands. Your motions are identical. Well, this is not rocket science, but still, sometimes it is important to remember that displacement is not equivalent to force.

[5] T.G. Carne. Design of tests. In *23rd International Modal Analysis Conference (IMAC XXIII)*, Orlando, Florida, USA, January 31 - February 3 2005. Society for Experimental Mechanics.

[6] T.G. Carne. Hit me baby one more time - the do's and don'ts of impact and transient excitation. In *23rd International Modal Analysis Conference (IMAC XXIII)*, Orlando, Florida, USA, January 31 - February 3 2005. Society for Experimental Mechanics.

And that's why usually an impedance head (force and acceleration sensor) is placed between the shaker and the structure: to measure both the incoming force and the system response to it. Now back to rocket science (giggle).

Information about the response of the system can be seized at one frequency at a time (like in a sine-sweep) or in a broad band of frequencies. In the latter case, broadband forces that the shaker can impart on the structure can be transient, periodic or non-periodic.

A **transient** response can be obtained by applying a burst random or a burst chirp. What both share is the concept *burst*: a brief sudden excitation which declines to zero before the observation time is over. In the short period of time of a burst random the energy content of the force is randomly distributed within its spectrum. A chirp on the other hand is a signal whose frequency increases over time, basically a rapid sine-sweep. In a burst chirp, this happens very fast.

Periodic signals, which repeat continuously after a certain period T, can be divided in pseudo-random, periodic random and periodic chirp. We have already mentioned that a **chirp** is a very rapid sine-sweep, which in this case lasts through the whole measurement time window. The spectrum of a **pseudo-random** signal consists of integer multiples of the basic frequency $\omega_o = \frac{1}{T}$. This is to ensure that at the end of the period $t = T$ the signal is at the same amplitude than at the beginning $t = 0$. Should this not be verified, problems will arise in the signal post-processing. In short, it is a signal disguised as random, which repeats unchanged every period T: the amplitude and phase of the signal at each frequency is set in the first period, and then repeated exactly the same. In a **periodic random** excitation a randomly generated block, with the same frequency content as a pseudo-random signal, is repeated until a steady-state response is reached. At this point both the excitation and the response are measured. After that, a new block is randomly generated and repeated until steady-state is reached, and the measurement is averaged with the one from the previous block series. Somewhat less sneaky than a pseudo-random signal.

In the **non-periodic** signals we find the true unpredictable random, free to choose frequency, amplitude and phase (actually, even random signals might have to follow rules, like the distribution of the energy in its spectrum: a white noise for instance is a random signal whose energy is equally distributed to all frequencies in the range, while in pink noise the energy content per frequency is proportional to the reciprocal of the frequency self, thus resulting in a spectrum which decreases along the frequency axis).

But again, for some structures the shaker might not be an option. Consider a bridge, a building, a rotating machine, or a space station. Very often the regular operation of

the structure becomes the excitation, a fact which also ensures that the response remains within its realistic range. A modal analysis performed on running machines without a measurement of the force is called Operational Modal Analysis, and uses other techniques to derive the modal parameters. But this goes beyond the scope of this work. Going back to bridges and buildings, one of the preferred means of excitation are the people or cars proceeding in or on them. It might also be one person jumping up and down. There is a fascinating video on which an astronaut onboard the International Space Station is seen thrusting himself and floating from one side of the cubicle to the other, bouncing back and forth, to provide a periodic excitation to the station[3]. In this case as well valid data could be retrieved. Another ingenious idea applied to the same structure was to use thrusters bursts of the docked Space Shuttle to "scare" the structure into providing a transient response[32].

An enjoyable conference paper entitled *"What's shakin', dude?"*[38] discusses the effective use of shakers for experimental modal analysis.

9.2 Sensors

The most popular sensor used for response detection is the **accelerometer**. As the name suggests, it senses its own acceleration and generates an electrical output proportional to it. Since the motion which it senses is its own, it has to be rigidly attached to the structure whose motion is investigated. A loose connection is obviously a bias in the measured values.

Accelerometers come in different sizes and shapes, according to the application they are used for. Since they are firmly attached to the system, their mass has the potential of changing the structural dynamic response. Therefore its mass has to be definitely smaller than the mass of the structure[1]. Moreover, the application at hand determines

---

[1]Actually, the influence of the mass of the accelerometer depends on the vibration shape of the structure as well: a sensor sitting exactly on a node of the mode shape has no influence, since it won't move. But it won't measure either.

[3]   T.J. Bartkowicz. On-orbit testing of the International Space Station: challenges of implementation. Oral presentation 24th International Modal Analysis Conference (IMAC XXIV), January 30 - February 2 2006. St. Louis, Missouri, USA.

[32] M. Kaouk, S. McNeill, S. Haley, M. Grygier, T.J. Bartkowicz, P.B. Rachal, and W. Peart. Shuttle-ISS Flight-7A on orbit test verification: pre and post flight analysis. In *22nd International Modal Analysis Conference (IMAC XXII)*, Dearborn, Michigan, USA, January 26-29 2004. Society for Experimental Mechanics.

[38] R.L. Mayes and A.J.Gomez. What's shakin' dude? Effective use of modal shakers. In *23rd International Modal Analysis Conference (IMAC XXIII)*, Orlando, Florida, USA, January 31 - February 3 2005. Society for Experimental Mechanics.

the choice of the built-in technology as well: frequency range and sensitivity are two important criteria. Accelerometer manufacturers usually concentrate their efforts in two major technologies: the piezoelectric and the capacitive.

Piezoelectric accelerometers rely on the piezoelectric effect of certain materials (e.g. quartz crystals or ceramics), in which a voltage is generated in response to a change in applied mechanical stress, as a result of the rearrangement of ions. In order to measure acceleration, the piezoelectric layer is attached onto a small mass called seismic mass (due to the fact that the excitation for this mass comes from the vibrating casing of the sensor, as if it was a shaking ground in an earthquake). According to Newton's second law Eq. (4.2), the vibrating mass will create a changing inertia force which is proportional to its mass and acceleration. This force will be imparted on the piezo-electric layer, whose ions will undergo rearrangement. Although they can respond to low-frequency phenomena, piezoelectric accelerometers cannot measure uniform acceleration such as the gravitational pull.

How the charge accumulation is then transformed in an output determines the sub-type of piezoelectric accelerometer: circuitry can be integrated in the sensor to convert the surface charge in voltage, or the charge itself can be used as output through a charge amplifier. In the first case, the sensor needs to be powered from the outside.

Capacitive accelerometers on the other hand are capable of sensing constant accelerations. This is due to the principle underlying their functionality: a membrane is placed between two parallel plate capacitors, forming two condensators sharing a movable plate, as shown in Fig. 9.2. The position (or deflexion) of the membrane determines the capacitance difference between the two, which is then translated in an electric signal proportional to the acceleration. The static flexion of this membrane under the gravitational pull already creates a difference in capacitance, and is therefore detected.

Another popular way of sensing motion is the **laser vibrometer**. This contact-free measurement technique is based on the Doppler effect: the laser light being reflected back from a vibrating target will show a frequency shift which is proportional to the velocity of the target (the frequency will increase when the object moves towards the light detector, while decrease when the object is moving away). The frequency shift contains therefore the information of the motion of the target with respect to the position of the detector.

The advantages of such systems are the accessibility to locations which are otherwise unreachable, the absence of added mass, and the high precision in large frequency bands. The technology is now so advanced that three-dimensional measurements can be taken at several points during one single scan.
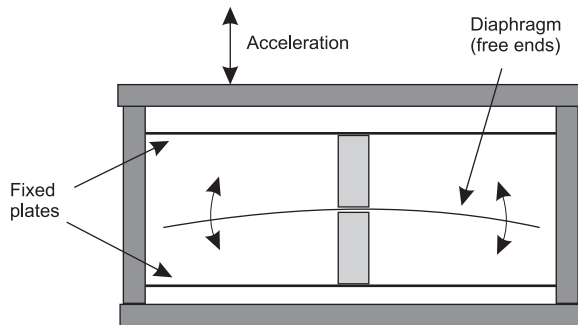
Figure 9.2: Capacitive accelerometer.

Fig. 9.3 shows the laser vibrometer at disposal in our lab (Polytec OFV505 with controller Polytec OFV5000), in operation during an early test with a fresh-frozen human specimen.
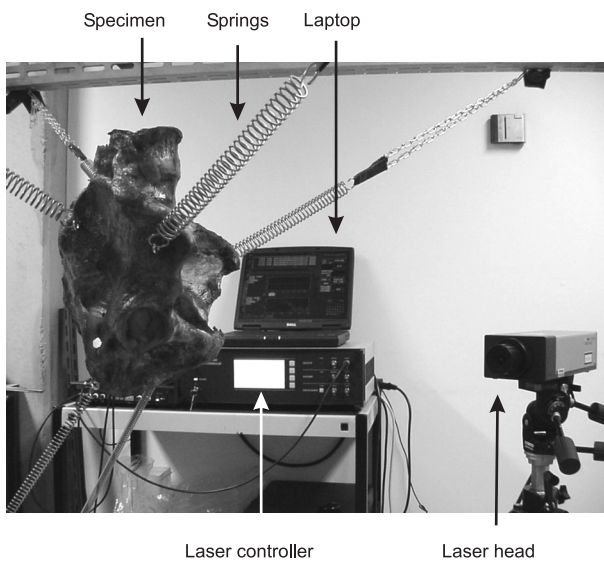
Figure 9.3: Laser vibrometer set-up during an experiment on a fresh-frozen human pelvis.

117

Impact test on an embalmed pelvis

The tools
Chapter 9

	In vitro		*In vivo*
Human	**Impact test on an embalmed pelvis Chapter 10**		*In vivo* ultrasound measurements Chapter 13
	Sine-sweep test on a fresh-frozen pelvis Chapter 11		
Animal	Dynamic test on rabbit ligaments Chapter 12		

This chapter describes methods and results of the first series of experiments performed on embalmed human specimens.

10.1   Oh dear... how do we do this?

UR FIRST ENCOUNTER with (dead) human material dates back to the beginning of 2003. It wasn't a loud battle, but neither a smooth victory. It did necessitate some adjustment and desensitization, and to us engineers felt like a true triumph. In hindsight, the fact that the anatomical specimens available[1] were embalmed made this initiation somewhat gentle.

Three embalmed specimens were put at our disposal for our first attempt at performing an experimental modal analysis. The objective was to obtain indications on their dynamic response (mode shapes, frequencies and damping ratios), in order to establish a suitable protocol and estimate the systems characteristics. The embalmment of the integral adult male human bodies was performed according to the standard protocol. After separation of the pelvic girdles at the level of the fourth lumbar vertebra, skin, subcutaneous tissue and muscles were removed, leaving the osseous and ligamentous systems intact. One of the specimens weighed 1.64 kg (value taken as reference for the inertia properties, as explained in Chapter 5.2), while the specimen used in this experiment session weighed 1.465 kg.

Various preliminary tests were performed in order to establish a valid protocol. In the end the data were collected with the pelvis laid in prone position with the two anterior superior iliac spines (SIAS) and the fourth lumbar vertebra supported by a layer of soft material (foam)[9], as seen in Fig. 10.1b.

The transient response was excited with impact hammer hits (PCB Piezotronics, Model 086C03) perpendicular to the surface of the bone on three different locations of the pelvis (externally on each side in the center of the iliac fossa, and on the midline of the second sacral vertebra). The response of the pelvis was sequentially measured at fourteen locations (five per innominate bone, four on the sacrum) by means of a three-dimensional accelerometer (PCB Piezotronics, Model 356B21) attached to the bone by screw fixation. The signals from the accelerometer and the hammer impact force were recorded by means of an acquisition system (Siglab Mod. 42-20, vna v3.2).

The Frequency Response Functions were obtained via Fast Fourier Transform (FFT) of the acquired signals and imported in the STAR System modal analysis programme (Spectral Dynamics, v5.1). The natural frequency, damping ratio and mode shape of the principal resonances were identified by polynomial curve fitting. The characterization of the mode shapes was based on the visual reproduction of the motion of

---

[1]Department of Anatomy, Erasmus Medical Center, Rotterdam, The Netherlands.

---

[9]   N.E. Conza and D.J. Rixen. Dynamic response of an embalmed human pelvis - A pilot study. In *World Congress in Medical Physics and Biomedical Engineering*, Sydney, Australia, August 24-29 2003.

each measured point. To that intent, the positions and local orientations of each three-dimensional measurement were assessed by means of infrared images taken from two infrared cameras, and two sets of three retroflective markers attached to the accelerometer and to the pelvis for reference, as depicted in Fig. 10.1.
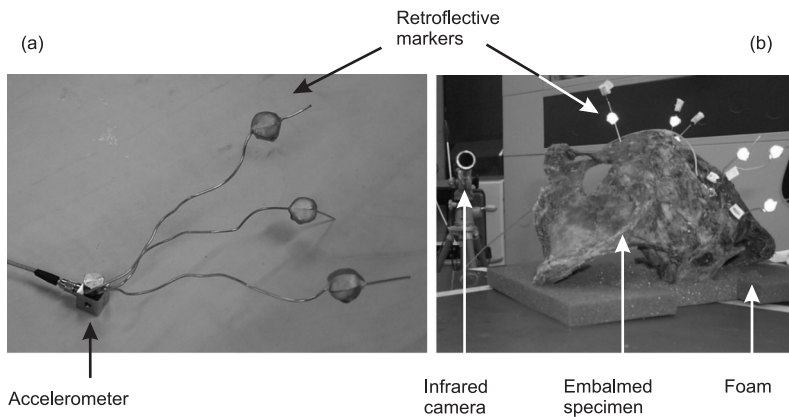
Figure 10.1: System for the determination of the sensor orientation. (a) The accelerometer with the cluster of retroflective markers, (b) the measurement setup with the infrared camera, the pelvis and the clusters of retroflective markers.

10.2 Results, indeed

The two measurement sets obtained by exciting the system on the ilia were good enough for a modal analysis (good coherence[2]). Unfortunately, the signals obtained via excitation on the sacrum were not useful (bad coherence) probably due to the fact that the osseous surface was not completely exposed. Separate analysis of the two mentioned successful measurement sessions revealed three main resonances with similar frequencies and damping ratios, as shown in Table 10.1.

The visualization of the first two resonances seemed to indicate the presence of (quasi) rigid body motions, which appeared to be translational along the anterior-

---

[2]The coherence is an indicator of the linear relation and the causality between the output (displacement, velocity or acceleration) and the input signals (force). The highest score is 1. It is obtained by comparing two different ways of calculating the Frequency Response Function starting from the spectra of the signals. In structural dynamics a coherence of > 0.98 is considered good[30].

[30] W. Heylen, S. Lammens, and P. Sas.   Modal analysis theory and testing.   Lecture notes Katholieke Universiteit Leuven, 1998.

Table 10.1: Frequency and damping ratio of the three identified resonances following impact on the right and on the left ilium.

	Impact on right ilium		Impact on left ilium	
Mode	Frequency Hz	Damping ratio %	Frequency Hz	Damping ratio %
1	16.66	9.28	17.52	7.72
2	35.91	5.91	37.05	5.24
3	187.77	3.02	187.50	2.96

posterior axis of the body (vertical in the experimental set-up) and rotational around the longitudinal axis of the body (horizontal in the experimental set-up), respectively (Fig. 10.2a and b). Additional tests performed to identify the influence of the supporting foam suggested indeed a translational and a rotational resonance at about 15 Hz, which could at least explain the first identified mode. After numeric filtering of the motion of the sacrum at the two first resonances, globally projected on all the points of the pelvis to simulate rigid body modes, no plausible vibration mode was left to be recognized. The residual motions could be explained as a result of the interaction between the foam and the pelvis, as well as inaccuracies in the measurements. The visualization of the third resonance on the other hand suggested a symmetric vibration mode where the two innominate bones opened and closed with the two sacroiliac joints acting as hinges, as illustrated in Fig. 10.2c.
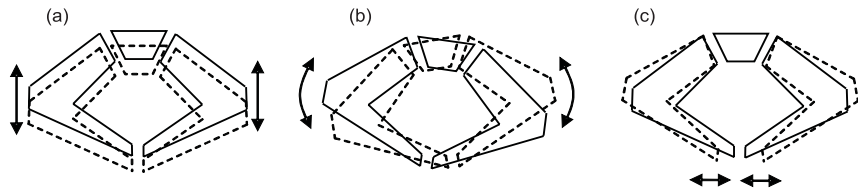
Figure 10.2: Resonance modes identified by the modal analysis tools: (a) around 17 Hz, (b) around 36 Hz, (c) around 187 Hz.

The preliminary indication of the existence of a resonance around 187 Hz was very important to free us from the absolute ignorance we were dwelling in. However, doubts were still hanging like a Damocles's sword on the reliability of such results. What really happened between the foam and the pelvis? Preliminary tests on a plastic pelvis had shown that hanging the structure on rubber bands resulted in very low-frequency rigid body motions (about 3 Hz), which would have been preferable to the 15 Hz resonance noticed with a foam support. Unfortunately in our case the accessibility of all points by the infrared cameras was the limiting factor which made us opt

for a prone position on a soft support. Similarly, other issues were still open. What is the effects of the embalmment on the dynamic behaviour of an organic structure? Are there alternatives? Other specimens? Other solutions for fixture?

Very much will happen between now and the next Chapter.

Sine-sweep test on a fresh-frozen pelvis

The tools
Chapter 9

	In vitro	*In vivo*
Human	Impact test on an embalmed pelvis Chapter 10	*In vivo* ultrasound measurements Chapter 13
	Sine-sweep test on a fresh-frozen pelvis Chapter 11	
Animal	Dynamic test on rabbit ligaments Chapter 12	

In this chapter the transition from embalmed to fresh-frozen specimens is presented. The process of establishing the method is described, and a curious event of serendipity is illustrated, which lead to the exclusion of three main ligaments from the model.

125

11.1 Perfecting the methods

URNING THIS ONE PAGE meant for us turning more than a year. That's how long it took us to set up a series of experiments on fresh-frozen human pelvises. At first it looked like we had to go all the way to Australia to find human specimens. Then the projections improved and Bruxelles showed up as the lucky place. In the end it was just next door that we found the material we were looking for, and a helpful friendly environment for a fruitful cooperation[1].

And it took us almost as much additional time to do all the mistakes and learn all the lessons to collect good data.

The test objects were fresh-frozen human pelvises, comprising the three bones of the pelvic girdle and the ligamentous tissue around the three joints. The femurs were removed completely and the spines were cut at the level of the fourth lumbar vertebra, to allow for ligaments integrity. The specimens were harvested short after death and frozen at -20 °C. They were removed from storage the day before the experiment and thawed overnight at room temperature.

During the first experiment in April 2004 we thought of exciting the pelvises (innocent as we were, we really did intend to measure two specimens in one session!) with an impact hammer and measuring the response with the laser vibrometer. The specimens were to be hung on a (supposedly rigid) heavyset metal frame by means of springs, which we had tailor-made for the expected weight and the desired low-frequency support resonance. Our modest goal was to gather some preliminary indications on support frequency, repeatability, effects of gravity, effects of drying-out. Well, the path was more arduous than imagined, and the goal already too ambitious. We didn't foresee the tenacious resistance of the bone to our attempts to insert a screw, and we didn't have a drill. But Utrecht was too far away to have come for nothing, and we succeeded eventually. But from that moment, puzzlement reigned unchallenged. The response was damped above expectations, and no matter how hard we tried, we were not able to discriminate between the FRF "hills" of the support and the ones of the system itself (usually in the jargon they are called "peaks", but as a Swiss citizen, grown up at the feet of the Alps, those really didn't look peaks to me). We thought that we could outsmart the situation and remove springs, or place weights on them, or substitute them with rubber bands. All logic actions which alas proved insufficient. Moreover, we didn't anticipate the amount of bouncing that the pelvis performed after each hammer hit, and how this would (now we think rather obviously) impair a laser measurement, where the light spot should more or less remain on the same point of

---

[1]Department of Pharmacology and Anatomy of the Rudolf Magnus Institute of Neuroscience at the University Medical Center in Utrecht, The Netherlands.

the structure. We capitulated half way through the protocol, rich with our first learned lessons (we needed a drill, and a shaker!), and returned the undisputable winner of the battle and his untried loyal colleague back to the freezer.

Two weeks later we tried again, this time with just one pelvis, with a shaker instead of the impact hammer, and with accelerometers in addition to the laser vibrometer. We wanted to investigate the support and the reciprocity, but we ran into difficulties of all sorts. Again, laden with new insight and an incipient sense of frustration, we returned home that night with the resolution to attempt a modal analysis with triaxial accelerometers.

This happened two more weeks down the calender. The main issue that time was the determination of the position and orientation of the accelerometers placed on the pelvis, an absolute essential for an experimental modal analysis. To that end we had arranged for a magnetic tracking system, whose operation required not little strategic undoing: we realized after the whole system inclusive fixture and shaker were in place, that the shaker with its coil would annihilate the reliability of the magnetic tracking system readings. Again the day ended with wonderful new ideas.

And so it continued for quite a while. At one point we even tried to fix one half of the pelvis in quick-setting cement, feeling like some sort of gangsters. But the cement never set, with our dismay and some amused curiosity about the missing trick (undeniably, criminal practice teaches that it can be done). In another session we performed dynamic measurements on the bones separately and could confirm that they can be considered rigid below a frequency of 300 Hz.

And on we went in our quest, until, wise enough to lower the expectations, we thought that we might have just the right procedure to obtain sufficiently good modal data[12]. But that very day something different happened.

11.2 Bad luck... or is it?

It was a summer day in 2005 when a little unexpected accident occurred to the pelvis we were about to test: the sacrotuberous and sacrospinous ligaments on one side got severed (see Fig. 2.2). Within minutes the automatic disappointment turned into a sense of expectation: by testing a specimen with only partial ligamentous system we could gather relevant information indeed, and maybe sever a few more and repeat and compare. The results of that day showed that cutting through the pubic symphysis would cause noticeable frequency shifts and mode shape changes, while severing

[12] N.E. Conza and D.J. Rixen. Experimental modal analysis on a human specimen: lessons learned. *Experimental Techniques*, 30(6):(to appear), 2006.

the iliolumbar ligaments would maintain the results. Of course we had no indication on the role of the sacrotuberous and sacrospinous ligaments, since they were severed from the beginning. The suspicion that such obviously visible ligaments might not contribute to the dynamic of the pelvis was indeed intriguing.

So we decided to pursue this unconventional idea and to schedule an experiment session with the purpose of performing a modal analysis on an intact specimen, then resect first the sacrospinous and sacrotuberous ligaments, repeat the measurements, and finally resect the iliolumbar ligaments and measure one last time.

In that session the excitation was introduced by an electromechanical shaker (TIRA Model S 513 TV51110) current-driven by its amplifier (TIRA Model BAA120 TV51110). The imparted force was measured by means of an impedance head (PCB Piezotronics Model PCB 288M25), and the response of the system by means of two triaxial accelerometers (PCB Piezotronics Model PCB 356B21) powered by signal conditioners (PCB Piezotronics Model PCB 442C04). The preparation of the pelvis foresaw the drilling of thirteen holes at the desired sensor locations (five per innominate bone and three on the sacrum, as shown in Figures 11.1 and 11.2) so that the screws axes would be horizontal upon hanging. In fact we had decided to discard the idea of the magnetic tracking system as it was too time-consuming and not really accurate, and we opted for a new protocol in which small horizontal aluminum platforms were to be mounted on the screws for the accelerometers to be positioned horizontally and along the reference axes (see Fig. 11.3). The positions of the accelerometers were estimated using rulers, as seen in Fig. 11.3a. Other four holes were drilled along the iliac crests to attach rubber bands, through which the pelvis was then hung to the frame. A plexiglas rod
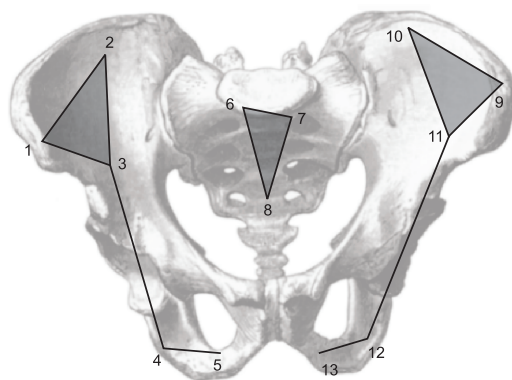
Figure 11.1: Points on the pelvis where measurements have been taken.

Figure 11.2: Drilling of the screw holes.

(15 cm in length, 0.4 cm in diameter) transmitted the vibration of the shaker to an impedance head which was screwed to the pelvis. The excitation was imparted in form of sine-sweeps in the frequency range 10 to 340 Hz. The coherence was very good except below 30 Hz. After completion of the first series of measurements (lasted about 3 hours) the sacrospinous and the sacrotuberous ligaments were resected on both sides. Measurements at four locations (two near the attachment points of the ligaments (positions 4 and 12), and two at the SIAS (positions 1 and 9), Fig. 11.1) were performed. Then the iliolumbar ligaments were resected on both sides. Again, measurements at four locations (two near the attachment points of the ligaments (positions 2 and 10), and two at the SIAS (positions 1 and 9), Fig. 11.1) were obtained.

A first analysis of the measured FRFs by means of ME'scope is described in a publication[14]. However, since its submittal, a second analysis of the data performed with SDT added new insight to the conclusions without discarding any of them. The next section will present both sets of results.

[14] N.E. Conza, D.J. Rixen, and S. Plomp. Vibration testing of a fresh-frozen human pelvis: the role of the pelvic ligaments. *Journal of Biomechanics*, Epub ahead of print, 2006.
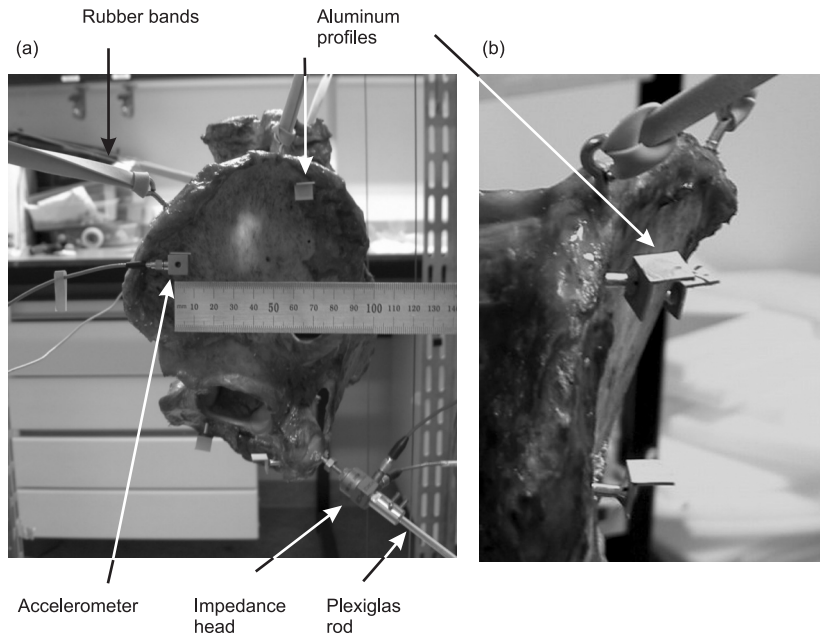
Figure 11.3: Pelvis fixture: (a) pelvis hanging on the frame, with aluminum profiles as horizontal platforms for the accelerometer, (b) close-up on the aluminum profiles.

11.3   Surprise! (alias: Results)

What was very different in this second modal analysis, performed with SDT instead of ME'scope, was our attitude. In the results reported in the above mentioned article we clearly saw a resonance around 80 Hz, but we decided quite fast, after visualization of the mode shape, that it must be a rigid body mode caused by the support, and that it was not an elastic mode of the pelvis. Also, the first analysis was approached in a top-down fashion, looking at the Frequency Response Functions and estimating a priori which few "hills" were resonances and which little ripples were just noise. This almost unconscious carelessness was not due to arrogance, on the contrary: after years of data collection on human pelvises we had developed a feeling of resignation towards the unsoundable mysteries of the pelvic dynamics, and we thought that a simplistic approach, to be discarded only in presence of strong evidence of the contrary, was to be preferred to trying to interpret uncountable little bumps. Nevertheless we still had our spark of healthy scientific suspicion, and we investigated the matter further.

But first things first. The linearity of the system for the imparted vibration level was

checked by comparing reciprocals and by attesting that change in the intensity of the excitation did not result in change in the FRFs. Also, the possible impact of humidity loss during the experiment was investigated by repeating the first measurement at the end of the session. No change in the FRFs could be detected.

Our interpretation of the analysis performed with ME'scope indicated main resonances at 80 Hz, 133 Hz, 226 Hz, and 244 Hz, of which, as said, the first one appeared to be a rigid body mode with the pelvis moving as an undeformed whole (and was for the time ignored).

The mode shape of the second resonance seemed to indicate an antisymmetric rotation of the upper part of the innominate bones around a horizontal coronal axis, with the two halves of the pubic symphysis moving together (Fig. 11.4a). The mode shape of the third resonance showed a symmetric opening-closing motion of the two SIAS generated by a rotation around what could be a vertical axis, and an antisymmetric back and forth gliding of the two pubic symphysis halves (Fig. 11.4b). The mode shape of the fourth resonance seemed to indicate a symmetric inwards rotation of the two innominate bones, and a back and forth motion of the pubic symphysis with opening and closing of the tuberi (Fig. 11.4c).

The exciting part came from the analysis of the data collected after ligaments resection. After bilateral resection of the sacrospinous and the sacrotuberous ligaments analysis showed three resonances: at 132 Hz, 226 Hz and 245 Hz. The mode shapes were compared at the four measured locations to the results obtained with intact ligamentous system, and **did not indicate any change**. The MAC values (see Chapter 4.3) of the three modes before and after ligaments resection were 0.954, 0.913 and 0.970. The **dynamic response** of the system was also **unaffected** after additional bilateral resection of the iliolumbar ligaments. The results showed three resonances, identified at 132 Hz, 226 Hz and 246 Hz, whose MAC values with respect to the intact pelvis were 0.984, 0.976 and 0.973. In fact, that the response of the system seemed not to be affected by the change in ligamentous configuration was already visible in the drive point FRFs (Fig. 11.5), and was the reason why we had decided to measure only four points after both ligament resections, instead of the whole complement of 13.

The finding that the sacrospinous, sacrotuberous and especially the iliolumbar ligaments seemed not to play a role in the vibration response of the pelvis is at first glance surprising. Literature reports of many studies in which the importance of the iliolum-
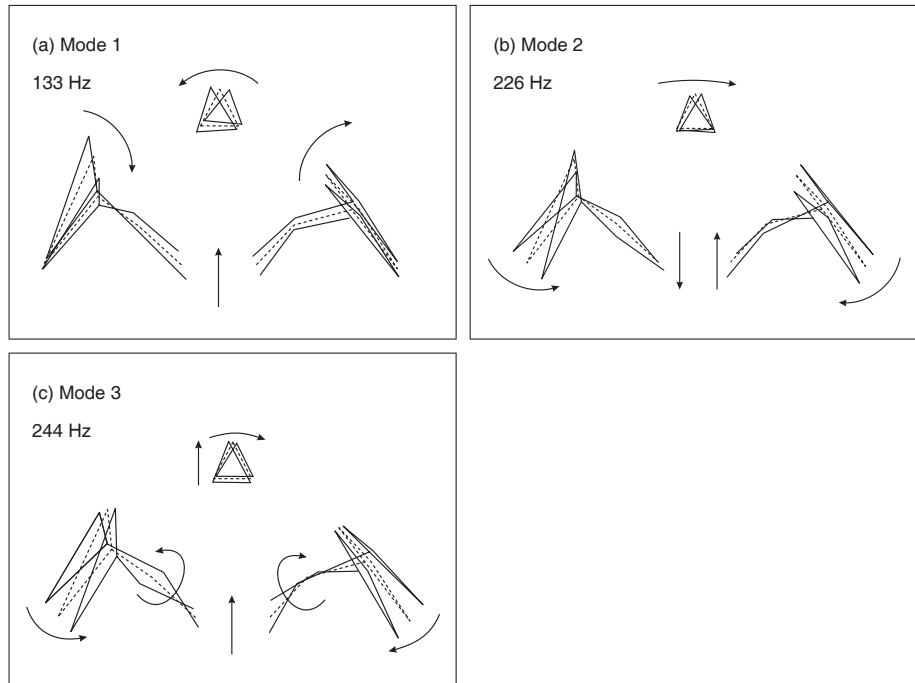
Figure 11.4: The three identified vibration mode shapes. The dashed lines represent the undeformed configuration, the solid lines the extreme positions during one vibration cycle. Arrows are added to simplify the interpretation of the motion.

bar ligaments for the stability of the pelvis is demonstrated [8,33,42]. However in all cases their role was investigated for static stability and not for dynamic vibrations.

Still, that resonance at 80 Hz bothered our conscience. We decided therefore to perform the analysis with SDT, which we deemed mathematically more suitable for the subtleties of the task at hand. In fact, SDT optimizes both the poles (frequencies and damping factors) and the residues (see Chapter 4.4) until convergence, while ME'scope identifies the poles first, and then, with the poles fixed, the residues. Moreover, in this

[8] D.H. Chow, K.D. Luk, J.C. Leong, and C.W. Woo.   Torsional stability of the lumbosacral junction. Significance of the iliolumbar ligament. *Spine*, 14(6):611–615, 1989.

[33] J.C. Leong, K.D. Luk, and D.H. Chow nad C.W. Woo.   The biomechanical functions of the iliolumbar ligament in maintaining stability of the lumbosacral junction. *Spine*, 12(7):669–674, 1987.

[42] A. Pool-Goudzwaard, G. Hoek van Dijke, P. Mulder, C. Spoor, and C.J. Snijders amnd A. Stoekart.   The iliolumbar ligament: its influence on the stability of the sacroiliac joint. *Clinical Biomechanics*, 18(2):99–105, 2003.
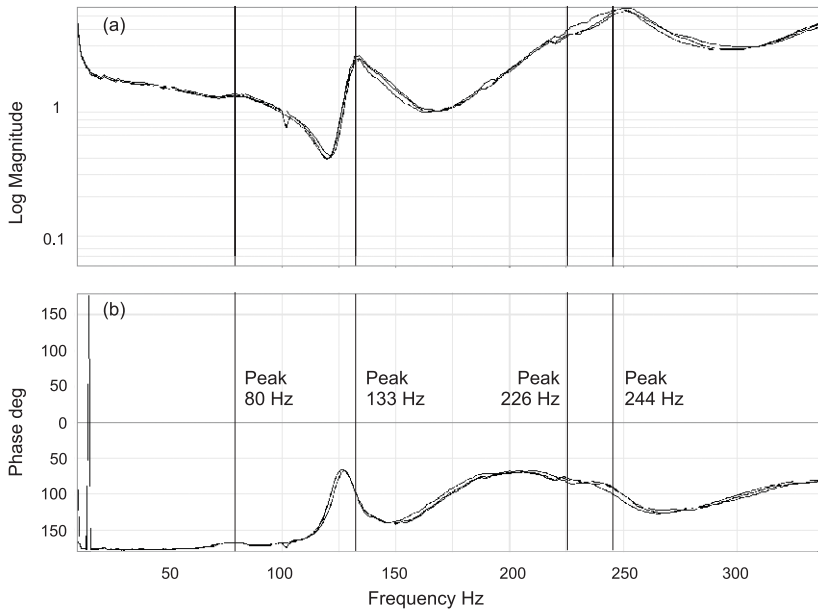
Figure 11.5: Superposition of (a) amplitude and (b) phase of Frequency Response Functions at the drive point: with intact ligamentous system, after sacrospinous and sacrotuberous ligaments resection, and after iliolumbar ligaments resection. Legend is not added since the response does not show any change. The four vertical lines indicate the frequency of the peaks as identified by ME'scope.

second analysis we reversed the approach by manually placing potential resonances at almost all ripples, and letting SDT sort them out. Our only criterium for plausibility was a good fit of the measured curves. After a struggle which lasted a couple of months we eventually found a set of fulfilling results, shown in Table 11.1.

Table 11.1: Frequencies and damping ratios of the modes identified by SDT.

Mode	Frequency Hz	Damping ratio %
1	75.6	13.4
2	132.5	3.2
3	139.3	4.4
4	230.6	14.7
5	245.0	6.4
6	340.0	7.6
7	503.0	72.8

If you recall from the previous section, the frequency range in which we measured the response was from 10 to 340 Hz. This does not mean that the modal analysis tool will suggest resonances only within this range. In fact, the contribution of so called out-of-range modes can have quite an impact, and is often necessary to achieve a good fit of the curves. The mode at 503 Hz is one of them: with a damping of 72% it is virtually a flat line, which compensates also for all the modes at higher frequencies, which contribute to the response in a quasi-static manner. In addition, SDT was allowed to assume the existence of a mode at a frequency much lower than 10 Hz, which represents a quasi-rigid body mode. This additional mode will be referred to as mode 0, and will be discussed in the next sections.

Global modes filtering

With the obtained mode shapes we did many things, the first one of which was to filter out the global motion of the pelvis in the three translations and three rotations. One question we wanted to answer was whether the mode around 80 Hz (here identified at 75 Hz) was a rigid body mode or not. To do this, we **numerically filtered out all global rigid motions** and we checked the nature of the residual motions. This was done by expressing each identified mode shape as:

$$\boldsymbol{x}_{raw} = \boldsymbol{R}_g \boldsymbol{\alpha}_g + \boldsymbol{x}_{el}, \tag{11.1}$$

where $\boldsymbol{x}_{raw}$ is a vector containing the 39 residuals of the considered mode (13 measurement points in three directions), $\boldsymbol{R}_g$ is a (39×6) matrix whose columns contain the amplitude of the 39 degrees of freedom belonging to the six global rigid body modes (three global translations and three global rotations), $\boldsymbol{\alpha}_g$ is a (6×1) vector containing the contribution of each rigid body mode to the measured residuals, and $\boldsymbol{x}_{el}$ represents what is left on top of those rigid contributions. The matrix $\boldsymbol{R}_g$ has been constructed geometrically based on the measured positions of the thirteen points. The subscript g in the equations stands for "global". Should the identified mode be perfectly globally rigid, $\boldsymbol{x}_{el}$ would contain a series of zeroes.

Premultiplication of Eq. (11.1) by $\boldsymbol{R}_g^T$ and resolution for $\boldsymbol{\alpha}_g$ with the assumption that $\boldsymbol{R}_g^T \boldsymbol{x}_{el} = \boldsymbol{0}$ (which means that the remaining motion must be orthogonal to the rigid body modes defined in $\boldsymbol{R}_g$) results in

$$\boldsymbol{\alpha}_g = (\boldsymbol{R}_g^T \boldsymbol{R}_g)^{-1} \boldsymbol{R}_g^T \boldsymbol{x}_{raw}, \tag{11.2}$$

which leads to the expression of the remaining motion as

$$\boldsymbol{x}_{el} = \boldsymbol{x}_{raw} - \boldsymbol{R}_g \boldsymbol{\alpha}_g = \boldsymbol{x}_{raw} - \boldsymbol{R}_g (\boldsymbol{R}_g^T \boldsymbol{R}_g)^{-1} \boldsymbol{R}_g^T \boldsymbol{x}_{raw}. \qquad (11.3)$$

A ratio defined as

$$\frac{\|\boldsymbol{x}_{raw}\|_2 - \|\boldsymbol{x}_{el}\|_2}{\|\boldsymbol{x}_{raw}\|_2} \qquad (11.4)$$

provides an indication of the amount of global rigid body motion in each mode. Table 11.2 provides these values for the seven identified modes, plus the quasi-rigid body mode 0.

Table 11.2: Frequencies and global rigid body content of the modes identified by SDT.

Mode	Frequency Hz	Rigid body content
0	-	0.91
1	75.6	0.83
2	132.5	0.51
3	139.3	0.48
4	230.6	0.06
5	245.0	0.03
6	340.0	0.05
7	503.0	0.10

As Table 11.2 shows, modes 0 through 3 contain a noticeable amount of rigidity in the movement. This is actually to be expected for mode 0 which, as said before, has been numerically added as a quasi-rigid body mode at a frequency close to zero, thus virtually **rigid**. Even though its rigidity content is less than 1, as it should theoretically be, it is already a satisfactory result. In fact it should not be forgotten that it results from the numerical fitting of non-perfect real measurements performed by a software which had no mathematical knowledge that the measurement points belonged to the same body.

Nevertheless, an inspection was performed to check whether this less-than-one rigidity of mode 0 might have been caused by one single measured point, which, beside the possible inaccuracy of the dynamic response measurement, could carry the consequences of inaccuracies in both the position and orientation estimations. This was obtained by ignoring the three-dimensional measurement taken at one point at a time, and perform global rigid body mode filtering without it. A sudden increase in global rigidity should directly indicate the culprit. But there was no sudden jump, and no culprit.

For the other seven modes, on the other hand, a considerable rigid body contri-

bution is unwelcome, since it means that the dynamics of the support structure was possibly driving the response, making the information on the mode frequency less reliable. In fact, a strategic mistake was done when setting up the experiment: the shaker and the pelvis were both hung at the same frame. The fact that the pelvis was attached by rubber bands to the frame would probably have been sufficient to isolate it from the vibrations of the frame. However, the shaker was hung by a strap to the same frame, which received part of the vibration, and responded to it at its own resonance frequencies. This response would then be transmitted back into the shaker, which would then transmit it to the pelvis. Fatal mistake.

Bone rigidity filtering

The next step taken in the post-processing of the results is similar in concept to what has been just described, but aims at the "rigidification" of the motion of the individual bones. The idea is to take the modes which were left over from the global modes filtering (thus what we assume are the elastic modes of the pelvis) and extract from them and retain the rigid motions of the three individual bones. In this manner we hope to clean the modes from measurement noise and errors, since findings from previous tests indicated that under 300 Hz the bones can be considered rigid.

Data on the rigidity of the individual bones in the identified modes could provide indications relevant for many purposes. High rigidity levels would increase our confidence in the estimation of the sensor positions and orientations, and in the assumed rigid behaviour of the bones under 300 Hz. Moreover, a very low rigid body content of a mode could indicate that it is just a numerical artefact. And last but not least, since the individual filtering has been performed with rigid body modes of unit displacements and rotations, it provides us directly with the elastic modes of the rigid bones which we can use for correlation.

Mathematically, this is performed as follows. The modes left over from the global filtering x_{el} can be expressed as:

$$x_{el,i} = R_i \alpha_i + x_{res,i}, \tag{11.5}$$

where each bone has its own R_i, whose 6 columns contain the six rigid movements of that particular bone geometrically transformed at the measured degrees of freedom (15 in case of the innominate, and 9 in case of the sacrum), and $x_{res,i}$ are the remnants satisfying $R_i^T x_{res,i} = 0$. The **rigid motion of the three bones** independently to one

another is extracted as follows:

$$\boldsymbol{\alpha}_i = (\boldsymbol{R}_i^T \boldsymbol{R}_i)^{-1} \boldsymbol{R}_i^T \boldsymbol{x}_{el,i}. \tag{11.6}$$

Unlike before, what is retained from this calculation is not the remaining motion for all bones, but their rigid body content, thus their $\boldsymbol{\alpha}_i$. Dutifully reorganized and combined, the three $\boldsymbol{\alpha}_i$ represent the mode shapes (the $\boldsymbol{z}_s$ of Chapter 4.3) expressed at the 18 degrees of freedom of the model, and can therefore be compared to simulated modal response. Here as well the same ratio defined in Eq. (11.4), adapted to

$$\frac{\|\boldsymbol{x}_{el,i}\|_2 - \|\boldsymbol{x}_{res,i}\|_2}{\|\boldsymbol{x}_{el,i}\|_2} \tag{11.7}$$

can provide indication on the level of rigidity of the bones, and can be used as a thermometer to guess the health condition of each identified mode. Table 11.3 shows the values obtained for the three bones for the eight modes.

Table 11.3: Rigidity of the individual bones at the modes identified by SDT.

Mode	Frequency Hz	Bone		
		R	S	L
0	-	0.10	0.80	0.20
1	75.6	0.17	0.66	0.29
2	132.5	0.65	0.72	0.83
3	139.3	0.49	0.83	0.70
4	230.6	0.71	0.83	0.67
5	245.0	0.66	0.91	0.52
6	340.0	0.40	0.74	0.52
7	503.0	0.51	0.46	0.50

A first point of discussion is that it is not really meaningful to want to extrapolate the elastic mode underneath mode 0, since we consider it a quasi-rigid body mode. However, the visualization of the remaining motion can always bring insight. Second, considering the aspects mentioned above related to the rigidity level of the individual bones, the question might arise over mode 1, which shows a bad rigidity in the two innominate bones. The sufficiently accurate sensor position measurement is confirmed by the relatively high values in the other modes, and is therefore not the problem. A deformation of the bone is also not plausible, since modes at higher frequencies show much better rigidity. And visualization of the mode indicates an antisymmetric mode, too credible to be discarded. A possible explanation comes from the fact that the content of global rigidity was as high as 83%. Once that this motion is removed, what is left is a low intensity response, in which noise comes to play an important role

in disrupting the rigidity.

The last step, which is the result of a choice more than a necessity, was to transform the thus filtered modes, the $\boldsymbol{\alpha}_i$, expressed at the degrees of freedom of the model and comprising the rigid modes of three separate bodies, back to the points at the periphery: $\boldsymbol{x}_{corr,i} = \boldsymbol{R}_i\alpha_i$ (*corr* for "correlation"). That's where the comparison to the simulated motion will take place. The other option, to compare the filtered modes $\boldsymbol{\alpha}_i$ (dutifully combined) at the 18 model degrees of freedom, would seem to be more logical, since that's what the solution of the eigenproblem provides in the first place. However, this option would force us to compare vectors containing translation and rotation values, which is very tricky due the different nature of the quantities contained (displacements, angle variations). In fact, a unit transformation, for instance from meters to millimeters on the translation values, would accrue the role that the translation plays with respect to the rotation, without any physical reflection of it. At the periphery, all that is compared are displacements.

The results, visualized at the periphery, were very good. In fact they showed plausible (anti)symmetric motions between the right and left innominate bones, which is something that anatomy would suggest. Intriguing is the fact that the remaining motion of mode 0 does not seem to be just noise. Fig. 11.6 shows the identified and double-filtered mode shapes.

But to know how the model compares to these modes, you will have to wait for Part V. Sorry.

138

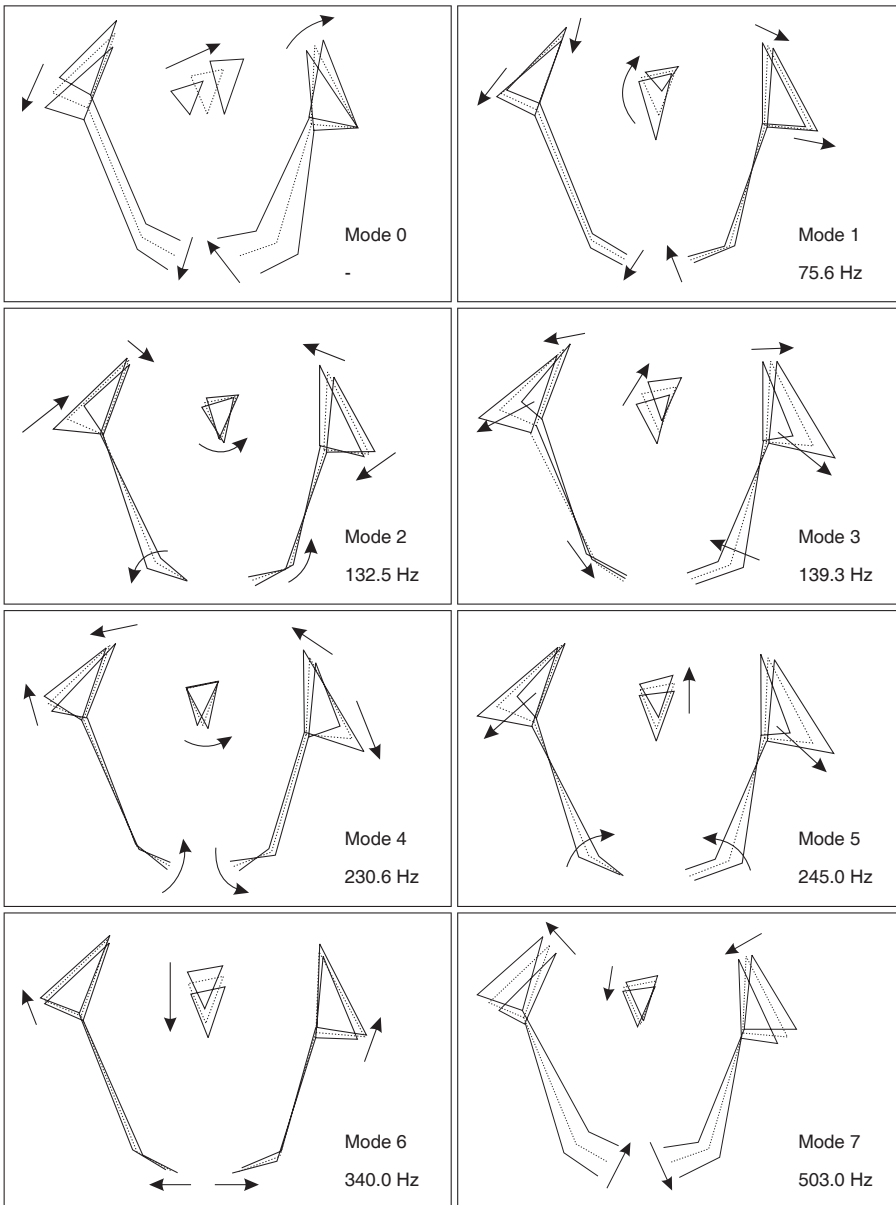Figure 11.6: Resonance mode shapes identified by the modal analysis tools and double-filtered.

Dynamic test on rabbit ligaments

This chapter resumes the discourse about the frequency dependence in the mechanical properties of the ligaments, as introduced earlier in this work. Here pilot experiments on rabbit ligaments, performed with the aim of assessing the existence of such dependence, are described.

12.1 Home cooking

N CHAPTER 7 we have learned that the "conventional" analysis of data collected on an "unconventional" structure might lead to false conclusions, where with conventional we mean related to a viscously damped structure whose mechanical properties are assumed constant. More precisely, we suggested that ligaments might fall in this category due to a possible dependence of their biomechanical properties on the frequency of the dynamic excitation.

To investigate this intriguing possibility, pilot dynamic tensile experiments were performed on medial collateral ligament (MCL) complexes of rabbit knees. We consider these experiments "pilots" not only for their unique home-made nature, but also for the quite unsophisticated choice of biological samples. For a brief moment we considered ordering "animal models" (the euphemism currently in use to indicate laboratory animals), but the additional information that they were to be delivered alive immediately made us run for retreat. We resorted to MCL-complexes harvested from frozen rabbit posterior legs otherwise destined for culinary purposes.

A set-up was built with an electromechanical shaker (TIRA Model S 513 TV51110, amplifier TIRA Model BAA120 TV51110), an impedance head (PCB Piezotronics Model PCB 288M25), the ligament complex and a metal wire in vertical sequence (Fig. 12.1). The metal wire was attached to the environment at the top and passed through a hole in the upper bone part. A small aluminum ring was inserted in the hole to prevent the metal wire to cut through the bone. The same connection was provided at the bottom bone part, below which the metal wire was attached to the impedance head, screwed to the shaker platform. In physiologic conditions *in vivo* the axes of the femur and the tibia of rabbits lie with an angle of about $70°$ with respect to each other. To avoid the construction of clamps designed to reproduce this angle in the test set-up, the two holes on the upper and lower bone parts were aligned with the ligament axis in physiologic configuration, so that the bone parts would, under tension, automatically orient themselves in the correct direction.

Sine sweeps were performed in the frequency range between 20 Hz and 300 Hz, with a frequency increment of 2.5 Hz and for four different pre-strains (approximatively 2%, 3%, 4% and 5%). The dynamic stiffness in frequency domain is normally obtained by dividing the measured force by the measured displacement (converted from the acceleration signal), and includes also the inertia component due to the acceleration of the lower mass (bone and connector). This inertia component had to be removed from the measured force in the post-processing phase in order to obtain $k(\omega)$,

(a)   (b)

Connection
to fixed
environment

Metal wire

Hole in
the bone

Bone
fragments

Ligament

Connection
to the shaker

Impedance
head

Hole in
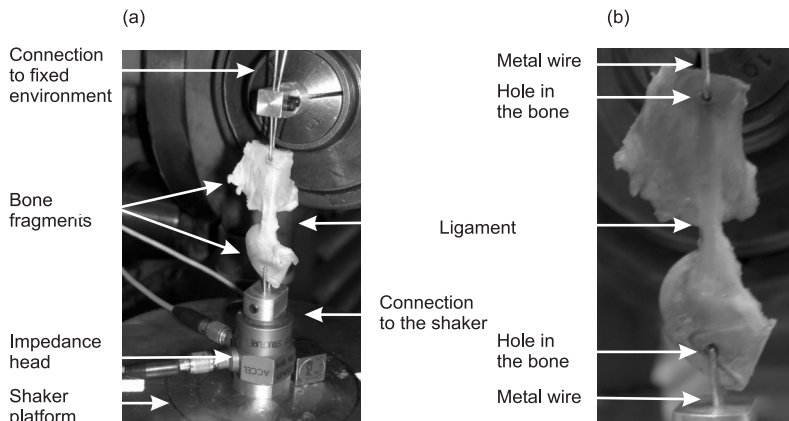the bone

Shaker
platform

Metal wire

Figure 12.1: Dynamic tensile test setup: (a) general view with shaker at the bottom, impedance head, connector for the metal wire, rabbit MCL-complex, wire and connection to the environment, (b) close-up on the MCL-complex.

since:

$$f = (-\omega^2 m + k(\omega))z, \tag{12.1}$$

where f is the measured force, m the mass of bone and connector, and z the measured displacement.

12.2 The verdict

Analysis of the complex $k(\omega)$ seemed to indicate that the stiffness (real part) is constant along the frequency axis, and that it increases with increasing pre-strain (Fig. 12.2a). The imaginary part (providing indications on the damping) on the contrary seems to suggest a slight linear relationship with the frequency, and it shows values one order of magnitude smaller than the amplitude of the stiffness (Fig. 12.2b). The fact that the stiffness depends on the pre-strain might not come as a surprise, but is for sure a complication. A methodology designed to identify the mechanical properties of the sacroiliac ligaments will not discriminate between the causes of a change in stiffness, be it pre-strain or an actual stiffening of the ligament.

Following these pilot tests, we drew the pilot conclusion that the stiffness of the ligaments was "innocent until proven guilty" of the charge of frequency dependence. As for the damping, we decided that these results were too pilot at this time, too late in the project timeline (it's April 2006), and too akin to the fuzzy aura of mystery around
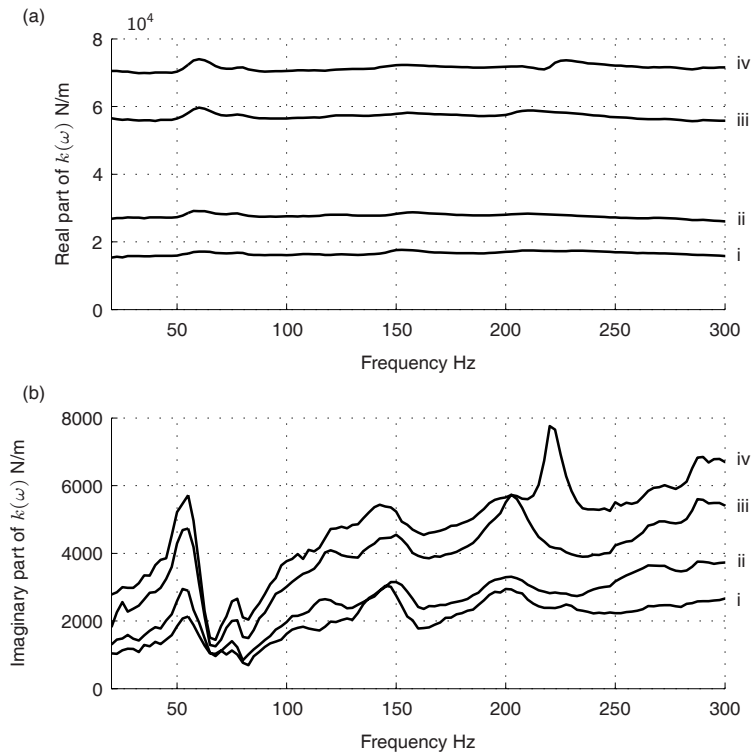
Figure 12.2: Real part (a) and imaginary part (b) of the complex stiffness $k(\omega)$ for the four levels of pre-strain: (i) 2%, (ii) 3%, (iii) 4%, and (iv) 5%.

the damping of the pelvis as a whole, to justify the implementation and investigation of the glimpsed linear dependence. This task will be part of the legacy of this project.

In vivo ultrasound measurements

This chapter reports of the pilot experiments performed on subjects. In the first section the functionality of the ultrasound technique is briefly illustrated, while the second section describes results obtained, in a more practical way, by pressing accelerometers against the skin.

13.1   The ultrasound technique works!

UT ALL THIS wouldn't have its exquisite thrill of expectation if we didn't try on (our) warm pulsating living bodies. As we have discovered in Chapter 8, it is not all about dry runs in a computer chip, or a handicraft exhibition with drills and screws mounted on human specimens. We also dispose of an ingenious piece of technology to measure vibrations at a micrometer level non-invasively, non-painfully and non-destructively through layers of tissue.

To check the functionality of the ultrasound technique, an experiment was performed on a very accessible bone (the proximal phalange of the forefinger of the hand). The dorsal side of the finger was pressed against an accelerometer which was attached to the platform of a shaker. As the shaker vibrated with an amplitude of 10 μm, its motion was transmitted through the accelerometer to the bone. The vibration was measured on the palmar side of the phalanx by means of the ultrasound prototype, at four frequencies and twenty times per frequency, and compared to the measurement of the accelerometer. The difference between the two was of about 2%, which, since the transmission of the motion was performed through the tissue itself and the accelerometer was actually measuring the vibration of the shaker and not of the bone, is already a good result.

13.2   And so do the accelerometers

In the last months of the project we were armed with a very simple idea, which had escaped us until the fresh mind of our lastly appointed colleague Mr Bram Soethoudt catched it: measure the bone vibration by pressing an accelerometer on the skin atop a protruding bony landmark.

Many pilot experiments were performed, in many different configurations (but always with the same two willing subjects: the two young researchers of this project). A hole of about 15 cm was made in an examination bed, through which the shaker, placed on the ground, could come in contact with the exposed pelvis of a lying person. The measurements were taken with the accelerometers on the opposite site of the pelvis. In another configuration the subject would stand, and the excitation would be imparted my hammer and picked up by accelerometer, as seen in Fig. 13.1.

This measurement technique is obviously limited in the number of points that can be measured and is applicable only to subjects with a lean body type. It is not to substitute the ultrasound apparatus. Nevertheless it is a quick-fix to gather information in an easy and practical manner. In fact, the very nature of the dynamic response of

(a) (b)
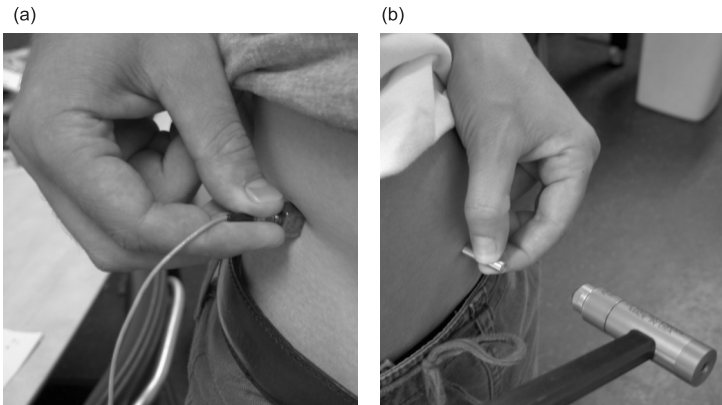
Figure 13.1: Experiments *in vivo* by different subjects: (a) response measurement on the right anterior superior iliac spine (SIAS), (b) hammer hit on the left SIAS.

the human pelvis *in vivo* is still to be unfold, and crucial for the deliberation about the future of the project.

Preliminary result show very flat response curves. An example of such a response can be seen in Fig. 13.2, showing the transfer function between an excitation at the anterior superior iliac spine (the drive point has also been measured) and a measurement at the posterior superior iliac spine of the same innominate bone. If the dynamic responses of the fresh-frozen specimens were just about hilly, this is definitely more like the Netherlands. Moreover, a repeatability check revealed that after a five minute interval, in which the subject was asked to walk around, the response could not be reproduced.

Alas.

(a)

(b)
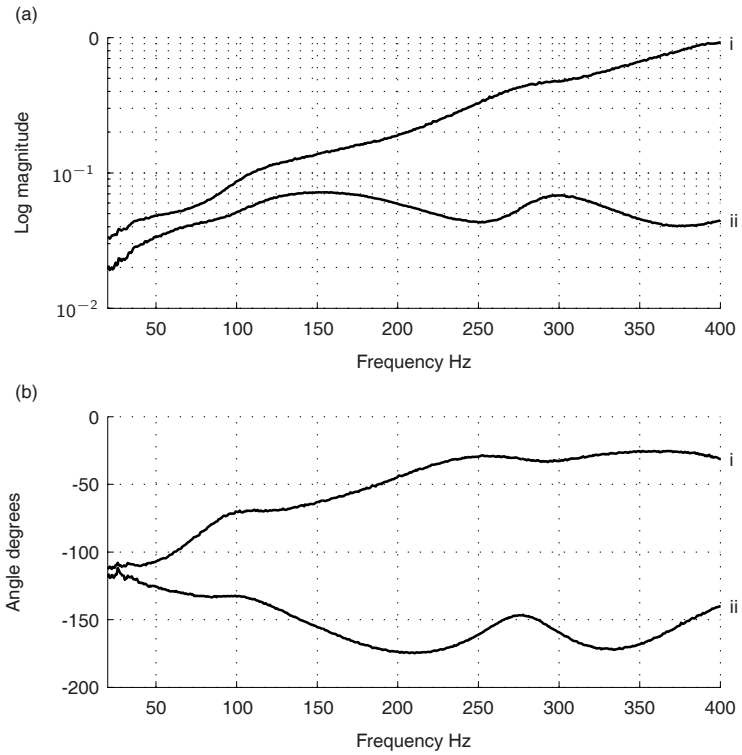
Figure 13.2: Amplitude (a) and phase (b) of Frequency Response Functions measured *in vivo*: (i) drive point response on the anterior superior iliac spine, (ii) response function between the drive point and the posterior superior iliac spine of the same hip bone.

PART V

THE INTERPRETATION

אב

18 June 2006

It was painstaking. And long.

Three and a half years to develop a theory on the semantics
of the scroll. I have a draft model of the meanings, and
I think I can distinguish between random variations and
meaningful differences in the simple hieroglyphs.
This is my reading guide, now I only have to try and read it.

Should it truly be of divine origin and should I have got it
all wrong, which I deem quite possible, I might give God
a good laugh.
Considering the mess down here, he badly needs one.

Correlation between model and measurements

This section explains the process of bringing the model to match the experimental dynamic behaviour obtained from the fresh-frozen human specimen. The model parameters are tuned with the objective to minimize the difference between simulated and measured response.

O HERE YOU ARE, eventually entering Part V, facing its only chapter with that sense of suspense left over from the end of Chapter 11. We were discussing the results from the experiments on fresh-frozen specimens, and what had to be done to them to make them fit for this: the correlation.

The model used for this study has been updated after realizing that the sacrotuberous, the sacrospinous and the iliolumbar ligaments don't contribute to the dynamic response of the pelvis, and is configured with two springs representing the ligaments of the pubic symphysis, three springs per side representing the interosseous, the long sacroiliac and the short sacroiliac ligaments on the posterior side of the sacroiliac joints, and two springs representing the anterior sacroiliac ligaments (one ascending from the sacrum across to the ilium, and one descending), as shown in Fig. 5.4. Three dashpots per sacroiliac joint, and two in the pubic symphysis are responsible for the damping.

However the identification method has to undergo a major modification, again. As we have seen and discussed in Chapter 11 the data obtained from the fresh-frozen specimen were most probably partially driven by the resonances of the supporting frame. This fact makes the Frequency Response Functions not suitable for an identification algorithm as presented in Chapter 6.2. With the modal parameters at disposal, it is handy at this point to perform a correlation study based on a cost function representing the difference between experimental and analytical mode shapes. But this is also not as straight-forward as it sounds. In the next sections we will see why.

14.1 Survival of the fittest

If you remember, in Chapter 11 we were talking about a thermometer to measure the fitness of the identified modes: it was the level of rigidity of the single bones after filtering of the global modes, given in Table 11.3. To save you from having to turn back an undefined number of pages, here is the table again (Table 14.1).

All what will happen in this section is basically aimed at selecting mode shapes that could be used as targets for a correlation (meaning that the model will be updated based on them). Mode 0 is from now on set aside.

One information which is only partial is the frequency: as already mentioned, the modes which had a considerable content of global rigid motion might have occurred at that particular frequency because they got tangled in with a support mode. It is therefore difficult to decide whether the identified frequency is now of a support resonance, of a pelvis mode, or of a coupled mode.

For the same reason, it is also necessary to confirm that the identified modes are all different, and not a same highly damped mode being co-excited twice at two separate

Table 14.1: (alias Table 11.3): Rigidity of the individual bones at the modes identified by SDT.

Mode	Frequency	Bone		
	Hz	R	S	L
0	-	0.10	0.80	0.20
1	75.6	0.17	0.66	0.29
2	132.5	0.65	0.72	0.83
3	139.3	0.49	0.83	0.70
4	230.6	0.71	0.83	0.67
5	245.0	0.66	0.91	0.52
6	340.0	0.40	0.74	0.52
7	503.0	0.51	0.46	0.50

support resonances. A first survey was performed by calculating the MAC values among the seven modes (after having filtered out the global rigid body motion, thus the MAC values among the x_{el} introduced in Eq. (11.1)). Of course the values on the diagonal are a perfect 1, but what deserves our interest are the off-diagonal values. As shown in Table 14.2, there are indeed values between modes 2 and 5, and mode 3 and 5, which are not negligible: 0.47 and 0.50. Curiously enough, the MAC value between modes 2 and 3 is not high.

Table 14.2: MAC values in % within the seven identified modes, after having filtered out the global rigid body motion.

	1	2	3	4	5	6	7
1	100	6	17	3	12	4	10
2	6	100	17	38	47	9	17
3	17	17	100	13	50	1	2
4	3	38	13	100	13	12	27
5	12	47	50	13	100	7	8
6	4	9	1	12	7	100	16
7	10	17	2	27	8	16	100

To investigate a possible relation between the three modes 2, 3 and 5, additional tests were quickly performed. Visualization of modes 2 and 5 together, and of modes 3 and 5 together did not provide qualitative evidence that mode 5 was a resurgence of modes either 2 or 3. Moreover projecting mode 5 on the space created by mode 2 and 3 together left a component of mode 5 which, if evaluated in terms of ratio of norms, was still 55% of its original self (should mode 5 be a combination of modes 2 and 3, no residuals outside the space of modes 2 and 3 would be left after the projection). We therefore concluded that all seven modes had an independent right to be.

If we now look for the highest figures for the rigidity of three bones in Table 14.1, a first group of three modes stands up: modes 2, 4, and 5. The high level of rigidity of

the individual bones means that they were probably well identified and are thus "fit for correlation". In order of decreasing fitness, they are followed by mode 3, mode 6 and mode 1. That mode 1 appears to be the least reliable one is actually unfortunate, since one of the requirements for a satisfactory correlation is, in our view, that the first analytical mode corresponds to the first measured mode.

The consequence is that a correlation between the analytical and experimental first mode is to be based on the mode shape and not on the frequency, a limitation which applies to all other modes with high level of global (not individual!) rigidity.

The next course of action is to set up a model updating routine, which tunes the parameters of the model with the intent of obtaining the same mode shapes, possibly starting with mode 1, and continuing with the fittest modes 2, 4, and 5. Ok, but which parameters?

14.2   Evolution still in progress

This elliptic title wants at this point to sow and carefully cultivate a particular mind-set in you readers, which will accompany us into the conclusions, and in which we quietly realize that we have indeed come a long way, but that the fabulous journey is not over yet. At the same time it wants to inspire that glow of marvel which surrounds all things which, even though not having come to completion, bear an intrinsic drive for advancement, like evolution. There is no end and no failure. Only onward motion.

During this last phase several paths have been searched. In a first approach the parameters chosen for the updating of the model were the position of the attachment points of all springs except the two at the pubic symphysis. It is in fact our belief that the configuration of the springs is the key to effectively reach the desired mode shape scenario. The mentioned positions were allowed to change of 1 cm in each direction.

It has still to be mentioned that a very brief post-processing had to be performed on the analytical modes as well. As we have seen, the $\boldsymbol{\alpha}_g$ have been derived by assuming $\boldsymbol{R}_g^T \boldsymbol{x}_{el} = \boldsymbol{0}$, which means that the elastic mode shapes are orthogonal to the rigid body modes (contained in $\boldsymbol{R}_g$). As briefly introduced in Chapter 4.3 however, the analytical mode shapes are orthogonal to one other with respect to the mass (and stiffness) matrix, and not directly. Therefore, to obtain a comparable motion at the periphery, the analytical mode shapes at the model degrees of freedom had to be transformed in displacements at the periphery, and then filtered, exactly as the measurements were, with the same matrix $\boldsymbol{R}_g$. The equivalent of $\boldsymbol{x}_{el}$, but now of the **model** and which we call $\boldsymbol{x}_{model,corr}$, is such that $\boldsymbol{R}_g^T \boldsymbol{x}_{model,corr} = \boldsymbol{0}$ (mode shapes this time directly orthogonal to the rigid body modes, and not through the mass matrix), and is what was used for

the correlation. We realize that this might be confusing, so here is a scheme that might help (Fig. 14.1). The correlation is thus performed between $\boldsymbol{x}_{model,corr}$ and $\boldsymbol{x}_{corr}$.
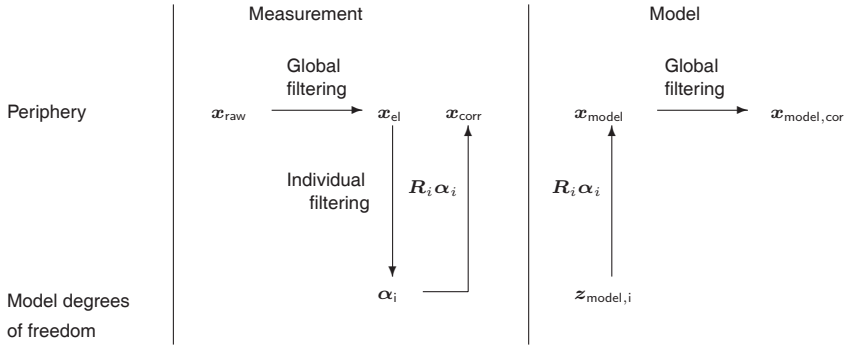

Figure 14.1: Scheme depicting the filtering and transformation necessary to obtain comparable motions at the periphery from the model and the measured data.

Cost-function optimization in modal domain

The updating was performed by creating a cost function $J(p)$. In this function the MAC values (Eq. (4.49)) were calculated between a predefined set of measured-filtered modes and a predefined set of analytical modes, expressed at the periphery. The sum of the obtained MAC values was subtracted from its maximal theoretical value (1 times the number of modes to match N_{modes}), and given as the cost of the function, as follows:

$$J(p) = N_{modes} - \sum_{modes} MAC(\boldsymbol{x}_{corr}, \boldsymbol{x}_{model,corr}(p)). \qquad (14.1)$$

A perfect match of all the considered modes would result in a cost value of zero. The cost function therefore just had to be minimized with the coordinates of the attachment points of the springs (except the two at the pubic symphysis) as parameters for updating. This was performed using the standard optimization tools available in the mathematical environment where the model was created[1].

With no exception, the experimental mode 1 was always paired with the analytical mode 1, since this was one of our target points. The updating with this mode alone was actually very successful: the positions of the springs were changed to obtain a

---

[1]Matlab, function *fminsearch*.

MAC value of 0.95. Similar brilliant results were achieved by the matching of any one mode. But what happens with more modes?

A first step in a systematic approach was to perform a series of optimization of experimental mode shapes 1 and 2, to be matched with analytical mode shapes 1 and x (with $x = 2, 3, 4, 5$). The results showed quite promising values (see Table 14.3).

Table 14.3: MAC values in % calculated between experimental modes 1-2 (indicated as Exp. m.), and updated analytical modes 1-2, 1-3, 1-4 and 1-5 (indicated as An. m.).

Exp. m.	1	2	1	2	1	2	1	2
An. m.	1	2	1	3	1	4	1	5
MAC %	68	75	54	79	77	95	76	88

The next step was to select the best combination and continue by adding a third mode matching. This was performed for experimental modes 1-2-3, and analytical modes 1-4-x (with $x = 5, 6, 7, 8$). Table 14.4 shows the calculated MAC values.

Table 14.4: MAC values in % calculated between experimental modes 1-2-3 (indicated as Exp. m.), and updated analytical modes 1-4-5, 1-4-6, 1-4-7 and 1-4-8 (indicated as An. m.).

Exp. m.	1	2	3	1	2	3	1	2	3	1	2	3
An. m.	1	4	5	1	4	6	1	4	7	1	4	8
MAC %	67	91	25	63	83	51	74	89	10	75	93	16

The idea was to continue like this until a good matching was obtained. The best combination in this second step was experimental modes 1-2-3 versus analytical modes 1-4-6, and the fourth mode matching was introduced similarly as before. This path unfortunately became less and less enlightening the more we followed it, and soon we were lost in a forest of equally modest results, unable to make a choice between the best way to go. Moreover there were combinations the optimization routine could not make head or tail of, and just quit.

One interesting lead was provided by the observation that experimental mode 5 could just not find a suitable match with the mode it was assigned to: its highest MAC score was of 0.31, which was achieved by relegating the otherwise respectable match of experimental mode 4 to a mere 0.08. A closer observation of experimental mode 5 revealed that indeed it was a "difficult" mode, very complex in the sense that the 39 measurements composing it showed a wide range of phase shift between one another (a normal mode is real and all degrees of freedom show synchronized motions, while a complex mode, resulting from heavy non-proportional damping, show highly out-of-phase motions, see Chapter 4.3).

At this point a check was performed on the efficacy of the updating procedure to produce an analytical mode which bore the same level of complexity as experimental mode 5. Single mode matchings were then performed between experimental mode 2 (an almost "real" one) and analytical mode 2, and afterwards between experimental mode 5 (the quite "complex" one) and analytical mode 5. The results were evaluated by plotting the 39 complex values in the complex plane: the values of a normal mode all lie on a line which goes through the origin (they don't have to be real, but they do have to have 0 or 180° phase shift between one another). Fig. 14.2 illustrates the complexity of experimental modes 2 and 5, and the analytical match that the update procedure produced, and show that the level of complexity can be successfully reproduced when one single mode is optimized.

Encouraged by this, we tried to match some arbitrary combinations of analytical modes (the ones that the optimization routine could handle) to the experimental modes 1, 2 and 5, since what we wanted to see was whether the updating procedure could create at the same time a very "real" mode and a very "complex" one. One combination was successful: experimental modes 1-2-5 versus analytical modes 1-3-6. Visualization of the complexity plots of the analytical modes showed that while the (faint) level of complexity of experimental modes 1 and 2 was satisfactorily reproduced, the matching of mode 5 was much more "real" than its target.

The next logic course of action was to give the update routine the possibility to use the damping coefficients of the three joints as additional parameters for tuning (remember that until now only the positions of the springs were the updating parameters). Repeating the matching of experimental modes 1-2-5 versus analytical modes 1-3-6 showed no change: the damping coefficients were indeed slightly changed, but with no influence on the results.

The obvious suspect at this point was that the damping model was simply wrong. We needed a clue, and we found it by looking at the MAC tables where both experimental modes 2 and 5 were used. Very curiously, experimental mode 5 kept having little correlation to the analytical mode it was assigned to, but a much better MAC value with the analytical mode already assigned to reproduce experimental mode 2. It seemed that experimental mode 5 was "following" in a way what experimental mode 2 was doing, and ending up matching with the counterpart of mode 2 a lot better than its own counterpart. And this is almost puzzling if we remember how "real" mode 2 is, and how "complex" mode 5.

Somehow there was something similar about those two modes, and at the same time so profoundly different to cause such a drastic "complexification" (forgive me the neologism). The mysterious damping must be considerably activated by mode 5 and

159

Figure 14.2: Complex decomposition of the displacements of experimental modes (solid lines) and its optimal analytical match (dotted lines) for (a) experimental mode 2 versus analytical mode 2, and (b) experimental mode 5 versus analytical mode 5. The lines go from measurement 1 to measurement 39, decomposed in their real and imaginary parts, and are scaled so that measurements 1 of the experimental mode and the analytical mode coincide.

Table 14.5: MAC values in % calculated between experimental modes 1 through 7, and analytical modes 1 through 12, obtained by optimizing the matching between experimental modes 1-2-4-5 and analytical modes 1-3-6-7, indicated by the shaded cells.

	Experimental modes						
	1	2	3	4	5	6	7
1	66	7	32	6	33	16	2
2	27	0	31	20	22	11	1
3	2	81	19	21	51	8	7
4	11	5	16	6	10	20	9
5	4	4	3	0	1	0	0
6	2	46	22	54	21	11	24
7	14	21	27	1	33	18	2
8	0	2	3	7	0	2	16
9	8	1	3	0	0	10	8
10	3	8	1	6	2	1	19
11	13	3	2	5	1	19	7
12	0	0	3	3	1	8	10

(Analytical modes label the rows 1 through 12.)

not by mode 2. To unravel this puzzle we visualized the two modes together in search of a distance between two points (or more distances between more points), which was not or barely changing in one mode, and obviously changing in the other (a dashpot between those two points could then explain the difference in complexity). But the eureka moment never came.

However, we were not ready to capitulate yet. We replaced the threesome of dashpots in the sacroiliac joints with just one dashpot (per joint), and we used their attachment points as parameters for the updating. At this point the parameters were the attachment points of the five springs per side, of the one dashpot per side, and of the damping coefficients in the pubic symphysis and in the sacroiliac joints. The optimization between experimental modes 1-2-4-5 and analytical modes 1-3-6-7 bravely ran a whole night (other combinations would bring the optimization routine to a complete shut-down), and indeed the results showed a slightly better MAC for mode 5, as shown in Table 14.5, and a decidedly better matching of the level of "complexity", as depicted in Fig. 14.3 and 14.4. Table 14.5 reports the whole MAC table, to provide a feeling for the matching results obtained between the other modes as well.

A glance at the optimal parameters however stroke us with something peculiar: many of the parameters just showed either their maximum or minimum value allowed (provided by us as constraints). Did that mean that they had not even been touched by the standard optimization routine, or that they had settled on the extremes because
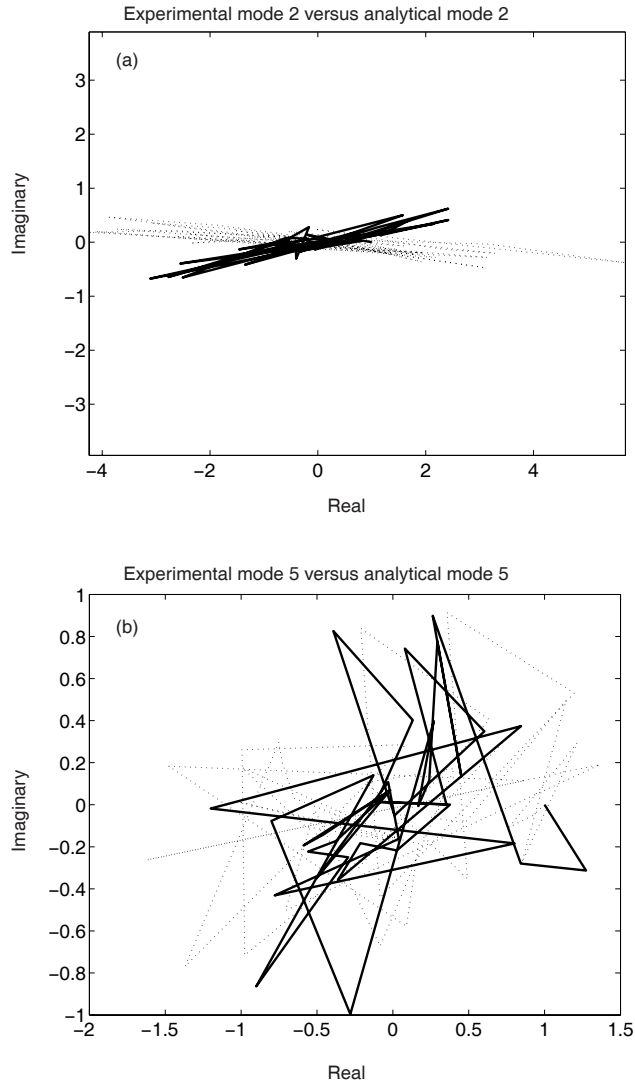
Figure 14.3: Complex decomposition of the displacements of experimental modes (gray line) and its optimal analytical match (black line) for (a) experimental mode 1 versus analytical mode 1, and (b) experimental mode 2 versus analytical mode 3. The lines go from measurement 1 to measurement 39, decomposed in their real and imaginary parts, and are scaled so that measurements 1 of the experimental mode and the analytical mode coincide.
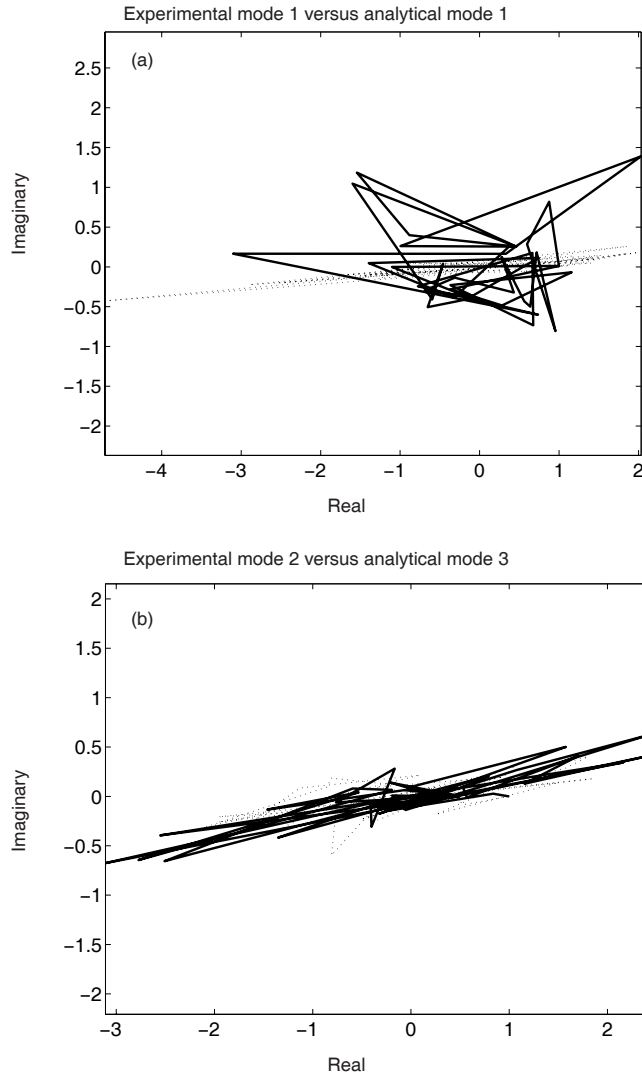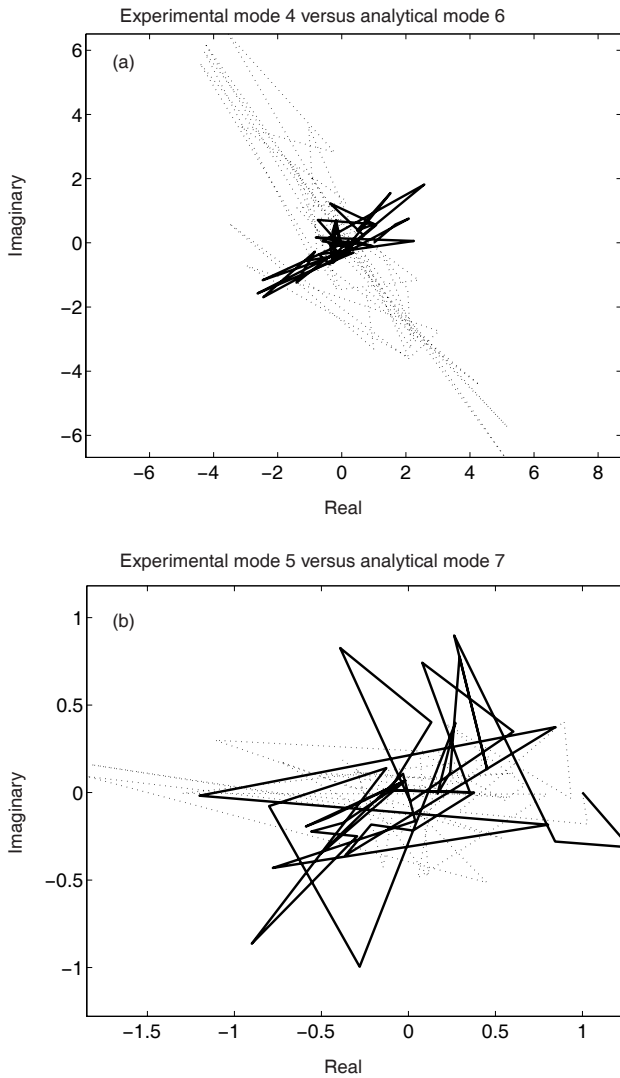
Figure 14.4: Complex decomposition of the displacements of experimental modes (gray line) and its optimal analytical match (black line) for (a) experimental mode 4 versus analytical mode 6, and (b) experimental mode 5 versus analytical mode 7. The lines go from measurement 1 to measurement 39, decomposed in their real and imaginary parts, and are scaled so that measurements 1 of the experimental mode and the analytical mode coincide.

163

they could go no further, even though that was the direction involving improvement? Was the minimum search routine actually able to deal with an otherwise sound and well-put minimization problem? Was it to be trusted at all?!?

These questions are still very clear in my mind, since they date only two months back at the time I am writing these words. That was the last entry in my work journal: May 21, 2006.

Today is July 21, 2006.

PART VI

THE CLOSURE

אב

9 August 2006

That's it.

Almost four years have gone by. I am about to pack my
stuff and leave again. I have survived life's siege, even
if at times I thought I was going to lose my sanity, and
everything else. It really seems just a last minute twitch,
doesn't it? Surviving or dying. Some say that what matters
is what we learn along the way. That's all well and good:
but as a survivor I might benefit from this newly acquired
wisdom. What would a victim benefit from?

Regarding the scroll, I have explained my theory, the
difficulties, the frustration and the tentative conclusions.
Hopefully I have also transmitted between the lines the beauty
and fascination of its symbolism.
Would it have been more beautiful had I succeeded in
unraveling the whole mystery? On the contrary.

The only thing that is not in question, set there almost
as a warning (I see it now), is the word on the cover:
the alphabet.

 "Caution: God inside.
  All attempts to reproduce this work will fail".

Conclusions and recommendations

T HAS BEEN a long journey, in which we have encountered more questions than answers. But isn't it so that the crude taste of an unrefined answer is in fact the drive to refine it? The combined efforts of three PhD students (see pages 8 and 102) aimed at the development of a diagnostic tool for the detection of abnormalities in the mechanical properties of the sacroiliac region, which in our idea lead to low back pain.

Apparatus

The hardware part of the tool - the apparatus - exists now in form of an ensemble of functional units. An electromechanical shaker introduces the excitation in the system, while a validated two-channel ultrasound technique detects the dynamic response. The redesign of those functional units in a compact affordable apparatus is bound to success. And no matter what, the developed ultrasound technology has for sure broader perspectives ahead than our little dynamics lab.

Methodology

The methodology - the post-process of the raw data coming from the apparatus, as well as the subject of this dissertation - is also in an advanced state of development.

- A dynamic model of the human pelvis has been created, in which the modeling of stiffness and damping escapes its purely mathematical grid and assumes a reality-driven physical meaning. It might well be that the true meaning has not been fully grasped yet, but the knowledge gained in the process is priceless, and points in the right direction.

  Our feeling is that the model is close to representing reality: the pelvic girdle is composed of three bones, and in the range of frequencies where they behave as rigid bodies, they are to be modeled with three rigid bodies.

  It has been shown that the minimal number of springs is given. With two springs used to fix the pubic symphysis, the sacrospinous, the sacrotuberous and the iliolumbar ligaments as the Big Absents in the dynamic response of the pelvis, and the justifiable assumption of symmetry, the remaining ten are to be specu-

169

larly distributed at the sacroiliac joints on either side. There are just not so many anatomically sound ways of putting them.

The damping is for sure the most difficult characteristics. It is a plausible idea that it is generated in the cartilage, but tests on the ligaments suggest that they might be partly responsible for it, and after having worked with the fresh-frozen specimens, we have no doubts about it. The ligamentous system on the dorsal side of the sacroiliac joints is a heavy mass of tissue: it is very unlikely that there is no dissipation taking place in its weave. Moreover, the huge difference might have been noticed between the high damping level used in the cost-function optimization in frequency domain (Chapter 6.2) and the decidedly lower level applied in the following studies (the investigation on the frequency dependence in Chapter 7, and the correlation study in Chapter 14). In the first study mentioned here, the criterium to set the damping coefficient values was to obtain a simulated FRF whose peaks showed the same "sharpness" as the measured ones. By doing this we were forced (by our choice of damping model) to "drown" a number of modes in (very!) supercritical damping. In the following studies however we needed to resuscitate them, since our intent was to identify, by means of standard modal analysis tools, the modal parameters of all the modes present. No more "drowning" was allowed, on the contrary: it was purposefully avoided. In the end all comes down to the fact that we still have no appreciation for the nature of the damping in a human pelvis. This level of understanding can be obtained by repeated and reliable measurements *in vivo*. In our case, the learning process necessary to establish an experimental protocol allowing for reliable *in vitro* measurements already took all the time we had, and we had just started measuring *in vivo*. Now it is left to the successors to develop a feeling for this eluding damping nature, and revisit both the damping of the ligaments and of the model.

- Nevertheless, the skeleton of the methodology has been born and nurtured for some time now: it is a developing creature who has already proven itself against some adversities. The identification algorithms are based on the model, and are therefore virtually correct. Since we have rectified our position and admitted that more modes are present in the range of frequency where the bones behave rigidly, an identification in modal domain is conceivable, but not in the form presented in Chapter 6.1. The inevitable presence of the noise and the probable imprecision in the measurements should be taken into account. A cost function based on the MAC values between mode shapes, however, as used in the corre-

lation study in Chapter 14 could be a possible alternative. In frequency domain, the efficacy of the cost function can indeed be further investigated against other formulations (e.g. magnitude and phase, instead of real and imaginary part), but the one implemented here proved to work in the simulations, and that was the achieved brick on which to build further. It should not be forgotten that, despite the commercially oriented goal, this research started from scratch and was basic to the core.

Difficult

However, this creature - the identification methodology - is not fully mature yet. It is healthy, determined and resilient, but it might be that its destiny is to fail in order to generate new ideas, a phoenix of the intellect.

- To start with, the target system, the human pelvis, has the elusiveness and the dignity unique to seniority: it has been around long before our little selves trying to describe it, and it might be just beyond our, or for that matter any, nicely formulated mathematical description. For those of you open to this, there might be just too much God in it to reveal itself so easily. The human body remains a wondrous machine.

- Moreover, the life flowing and pulsating and sometimes aching in a living body makes it very unquiet and urgent. It is a clockwork of processes, a maze of communication channels, a balance of chemistry that just cannot indulge us in our request for a sine-sweep long immobility. A human body cannot act a complete standstill, even with the strongest willpower (actually, functionality which resists cognitive boycott must be the primary failsafe mechanism embedded in sentient living organisms). And even if we could reduce the measurement time *in vivo* to a snapshot, there is no way to tell whether the same system ten minutes later would respond in the same way. *Panta rhei*, life more than anything.

- In addition, the strategy adopted to create the model was bottom-up, with the idea to start from the bare skeletal and ligamentous system and build in other structures should we deem it necessary. We actually never got that far as to think whether we should implement the various organs which are contained in, or surround the pelvis *in vivo*. Their presence adds mass, stiffness and damping to the system, which are necessarily going to influence the measurements *in vivo*, and which, since absent in our model, we are not able to interpret. However, a top-down approach, where all the organs and tissues of the trunk (and possibly

legs) were to be modeled from the beginning, would have probably seen us, after four years, still trying to enumerate and investigate the individual mechanical characteristics before combining them in a single model.

- As if this weren't enough, our methodology creature seems to have been rapt by this halo of mystery and elusion as well, and has decided, rascally, to play hide-and-seek. The formulation of the problem may be valid and sound, but if the answer to the cost minimization problem cannot be provided by the optimization routine, our creature, waiting impatiently for its playmate, might never be found. In fact the optimization routine was a stone in the shoe during the whole journey. We never really trusted it and tried repeatedly to improve on it, but it never gained our confidence. Many results in this work come from it. Our suggestion to the potential successors is to make the optimization robust and efficacious before upgrading or further developing the method. It is ancillary to the formulation of the problem, but it is primary for its solution.

Promising

All what we have shown in this work has been obtained with *in vitro* measurements which, despite our best efforts, had been affected by inaccuracies or plain mistakes. It is almost a cosmic injustice that just when we thought of having tried and erred all we could try and err, the time for experiments was up. We still nurture the idea that good dynamic measurements on a fresh-frozen pelvis can be obtained, and we think we know how. That would be the first thing to do, should this work be continued.

Much in these pages, however, seems to suggest that the mechanical properties of the sacroiliac joints are not to be directly identified. But even so, our little toddler - the identification method as it has been designed - does not just recite the identified values of springs and dashpots. It recites, period. Now that we have learned to listen to it, even if its baby talk remains unintelligible for us, we can still tell when and how its wording changes, or the accent, or the urgency in the voice. We can very well tell whether something is different. A longitudinal monitoring of a patient (the observation of a patient over time) might detect objective changes in the raw data collected by the ultrasound instrument, even though not associated to stiffness values of the sacroiliac ligaments. At least we would be able to inform the patient that the response of its pelvis is now shifted, and that symptoms might set in.

Between you and me

As suggested before, I have not many certainties to share with you at this time (forgive me the unadvised use of the first singular pronoun, but at this level of subjectivity it is imperative), and I commit these words to paper in pencil.

I have developed the very personal impression that the identification of the mechanical properties of the sacroiliac joints as attempted here is not feasible. There is, in my opinion, and I find it wonderful indeed, just too much life involved of which we have only a very vague idea: the organs surrounding the pelvis, the muscles, the ongoing processes. I still think, though, that the raw data obtained by the ultrasound technique can be used in many other ways (e.g. in a longitudinal follow-up of patients), and contain more information that we can realize now. Moreover, the know-how gathered throughout these years in experimenting with human specimens and divulged to the scientific community will remain.

For me, the purpose of this journey has been fulfilled through the journey itself. Set aside the valid contributions provided to science in terms of methods and expertise, I have learned a lot, and the fact that there is at present no outcome ready for marketing does not deprive me of the feeling of achievement. On the contrary. I have found a subtle noble sense of accomplishment in doing research with the unique purpose of accruing and sharing knowledge. A sense that wouldn't have been possible with a goal-oriented drive to distract me and lead the way.

And now, I have just this logbook to show, this contribution of mine, the attestation of having been here and thought these thoughts and fought these little battles. To me, unforgettable.

Appendices

Appendix A: Lagrange equations

The first step to obtain Hamilton's principle is the time integration of the virtual work principle:

$$\int_{t_1}^{t_2} \left(\sum_{k=1}^{n} (m_k \ddot{\vec{u}}_k(\boldsymbol{q}) - \vec{F}_k) \cdot \delta_{q_s} \vec{u}_k(\boldsymbol{q}) \right) dt = 0, \tag{A-1}$$

expressed here for a system with n masses subjected to the forces $\vec{F}_k$ and whose positions are defined by the vectors $\vec{u}_k(\boldsymbol{q})$ dependent on the N generalized coordinates $\boldsymbol{q}$. These forces can be internal and external, and can be conservative and non-conservative.

Conservative systems

If we assume that the applied forces $\vec{F}_k$ are conservative (e.g. internal elastic forces, external gravitational forces), we can express them as the gradient of a potential $\mathcal{V}$

$$\sum_{k=1}^{n} \vec{F}_k \cdot \delta \vec{u}_k = -\delta \mathcal{V}, \tag{A-2}$$

where $\delta \vec{u}_k$ stands for $\delta_{q_s} \vec{u}_k$.

If we consider that

$$\begin{aligned}
\frac{d}{dt}(m_k \dot{\vec{u}}_k \cdot \delta \vec{u}_k) &= m_k \ddot{\vec{u}}_k \cdot \delta \vec{u}_k + m_k \dot{\vec{u}}_k \delta \dot{\vec{u}}_k \\
&= m_k \ddot{\vec{u}}_k \cdot \delta \vec{u}_k + \delta \left(\frac{1}{2} m_k \dot{\vec{u}}_k \cdot \dot{\vec{u}}_k \right),
\end{aligned} \tag{A-3}$$

the inertia term in Eq. (A-1) can be written as

$$m_k \ddot{\vec{u}}_k \cdot \delta \vec{u}_k = \frac{d}{dt}(m_k \dot{\vec{u}}_k \cdot \delta \vec{u}_k) - \delta \left(\frac{1}{2} m_k \dot{\vec{u}}_k \cdot \dot{\vec{u}}_k \right). \tag{A-4}$$

By recalling the definition of kinetic energy $\mathcal{T}$ in the system being

$$\mathcal{T} = \frac{1}{2} \sum_{k=1}^{n} m_k \dot{\vec{u}}_k \cdot \dot{\vec{u}}_k \tag{A-5}$$

175

and by considering the expression in Eq. (A-4), Eq. A-1 can be rewritten as

$$\left[-\sum_{k=1}^{n} m_k \dot{\vec{u}}_k \delta \vec{u}_k \right]_{t_1}^{t_2} + \delta \int_{t_1}^{t_2} (\mathcal{T} - \mathcal{V}) dt = 0. \tag{A-6}$$

One of the assumptions on the virtual displacement is that $\delta \vec{u}_k(t_1) = \delta \vec{u}_k(t_2) = \mathbf{0}$, meaning that the first term of Eq. A-6 can be eliminated.

What is left leads to Hamilton's principle for a conservative system, which states that the integral

$$\int_{t_1}^{t_2} (\mathcal{T} - \mathcal{V}) dt \tag{A-7}$$

has a stationary value for the correct path of motion and for all compatible virtual displacements, arbitrary between t_1 and t_2 but zero at the end of the time interval, mathematically expressed as

$$\delta \int_{t_1}^{t_2} (\mathcal{T} - \mathcal{V}) dt = 0. \tag{A-8}$$

Developing the expressions of $\mathcal{T}$ and $\mathcal{V}$ as functions of the N generalized coordinates q_s, the following results:

$$\delta \mathcal{T} = \sum_{s=1}^{N} \left(\frac{\partial \mathcal{T}}{\partial q_s} \delta q_s + \frac{\partial \mathcal{T}}{\partial \dot{q}_s} \delta \dot{q}_s \right), \tag{A-9}$$

and Eq. (A-8) becomes

$$\int_{t_1}^{t_2} \sum_{s=1}^{N} \left((\frac{\partial \mathcal{T}}{\partial q_s} + F_s) \delta q_s + \frac{\partial \mathcal{T}}{\partial \dot{q}_s} \delta \dot{q}_s \right) dt = 0. \tag{A-10}$$

The last term can be integrated by parts as follows:

$$\int_{t_1}^{t_2} \frac{\partial \mathcal{T}}{\partial \dot{q}_s} \delta \dot{q}_s dt = \left[\frac{\partial \mathcal{T}}{\partial \dot{q}_s} \delta q_s \right]_{t_1}^{t_2} - \int_{t_1}^{t_2} \frac{d}{dt} \left(\frac{\partial \mathcal{T}}{\partial \dot{q}_s} \right) \delta q_s dt, \tag{A-11}$$

which, considering that $\delta q_s(t_1) = \delta q_s(t_2) = 0$, turns Eq. (A-10) in the expression

$$\int_{t_1}^{t_2} \sum_{s=1}^{N} \left(-\frac{d}{dt} \left(\frac{\partial \mathcal{T}}{\partial \dot{q}_s} \right) + \frac{\partial \mathcal{T}}{\partial q_s} - \frac{\partial \mathcal{V}}{\partial q_s} \right) \delta q_s dt = 0. \tag{A-12}$$

Since δq_s is arbitrary in the time interval between t_1 and t_2, the Lagrange equation for

conservative systems results in

$$-\frac{d}{dt}\left(\frac{\partial \mathcal{T}}{\partial \dot{q}_s}\right) + \frac{\partial \mathcal{T}}{\partial q_s} - \frac{\partial \mathcal{V}}{\partial q_s} = 0.$$

(A-13)

Non-conservative systems

An internal dissipation force acts in the opposite direction as the velocity vector and is a function of its absolute value. Its amplitude can be expressed as

$$\boldsymbol{F}_k = -C f_k(\|\dot{\bar{\boldsymbol{u}}}_k\|_2)\frac{\dot{\bar{\boldsymbol{u}}}_k}{\|\dot{\bar{\boldsymbol{u}}}_k\|_2}.$$

(A-14)

It can be shown that by defining a dissipation function

$$\mathcal{D} = \sum_{k=1}^{n} \int_0^{\|\dot{\bar{\boldsymbol{u}}}_k\|_2} C f_k(\kappa) d\kappa,$$

(A-15)

the generalized dissipation force is given by

$$Q_s^D = -\frac{\partial \mathcal{D}}{\partial \dot{q}_s}.$$

(A-16)

With the ensemble of the other non-conservative forces defined with Q_s, the Lagrange equations can be thus expressed as

$$-\frac{d}{dt}(\frac{\partial \mathcal{T}}{\partial \dot{q}_s}) + \frac{\partial \mathcal{T}}{\partial q_s} - \frac{\partial \mathcal{V}}{\partial q_s} - \frac{\partial \mathcal{D}}{\partial \dot{q}_s} + Q_s = 0.$$

(A-17)

If we now define

$$\frac{\partial \mathcal{T}}{\partial \dot{q}_s} \equiv g(\boldsymbol{q}, \dot{\boldsymbol{q}}, t),$$

(A-18)

we can develop the first term as

$$\frac{d}{dt}(\frac{\partial \mathcal{T}}{\partial \dot{q}_s}) = \frac{dg}{dt} \quad = \quad \frac{\partial g}{\partial t} + \sum_r \frac{\partial g}{\partial q_r}\frac{\partial q_r}{\partial t} + \sum_r \frac{\partial g}{\partial \dot{q}_r}\frac{\partial \dot{q}_r}{\partial t}$$

(A-19)

$$= \quad \frac{\partial g}{\partial t} + \sum_r \frac{\partial g}{\partial q_r}\dot{q}_r + \sum_r \frac{\partial g}{\partial \dot{q}_r}\ddot{q}_r.$$

(A-20)

The term multiplied with $\ddot{q}_r$ is per definition the inertia term

$$M_{sr} \equiv \frac{\partial^2 \mathcal{T}}{\partial \dot{q}_s \partial \dot{q}_r},$$

(A-21)

177

and the remaining terms express the force involved

$$f_s \equiv \frac{\partial^2 \mathcal{T}}{\partial t \partial \dot{q}_s} + \sum_r \frac{\partial^2 \mathcal{T}}{\partial \dot{q}_s \partial q_r} \dot{q}_r - \frac{\partial \mathcal{T}}{\partial q_s} + \frac{\partial \mathcal{V}}{\partial q_s} + \frac{\partial \mathcal{D}}{\partial \dot{q}_s} - Q_s. \tag{A-22}$$

In matrix form the following expression results:

$$\boldsymbol{M}(\boldsymbol{q})\ddot{\boldsymbol{q}} + \boldsymbol{f}(\boldsymbol{q}, \dot{\boldsymbol{q}}) = \boldsymbol{0}. \tag{A-23}$$

Appendix B: Eigenproblem in state space

The equations of motion of a system with N degrees of freedom are formulated in state space as follows:

$$\begin{bmatrix} \boldsymbol{K} & \boldsymbol{0} \\ \boldsymbol{0} & -\boldsymbol{M} \end{bmatrix} \begin{pmatrix} \boldsymbol{q}(t) \\ \dot{\boldsymbol{q}}(t) \end{pmatrix} + \begin{bmatrix} \boldsymbol{C} & \boldsymbol{M} \\ \boldsymbol{M} & \boldsymbol{0} \end{bmatrix} \begin{pmatrix} \dot{\boldsymbol{q}}(t) \\ \ddot{\boldsymbol{q}}(t) \end{pmatrix} = \begin{pmatrix} \boldsymbol{f}(t) \\ \boldsymbol{0} \end{pmatrix}. \tag{B-1}$$

This can be expressed as a differential equation of first order:

$$\boldsymbol{A}\boldsymbol{r}(t) + \boldsymbol{B}\dot{\boldsymbol{r}}(t) = \boldsymbol{s}(t), \tag{B-2}$$

by defining

$$\boldsymbol{A} \equiv \begin{bmatrix} \boldsymbol{K} & \boldsymbol{0} \\ \boldsymbol{0} & -\boldsymbol{M} \end{bmatrix}, \tag{B-3}$$

$$\boldsymbol{B} \equiv \begin{bmatrix} \boldsymbol{C} & \boldsymbol{M} \\ \boldsymbol{M} & \boldsymbol{0} \end{bmatrix}, \tag{B-4}$$

$$\boldsymbol{r}(t) \equiv \begin{pmatrix} \boldsymbol{q}(t) \\ \dot{\boldsymbol{q}}(t) \end{pmatrix}, \tag{B-5}$$

$$\boldsymbol{s}(t) \equiv \begin{pmatrix} \boldsymbol{f}(t) \\ \boldsymbol{0} \end{pmatrix}. \tag{B-6}$$

The general solution of the homogeneous case is found by assuming

$$\boldsymbol{q}(t) = \boldsymbol{z}e^{\lambda t}, \tag{B-7}$$

so that the variable $\boldsymbol{r}(t)$ results in

$$\boldsymbol{r}(t) = \begin{pmatrix} \boldsymbol{z} \\ \lambda \boldsymbol{z} \end{pmatrix} e^{\lambda t} = \boldsymbol{y}e^{\lambda t}. \tag{B-8}$$

Substitution in the homogeneous version of (B-2) results in the eigenproblem

$$\boldsymbol{A}\boldsymbol{y} + \lambda \boldsymbol{B}\boldsymbol{y} = \boldsymbol{0}, \tag{B-9}$$

which generates $2N$ eigensolutions, composed by N eigenvalues $\lambda_s = -\sigma_s + i\omega_s$ and their complex conjugates $\bar{\lambda}_s = -\sigma_s - i\omega_s$, and N eigenvectors $\boldsymbol{y}_s$ and their N

179

complex conjugates $\bar{\boldsymbol{y}}_s$. In the following expressions, the index k is used to address the collection of $2N$ eigensolutions, instead of the index s which was used to designate the N solutions and their N complex conjugates.

For the particular solution of the inhomogeneous problem, we propose $\boldsymbol{r}(t)$ as being the superposition of the $2N$ eigenvectors just obtained, each modulated by a time function

$$\boldsymbol{r}(t) = \sum_{k=1}^{2N} \eta_k(t)\boldsymbol{y}_k. \tag{B-10}$$

By inserting this suggested solution in Eq. (B-2), premultiplying it by $\boldsymbol{y}_j$, and considering the orthogonality property of eigenvectors, we end up with $2N$ first order differential equations in η:

$$-\lambda_j \eta_j(t) + \dot{\eta}_j(t) = \varphi_j(t), \qquad j = 1..2N \tag{B-11}$$

with

$$\lambda_j = -\frac{\boldsymbol{y}_j^T \boldsymbol{A} \boldsymbol{y}_j}{\boldsymbol{y}_j^T \boldsymbol{B} \boldsymbol{y}_j}, \qquad \varphi_j(t) = \frac{\boldsymbol{y}_j^T \boldsymbol{s}(t)}{\boldsymbol{y}_j^T \boldsymbol{B} \boldsymbol{y}_j}. \tag{B-12}$$

By multiplying equation (B-11) by $e^{-\lambda_j t}$ and recognizing the form of the derivation of a product, we obtain

$$\frac{d}{dt}(e^{-\lambda_j t}\eta_j(t)) = e^{-\lambda_j t}\varphi_j(t), \tag{B-13}$$

which integrated becomes

$$\eta_j(t) = e^{\lambda_j t}\left[-\int_0^t \varphi_j(\tau)e^{-\lambda_j \tau}d\tau + \eta_j(0) \right]. \tag{B-14}$$

In case of a harmonic excitation

$$\boldsymbol{s}(t) = \boldsymbol{s}_o e^{i\omega t}, \qquad -\infty < t < +\infty,$$

$\varphi_j(t)$ assumes the form

$$\varphi_j(t) = \frac{\boldsymbol{y}_j^T \boldsymbol{s}_o e^{i\omega t}}{\boldsymbol{y}_j^T \boldsymbol{B} \boldsymbol{y}_j} = \varphi_{oj}e^{i\omega t}. \tag{B-15}$$

By assuming that the motion has been going on long enough for the transient component to have faded out, the function $\eta_j(t)$ is then obtained as follows:

$$\eta_j(t) = e^{\lambda_j t}\int_0^t \varphi_{oj}e^{(i\omega - \lambda_j)\tau}d\tau = \frac{\varphi_{oj}e^{i\omega t}}{i\omega - \lambda_j}. \tag{B-16}$$

Substitution in Eq. (B-10) results in the forced harmonic response

$$\boldsymbol{r}(t) = \sum_{s=1}^{N} \left(\frac{1}{\boldsymbol{y}_s^T \boldsymbol{B} \boldsymbol{y}_s} \frac{\boldsymbol{y}_s \boldsymbol{y}_s^T}{\sigma_s + i(\omega - \omega_s)} + \frac{1}{\bar{\boldsymbol{y}}_s^T \boldsymbol{B} \bar{\boldsymbol{y}}_s} \frac{\bar{\boldsymbol{y}}_s \bar{\boldsymbol{y}}_s^T}{\sigma_s + i(\omega + \omega_s)} \right) \boldsymbol{s}_o e^{i\omega t}. \qquad \text{(B-17)}$$

The expression $\boldsymbol{y}_s^T \boldsymbol{B} \boldsymbol{y}_s$ can be defined as

$$\rho_s \quad = \quad \boldsymbol{y}_s^T \boldsymbol{B} \boldsymbol{y}_s \qquad \qquad \text{(B-18)}$$

$$= \quad \begin{bmatrix} \boldsymbol{z}_s^T & \lambda_s \boldsymbol{z}_s^T \end{bmatrix} \begin{bmatrix} \boldsymbol{C} & \boldsymbol{M} \\ \boldsymbol{M} & \boldsymbol{0} \end{bmatrix} \begin{bmatrix} \boldsymbol{z}_s \\ \lambda_s \boldsymbol{z}_s \end{bmatrix} \qquad \text{(B-19)}$$

$$= \quad \boldsymbol{z}_s^T \boldsymbol{C} \boldsymbol{z}_s + 2\lambda_s \boldsymbol{z}_s^T \boldsymbol{M} \boldsymbol{z}_s. \qquad \qquad \text{(B-20)}$$

If we now recall that the Frequency Response Function $\boldsymbol{H}(\omega)$ is defined as the ratio between the response of the system and the force, and consider Eq. (B-8), we obtain the expression

$$\boldsymbol{H}(\omega) = \sum_{s=1}^{N} \left(\frac{1}{\sigma_s + i(\omega - \omega_s)} \frac{\boldsymbol{z}_s \boldsymbol{z}_s^T}{\rho_s} + \frac{1}{\sigma_s + i(\omega + \omega_s)} \frac{\bar{\boldsymbol{z}}_s \bar{\boldsymbol{z}}_s^T}{\rho_s} \right). \qquad \text{(B-21)}$$

Appendix C: Sensitivity

To obtain the sensitivity of the modal parameters, we start by formulating the equilibrium related to an eigensolution

$$(-\omega_s^2 M + K)z_s = 0. \tag{C-1}$$

This expression is then differentiated with respect to the parameters p as follows:

$$\left(-\omega_s^2 \frac{\partial M}{\partial p} + \frac{\partial K}{\partial p}\right) z_s - \frac{\partial \omega_s^2}{\partial p} M z_s + \left(-\omega_s^2 M + K\right) \frac{\partial z_s}{\partial p} = 0. \tag{C-2}$$

If we premultiply with z_s^T, and we remember that $(AB)^T = B^T A^T$, thus

$$\left((-\omega_s^2 M + K)z_s\right)^T = z_s^T(-\omega_s^2 M + K)^T = z_s^T(-\omega_s^2 M + K) = 0, \tag{C-3}$$

we obtain an analytical expression for the sensitivity of the eigenfrequency ω_s^2 as

$$\frac{\partial \omega_s^2}{\partial p} = \frac{z_s^T \left(-\omega_s^2 \frac{\partial M}{\partial p} + \frac{\partial K}{\partial p}\right) z_s}{\mu_s}, \tag{C-4}$$

with μ_s defined as the modal mass

$$\mu_s = z_s^T M z_s. \tag{C-5}$$

Once the sensitivity of the resonance frequency is available, the equation Eq. (C-2) can be solved for $\frac{\partial z_s}{\partial p}$, to obtain

$$\left(-\omega_s^2 M + K\right) \frac{\partial z_s}{\partial p} = \left(\omega_s^2 \frac{\partial M}{\partial p} + \frac{\partial \omega_s^2}{\partial p} M - \frac{\partial K}{\partial p}\right) z_s. \tag{C-6}$$

Since the matrix $-\omega_s^2 M + K$ is singular per definition, to solve for $\frac{\partial z_s}{\partial p}$ we have to use its generalized inverse $(-\omega_s^2 M + K)^+$. The equation becomes

$$\frac{\partial z_s}{\partial p} = \left(-\omega_s^2 M + K\right)^+ \left(\omega_s^2 \frac{\partial M}{\partial p} + \frac{\partial \omega_s^2}{\partial p} M - \frac{\partial K}{\partial p}\right) z_s, \tag{C-7}$$

which at the same time represents a particular solution $\tilde{z}_s$ of (C-6). It can also be seen that, intrinsically to the equation, αz_s is a solution as well, for all α.

A unique solution for $\frac{\partial z_s}{\partial p}$ is obtained by requesting that the modal mass μ_s be constant independently from the parameter modifications. Derivation of Eq. (C-5) with

respect to the parameters p leads to

$$z_s^T M \frac{z_s}{\partial p} = -\frac{1}{2} z_s^T \frac{\partial M}{\partial p} z_s, \qquad (C\text{-}8)$$

which substituted in the general solution $\frac{z_s}{\partial p} = \tilde{z}_s + \alpha z_s$ results in

$$\alpha = -\frac{1}{\mu_s} \left(\frac{1}{2} z_s^T \frac{\partial M}{\partial p} z_s + z_s^T M \tilde{z}_s \right). \qquad (C\text{-}9)$$

The mode shape sensitivity is thus expressed as

$$\frac{\partial z_s}{\partial p} = \tilde{z}_s - \frac{z_s}{\mu_s} \left(\frac{1}{2} z_s^T \frac{\partial M}{\partial p} z_s + z_s^T M \tilde{z}_s \right). \qquad (C\text{-}10)$$

Appendix D: State space eigensolution by frequency dependence

In Chapter 7 the frequency dependence is implemented in the equation of motion as follows:

$$\left(-\omega^2 \boldsymbol{M} + j\omega \boldsymbol{C} + j\boldsymbol{D} + \boldsymbol{K} + \omega \boldsymbol{K}'\right) \boldsymbol{z} = \boldsymbol{F} \,, \tag{D-1}$$

where $\boldsymbol{D}$ and $\boldsymbol{K}'$ are defined as in page 87:

$$\boldsymbol{D} = f_c \, \boldsymbol{C} \, \frac{\omega_{max}}{4} \,, \tag{D-2}$$

$$\boldsymbol{K}' = f_k \, \boldsymbol{K} \, \frac{1}{4 \, \omega_{max}} \,. \tag{D-3}$$

The eigenvalue problem for free vibrations writes

$$\left(-\omega_s^2 \boldsymbol{M} + j\omega_s \boldsymbol{C} + j\boldsymbol{D} + \boldsymbol{K} + \omega_s \boldsymbol{K}'\right) \boldsymbol{z}_s = \boldsymbol{0} \,. \tag{D-4}$$

Even expressed in state space, this problem has not a standard form as given in Eq. (B-9), and is thus solved iteratively. The state space matrices $\boldsymbol{A}$ and $\boldsymbol{B}$ are defined as

$$\boldsymbol{A}_i = \left[\begin{array}{cc} \boldsymbol{K} + \boldsymbol{K}'\omega_{s,i} & \boldsymbol{0} \\ \boldsymbol{0} & -\boldsymbol{M} \end{array} \right] \,, \tag{D-5}$$

$$\boldsymbol{B}_i = \left[\begin{array}{cc} \boldsymbol{C} + \frac{\boldsymbol{D}}{\omega_{s,i}} & \boldsymbol{M} \\ \boldsymbol{M} & \boldsymbol{0} \end{array} \right] \,, \tag{D-6}$$

where $\omega_{s,i}$ is the damped resonance frequency of mode s at the ith iteration step. The eigenproblem in state space is solved for each mode at each step i with the frequency dependent matrices as expressed in (D-5) and (D-6). The absolute value of the imaginary part of the obtained pole $\lambda_{s,i+1} = -\sigma_{s,i+1} \pm j\omega_{s,i+1}$ is then used to update the matrices $\boldsymbol{A}_i$ and $\boldsymbol{B}_i$ into $\boldsymbol{A}_{i+1}$ and $\boldsymbol{B}_{i+1}$, and the eigenproblem solved again. This iterative procedure is performed until convergence of the eigenvalue is reached. In mathematical form, solve

$$\left(\boldsymbol{A}_i + \lambda_{s,i+1}\boldsymbol{B}_i\right) \, \boldsymbol{z}_{s,i+1} = 0, \tag{D-7}$$

for $\lambda_{s,i+1}$ and $\boldsymbol{z}_{s,i+1}$, with

$$\omega_{s,i+1} \quad = \quad |Im(\lambda_{s,i+1})| \,, \tag{D-8}$$

$$\sigma_{s,i+1} \quad = \quad -Re(\lambda_{s,i+1}) \,, \tag{D-9}$$

until

$$\frac{\left|\omega_{s,i+1} - \omega_{s,i}\right|}{\omega_{s,i+1}} < 10^{-6} \quad and \quad \frac{\left|\sigma_{s,i+1} - \sigma_{s,i}\right|}{\sigma_{s,i+1}} < 10^{-6}, \tag{D-10}$$

where $\lambda_{s,i+1} = -\sigma_{s,i+1} \pm j\omega_{s,i+1}$ is the pole s of the system at the $i+1^{th}$ iteration step, and z_{i+1} is the mode shape for mode s at the $i+1^{th}$ iteration step. The cut-off value of 10^{-6} is the relative error in frequency and damping factor and is deemed sufficiently small.

The actual mode shape is the eigenvector obtained at convergence. The damping ratio is calculated from the converged λ_s, for each mode s:

$$\zeta_s = \frac{\sigma_s}{\sqrt{\omega_s^2 + \sigma_s^2}} \ . \tag{D-11}$$

Appendix E: Parameter values

The values used in the study of Chapter 14 are listed here. The index in indicates the innominate bone, the indexes R and L specify the right and left sides. The index scr indicates the sacrum. Where applicable, for the homologous coordinates on the left side just change the sign of the y-coordinate.

Masses of the bones in kg

$$
\begin{aligned}
m_{in} &= 0.64 \\
m_{sacrum} &= 0.36
\end{aligned}
$$

Centers of mass of the bodies in m

$$
\vec{u}_{CM,in,R} = \begin{pmatrix} -63.8\ 10^{-3} \\ -72.8\ 10^{-3} \\ -27\ 10^{-3} \end{pmatrix}
$$

$$
\vec{u}_{CM,scr} = \begin{pmatrix} -93.2\ 10^{-3} \\ 0 \\ 2.8\ 10^{-3} \end{pmatrix}
$$

Rotational inertia matrix of the left innominate bone in $kg\ m^2$

$$
\boldsymbol{I}_{in,L} = \begin{bmatrix} 1.4656\ 10^{-3} & -1.1120\ 10^{-4} & 1.3628\ 10^{-4} \\ -1.1120\ 10^{-4} & 1.5634\ 10^{-3} & -2.6670\ 10^{-4} \\ 1.3628\ 10^{-4} & -2.6670\ 10^{-4} & 7.4577\ 10^{-4} \end{bmatrix}
$$

Rotational inertia of the right innominate bone in $kg\ m^2$

$$
\boldsymbol{I}_{in,R} = \begin{bmatrix} 1.4656\ 10^{-3} & 1.1120\ 10^{-4} & 1.3628\ 10^{-4} \\ 1.1120\ 10^{-4} & 1.5634\ 10^{-3} & 2.6670\ 10^{-4} \\ 1.3628\ 10^{-4} & 2.6670\ 10^{-4} & 7.4577\ 10^{-4} \end{bmatrix}
$$

Rotational inertia of the sacrum in $kg\ m^2$

$$\boldsymbol{I}_{scr} = \begin{bmatrix} 3.3083\ 10^{-4} & 0 & -7.8333\ 10^{-5} \\ 0 & 2.2500\ 10^{-4} & 0 \\ -7.8333\ 10^{-5} & 0 & 3.1083\ 10^{-4} \end{bmatrix}$$

Attachment position of springs in mm IO: interosseus; ASA: anterior sacroiliac ascending; ASD: anterior sacroiliac descending; PSS: posterior sacroiliac short; PSL: posterior sacroiliac long; PUBH: pubic horizontal; PUBS: pubic sagittal.

$$\vec{\boldsymbol{u}}_{IO,in,R} = \begin{pmatrix} -105 \\ -30 \\ 10 \end{pmatrix} \qquad \vec{\boldsymbol{u}}_{IO,scr,R} = \begin{pmatrix} -75 \\ -25 \\ 10 \end{pmatrix}$$

$$\vec{\boldsymbol{u}}_{ASA,in,R} = \begin{pmatrix} -85 \\ -70 \\ 10 \end{pmatrix} \qquad \vec{\boldsymbol{u}}_{ASA,scr,R} = \begin{pmatrix} -75 \\ -50 \\ 0 \end{pmatrix}$$

$$\vec{\boldsymbol{u}}_{ASD,in,R} = \begin{pmatrix} -55 \\ -75 \\ -30 \end{pmatrix} \qquad \vec{\boldsymbol{u}}_{ASD,scr,R} = \begin{pmatrix} -65 \\ -55 \\ -20 \end{pmatrix}$$

$$\vec{\boldsymbol{u}}_{PSS,in,R} = \begin{pmatrix} -115 \\ -35 \\ 25 \end{pmatrix} \qquad \vec{\boldsymbol{u}}_{PSS,scr,R} = \begin{pmatrix} -110 \\ -5 \\ 15 \end{pmatrix}$$

$$\vec{\boldsymbol{u}}_{PSL,in,R} = \begin{pmatrix} -130 \\ -35 \\ -5 \end{pmatrix} \qquad \vec{\boldsymbol{u}}_{PSL,scr,R} = \begin{pmatrix} -145 \\ -5 \\ -50 \end{pmatrix}$$

$$\vec{\boldsymbol{u}}_{PUBH,in,R} = \begin{pmatrix} 0 \\ -5 \\ -95 \end{pmatrix}$$

$$\vec{\boldsymbol{u}}_{PUBS,in,R} = \begin{pmatrix} 0 \\ 0 \\ -90 \end{pmatrix} \qquad \vec{\boldsymbol{u}}_{PUBS,in,L} = \begin{pmatrix} -10 \\ 0 \\ -100 \end{pmatrix}$$

Attachment position of the dashpots in mm P1-2: dashpots 1 and 2 in the pubic symphysis; S1-3: dashpots 1 through 3 in the sacroiliac joints.

$$\vec{u}_{P1,in,R} = \begin{pmatrix} 0 \\ -35 \\ -95 \end{pmatrix}$$

$$\vec{u}_{P2,in,R} = \begin{pmatrix} -10 \\ -1 \\ -100 \end{pmatrix}$$

$$\vec{u}_{S1,in,R} = \begin{pmatrix} -79 \\ -45 \\ -0.2 \end{pmatrix} \qquad \vec{u}_{S2,scr,R} = \begin{pmatrix} -80 \\ -45 \\ 0 \end{pmatrix}$$

$$\vec{u}_{S2,in,R} = \begin{pmatrix} -92.867 \\ -58.8 \\ -0.233 \end{pmatrix} \qquad \vec{u}_{S2,scr,R} = \begin{pmatrix} -93.333 \\ -58.333 \\ 0 \end{pmatrix}$$

$$\vec{u}_{S3,in,R} = \begin{pmatrix} -79.533 \\ -38.8 \\ -13.567 \end{pmatrix} \qquad \vec{u}_{S3,scr,R} = \begin{pmatrix} -80 \\ -38.333 \\ -13.333 \end{pmatrix}$$

Stiffness coefficients in N/m io: interosseus; asa: anterior sacroiliac ascending; asd: anterior sacroiliac descending; pss: posterior sacroiliac short; psl: posterior sacroiliac long; $pubh$: pubic horizontal; $pubs$: pubic sagittal.

$$
\begin{aligned}
k_{io} &= 10^6 \\
k_{asa} &= 10^6 \\
k_{asd} &= 10^6 \\
k_{pss} &= 10^6 \\
k_{psl} &= 10^6 \\
k_{pubh} &= 10^5 \\
k_{pubs} &= 5 \, 10^3
\end{aligned}
$$

Damping coefficients in Ns/m sij: sacroiliac joint; pub: pubic symphysis.

$$c_{sij} = 0.8$$
$$c_{pub} = 0.8$$

Bibliography

[1] J.L. Bada and A. Lazcano. Origin of life: some like it hot, but not the first biomolecules. *Science*, 296(5575):1982–1983, 2002.

[2] E. Balmès. Frequency domain identification of structural dynamics using the pole/residue parametrization. In *14th International Modal Analysis Conference (IMAC XIV)*, Dearborn, Michigan, USA, February 12-15 1996. Society for Experimental Mechanics.

[3] T.J. Bartkowicz. On-orbit testing of the International Space Station: challenges of implementation. Oral presentation 24th International Modal Analysis Conference (IMAC XXIV), January 30 - February 2 2006. St. Louis, Missouri, USA.

[4] P. Canadas, S. Wendling-Mansuy, and D. Isabey. Frequency response of a viscoelastic tensegrity model: structural rearrangement contribution to cell dynamics. *Journal of Biomechanical Engineering*, 128(4):487–495, 2006.

[5] T.G. Carne. Design of tests. In *23rd International Modal Analysis Conference (IMAC XXIII)*, Orlando, Florida, USA, January 31 - February 3 2005. Society for Experimental Mechanics.

[6] T.G. Carne. Hit me baby one more time - the do's and don'ts of impact and transient excitation. In *23rd International Modal Analysis Conference (IMAC XXIII)*, Orlando, Florida, USA, January 31 - February 3 2005. Society for Experimental Mechanics.

[7] Y.C. Chen, M. Fredericson, and M. Smuck. Sacroiliac joint pain syndrome in active patients. A look behind the pain. *The Physician and sportsmedicine*, 30(11):30–37, 2002.

[8] D.H. Chow, K.D. Luk, J.C. Leong, and C.W. Woo. Torsional stability of the lumbosacral junction. Significance of the iliolumbar ligament. *Spine*, 14(6):611–615, 1989.

[9] N.E. Conza and D.J. Rixen. Dynamic response of an embalmed human pelvis - A pilot study. In *World Congress in Medical Physics and Biomedical Engineering*, Sydney, Australia, August 24-29 2003.

[10] N.E. Conza and D.J. Rixen. Dynamic model of the human pelvis - parameter identification. In *22nd International Modal Analysis Conference (IMAC XXII)*, Dearborn, Michigan, USA, January 26-29 2004. Society for Experimental Mechanics.

[11] N.E. Conza and D.J. Rixen. Biodynamical parameter estimation using frequency domain updating. In *23rd International Modal Analysis Conference (IMAC XXIII)*, Orlando, Florida, USA, January 31 - February 3 2005. Society for Experimental Mechanics.

[12] N.E. Conza and D.J. Rixen. Experimental modal analysis on a human specimen: lessons learned. *Experimental Techniques*, 30(6):(to appear), 2006.

[13] N.E. Conza and D.J. Rixen. Influence of frequency dependent properties on system identification: simulation study on a human pelvis model. *Submitted to Journal of Sound and Vibration*, 2006.

[14] N.E. Conza, D.J. Rixen, and S. Plomp. Vibration testing of a fresh-frozen human pelvis: the role of the pelvic ligaments. *Journal of Biomechanics*, Epub ahead of print, 2006.

[15] N.E. Conza, A. Soethoudt, E. Vlaanderen, and D.J. Rixen. In vivo bone vibration measurement by ultrasound. In *24th International Modal Analysis Conference (IMAC XXIV)*, St. Louis, Missouri, USA, January 30 - February 2 2006. Society for Experimental Mechanics.

[16] J.D. Currey. *Handbook of Biomaterial Properties*, chapter A1-Cortical bone, pages 3–14. Chapman & Hall, 1998.

[17] L. Damen. *Laxity Measurements of the Sacroiliac Joints in Women with Pregnancy-related Pelvic Pain*. PhD thesis, Erasmus University Rotterdam, 2002.

[18] L. Damen, T. Stijnen, M.E. Roebroeck, C.J. Snijders, and H.J. Stam. Reliability of sacroiliac joint laxity measurement with doppler imaging of vibrations. *Ultrasound in Medicine and Biology*, 28(4):407–414, 2002.

[19] W.J. Daum. The sacroiliac joint: an underappreciated pain generator. *The American Journal of Orthopedics*, 24(6):475–478, 1995.

[20] European Commission. European social statistics, accidents at work and work-related health problems. Technical report, Office for Official Publications of the European Communities, 2003.

[21] European Agency for Safety and Health at Work. Expert forecast on emerging physical risks related to occupational safety and health. Technical report, Office for Official Publications of the European Communities, 2005.

[22] European Foundation for the Improvement of Living and Working Conditions. Third european survey on working conditions 2000. Technical report, Office for Official Publications of the European Communities, 2001.

[23] Y.C. Fung. *Biomechanics. Mechanical Properties of Living Tissues*. Springer-Verlag, New York, 2 edition, 1993.

[24] C. Galli, S. Guizzardi, G. Passeri, G.M. Macaluso, and R. Scandroglio. Life on the wire: on tensegrity and force balance in cells. *Acta Biomedica Ateneo Parmense*, 76(1):5–12, 2005.

[25] M. Gérardin and A. Cardona. *Flexible multibody dynamics. A finite element approach*. John Wiley & Sons, Ltd, 2001.

[26] U.J. Gerlach and W. Lierse. Functional construction of the sacroiliac ligamentous apparatus. *Acta Anatomica*, 144(2):97–102, 1992.

[27] H. Gray. *Anatomy of the Human Body*. Lea & Febiger, Philadelphia, 20 edition, 1918.

[28] W.B. Greene and J.D. Heckman. *The Clinical Measurement of Joint Motion*. American Academy of Orthopedic Surgeons, Rosemont, 1 edition, 1994.

[29] M. Groot (de), C.W. Spoor, and C.J. Snijders. Critical notes on the technique of doppler imaging of vibrations (DIV). *Ultrasound in Medicine and Biology*, 30(3):363–367, 2004.

[30] W. Heylen, S. Lammens, and P. Sas. Modal analysis theory and testing. Lecture notes Katholieke Universiteit Leuven, 1998.

[31] D.E. Ingber. Cellular mechanotransduction: Putting all the pieces together again. *The FASEB Journal*, 20(7):811–827, 2006.

[32] M. Kaouk, S. McNeill, S. Haley, M. Grygier, T.J. Bartkowicz, P.B. Rachal, and W. Peart. Shuttle-ISS Flight-7A on orbit test verification: pre and post flight analysis. In *22nd International Modal Analysis Conference (IMAC XXII)*, Dearborn, Michigan, USA, January 26-29 2004. Society for Experimental Mechanics.

[33] J.C. Leong, K.D. Luk, and D.H. Chow nad C.W. Woo. The biomechanical functions of the iliolumbar ligament in maintaining stability of the lumbosacral junction. *Spine*, 12(7):669–674, 1987.

[34] C. Linnaeus. *Systema Naturae*. 1735.

[35] J.Y. Maigne, A. Aivaliklis, and F. Pfefer. Results of sacroiliac joint double block and value of sacroiliac pain provocation tests in 54 patients with low back pain. *Spine*, 21(16):1889–1892, 1996.

[36] J.Y. Maigne and C.A. Planchon. Sacroiliac joint pain after lumbar fusion. A study with anesthetic blocks. *European Spine Journal*, 14(7):654–658, 2005.

[37] J.N. Maina. Spectacularly robust! Tensegrity principle explains the mechanical strength of the avian lung. *Respiratory Physiology and Neurobiology*, Epub ahead of print, 2006.

[38] R.L. Mayes and A.J.Gomez. What's shakin' dude? Effective use of modal shakers. In *23rd International Modal Analysis Conference (IMAC XXIII)*, Orlando, Florida, USA, January 31 - February 3 2005. Society for Experimental Mechanics.

[39] J.T. McConville, T.D. Churchill, I. Kaleps, C.E. Clauser, and J. Cuzzi. Anthropometric relationships of body and body segment moment of inertia. Technical Report AFAMRL-TR-80-119, Wright-Patterson Air Force Base, 1980.

[40] R. Melzack and P. Wall. Pain mechanisms: A new theory. *Science*, 150(3699):971–978, 1965.

[41] K.T. Palmer, K. Walsh, H. Bendall H, C. Cooper C, and D. Coggon. Back pain in britain: comparison of two prevalence surveys at an interval of 10 years. *BMJ*, 320(7249):1577–1578, 2000.

[42] A. Pool-Goudzwaard, G. Hoek van Dijke, P. Mulder, C. Spoor, and C.J. Snijders amnd A. Stoekart. The iliolumbar ligament: its influence on the stability of the sacroiliac joint. *Clinical Biomechanics*, 18(2):99–105, 2003.

[43] P.P. Provenzano, R.S. Lakes, D.T. Corr, and R. Vanderby. Application of nonlinear viscoelastic models to describe ligament behavior. *Biomechanics and Modeling in Mechanobiology*, 1(1):45–57, 2002.

[44] J.S.W. Rayleigh. *The Theory of Sound*. Dover Publications, 1945.

[45] M.H. Richardson and D.L. Formenti. Global curve fitting of frequency response measurements using the rational fraction polynomial method. In *3rd International Modal Analysis Conference (IMAC III)*, Orlando, Florida, USA, January 28 - 31 1985. Society for Experimental Mechanics.

[46] A.C. Schwarzer, C.N. Aprill, and N. Bogduk. The sacroiliac joint in chronic low back pain. *Spine*, 20(1):31–37, 1995.

[47] C.J. Snijders, P.F.G. Hermans, R. Niesing, A.L. Pool-Goudzwaard, and G.J. Kleinrensink. New concepts and hypotheses; Sudden slouching in the upright posture is a possible cause of back sprain in view of a biomechanical model on sacroiliac joints and iliolumbar ligaments. *Accepted for publication Manual Therapy*, 2006.

[48] C.J. Snijders, P.F.G. Hermans, R. Niesing, C.W. Spoor, and R. Stoeckart. The influence of slouching and lumbar support on iliolumbar ligaments, intervertebral discs and sacroiliac joints. *Clinical Biomechanics*, 19(4):323–329, 2004.

[49] C.J. Snijders, A. Vleeming, and R. Stoeckart. Transfer of lumbosacral load to iliac bones and legs : Part 1: Biomechanics of self-bracing of the sacroiliac joints and its significance for treatment and exercise. *Clinical Biomechanics*, 8(6):285–294, 1993.

[50] A.N. Thite and D.J. Thompson. The quantification of structure-borne transmission paths by inverse methods. Part 1: Improved singular value rejection methods. *Journal of Sound and Vibration*, 264(2):411–431, 2003.

[51] E. Vlaanderen, N.E. Conza, C.J. Snijders, A. Bouakaz, and N. Jong (de). Low back disorders; the stiffness of the sacro iliac joint: A new method using ultrasound. *Ultrasound in Medicine and Biology*, 31(1):39–44, 2005.

[52] G. Waechtershaeuser. Origin of life: Life as we don't wkow it. *Science*, 289(5483):1307–1308, 2000.

[53] World Health Organization Statistical Information System (WHOSIS). Global burden of disease estimates for the year 2001. Technical report, World Health Organization, 2001.

Summary

Dynamics of the human pelvis - Identification methodology for low back pain diagnosis

Musculoskeletal disorders, especially in the low back region, are very present and widely spread all over the world, impacting the societies in their productivity and straining their health care management systems. Ironically, this kind of uncomfort is a direct consequence of life's increased comfort. Sedentariness, increased body weight and prolonged life span make people more susceptible to developing all sorts of problems, among which of musculoskeletal origin. In addition, biomedical research is driven by more urgent goals: the defeat of molecular diseases such as cancer and AIDS, and advances in surgery techniques are indeed a question of life and death. This cannot be said of low back pain.

This work nobly addresses exactly such a neglected diagnostic issue, picking up the discourse where medicine drops it once exhausted all possible diagnoses. The underlying assumption of this research is that unexplained pain on the low back region is a consequence of abnormal mechanical properties of the sacroiliac joints, which connect the sacrum to the two innominate bones of the pelvis. Laxity is an often heard term in physiotherapy, and it designates the compliance of the joints between bones under the constant force that a practician applies. As such it is not measurable nor objective.

During this research the development of a diagnostic tool for a non-invasive objective measurement of the mechanical properties of the sacroiliac joints is investigated. The physical principle enabling such identification is borrowed from the dynamics field: a vibrating force is applied to the pelvis and provokes a vibrating displacement pattern all around the structure which depends on the mechanical properties of the structure (such a stiffness, mass and damping) and on the frequency of the applied force. The development of the apparatus for the introduction of the force and the measurement of the response by means of ultrasound technology (now existing in form of a prototype) has been investigated in a parallel track. In this work it is only briefly described.

To correctly interpret the measured response, and from it to extract the mechanical properties of interest, a model has been developed, comprising three rigid bodies representing the three bones of the pelvic girdle, a number of springs representing the ligaments of the girdle, and dashpots between the joints to implement damping. The

anatomy of the pelvis, which has inspired the creation of the model, and the mathematics of the model derivation are presented and explained.

Based on this model several simulation studies were performed. Two algorithms for the identification of the mechanical properties of the model (especially stiffness) starting from the measured response have been devised and verified, one based on the first vibration mode shape of the model (thus in modal domain), and the other one based on the curve fitting of Frequency Response Functions in frequency domain. Moreover the question about the constancy of the mechanical properties has been addressed: the response of a system showing frequency dependent stiffness and damping properties has been simulated and analysed with commercially available tools (all assuming constant stiffness and (viscous) damping properties), to investigate the magnitude of the error on the analysis outcome. Results showed that resonance frequencies and mode shapes were accurately identified, but not so much the damping.

Interweaved into these numerical efforts, experiments have been performed on embalmed and fresh-frozen human pelvises, mainly to obtain data for the model validation. The adventure in setting up such experiments and the results are presented in this work. A different set of experiments, with a different goal, has been performed on rabbit knee ligaments to determine whether the stiffness is dependent on the excitation frequency or not. As it resulted, there is not enough evidence to confirm it.

Finally the success and the difficulties in correlating the established model to the results from the experiments are discussed, which lead directly to the last chapter of this dissertation, where the conclusions and recommendations are presented.

Nadine Conza, December 2006

Samenvatting

Dynamica van het menselijk bekken - Identificatie methodologie voor de diagnose van lage rugklachten

Gewrichts- en spierpijn, met name in de onderrug komen wereldwijd veel voor. Deze aandoeningen hebben een negatieve invloed op de productiviteit van de samenleving en zetten de gezondheidszorg onder druk. Dit discomfort is, ironisch genoeg een direct gevolg van het toegenomen comfort van het leven zelf. Gebrek aan lichaamsbeweging, hoger lichaamsgewicht en verlengde levensduur maken mensen ontvankelijker voor ziekten, waaronder aandoeningen aan het spierskeletstelsel. Bovendien wordt biomedisch onderzoek geleid door urgentere drijfveren: bij het overwinnen van moleculaire ziekten zoals kanker en AIDS en het verbeteren van chirurgische technieken gaat het daadwerkelijk om een kwestie van leven of dood. Dit is niet het geval voor lage rugklachten.

Dit onderzoek houdt zich op een nobele manier precies met dit achtergesteld diagnostisch vraagstuk bezig, en pakt de discussie op waar geneeskunde het laat vallen, nadat al de diagnosen uitgeput zijn. De onderliggende veronderstelling van dit werk is dat onverklaarbare onderrugpijn veroorzaakt wordt door abnormale mechanische eigenschappen van de sacroiliacale gewrichten, die het sacrum en de ilia verbinden. Laxiteit is een bekend begrip in de fysiotherapie en wordt gebruikt om de compliantie van gewrichten aan te duiden onder een constante kracht die de therapeut uitoefent. Het is dus noch meetbaar noch objectief.

Dit onderzoek richt zich op de ontwikkeling van een diagnostisch middel om de mechanische eigenschappen van de sacroiliacale gewrichten op een non-invasieve objectieve manier te bepalen. Het fysische principe dat dit mogelijk maakt is geleend vanuit de dynamica: een trillende kracht wordt opgelegd aan het bekken en resulteert in een trillend antwoordpatroon van het bekken. Dit antwoordpatroon is afhankelijk van de mechanische eigenschappen van de structuur (zoals stijfheid, massa en demping) en van de frequentie van de toegepaste kracht. De ontwikkeling van het apparaat voor het aanbrengen van de kracht en het meten van het antwoord op basis van ultrageluid technieken (nu bestaand in vorm van prototype) is in een parallel traject uitgevoerd. In dit werk zal het kort worden beschreven.

Om het gemeten dynamisch gedrag correct te interpreteren en om daaruit de mechanische eigenschappen te extraheren, is een model ontwikkeld, bestaand uit drie vaste lichamen die de drie botten van het bekken vertegenwoordigen, een aantal veren dat

de ligamenten vertegenwoordigt, en dempers tussen de gewrichten om de demping te implementeren. De anatomie van het bekken, waarop het model is geïnspireerd en de wiskunde waarmee het model is afgeleid, zijn uitgewerkt.

Gebaseerd op dit model is een aantal simulaties uitgevoerd. Twee algoritmen zijn ontwikkeld om de mechanische eigenschappen (vooral de stijfheid) van de sacroilicale gewrichten te bepalen vanuit het gemeten dynamische gedrag. Het eerste algoritme is gebaseerd op de eerste trillingsvorm (dus in modaal domein) en het tweede is gebaseerd op de curve fitting van Frequency Response Functions (dus in frequentie domein). Bovendien is onderzocht in welke mate de mechanische eigenschappen constant zijn: het gedrag van een systeem waarvan stijfheid en demping frequentie-afhankelijk zijn, is gesimuleerd. Dit gedrag is gebruikt als ingangswaarde voor commerciële analyse software, welke allen uitgaan van constante mechanische eigenschappen. Op deze manier is onderzocht hoe groot de fout in de resultaten van de analyse is. Uit de resultaten blijkt dat de frequenties en de trillingsvormen van de resonanties goed te identificeren zijn, maar de demping niet.

Met deze numerieke inspanningen verweven, zijn experimenten op gebalsemde en verse menselijke bekkens uitgevoerd, vooral om het model te valideren. Het avontuur om zulke experimenten op te zetten en de resultaten hiervan zijn beschreven in dit werk. Een ander soort experimenten, met als doel de vraag over de frequentie-afhankelijkheid van de ligamentenstijfheid te beantwoorden, is met ligamenten van konijnenknieën uitgevoerd. De uitkomst was niet doorslaggevend voor het bevestigen van de hypothese.

Tot slot worden het succes en de moeilijkheden van het correleren van het model met de resultaten van de experimenten besproken. Dit leidt rechtstreeks tot het laatste hoofdstuk van dit proefschrift, waarin de conclusies en aanbevelingen gegeven worden.

Nadine Conza, December 2006

Acknowledgements

This dissertation has been made possible by the concomitance of three essential factors: a project, a supervision network, and a PhD candidate.

For the first essential element, the project, I want to thank Prof. Snijders for having created this opportunity through his ingenious idea.

My gratitude and respect also to Dr. Boontje of STW for the management of this project, which he has done with benevolence and sympathy. Should I have to choose one adjective to describe him, I'd say "cool".

I thank the members of the associated user committee as well, especially Nico de Jong, Ayache Bouakaz, Charles Lancée and Peter Brands for their enthusiastic involvement during the STW meetings.

In the supervision network, the absolute and undiscussed protagonist is my first doctoral supervisor Prof. Rixen. He is an outstanding professor, who offers almost unreasonable availability to his students and excellent scientific support, and with whom it is a great pleasure to work.

For the indispensable daily mumbling and chewing and lamenting and discussing over the details of the research, I thank from the bottom of my heart my colleague Ester, who has been my faithful comrade in the ups and downs of this project for two and a half years, and her successor Bram during this final year. It is not always easy to work with me: I admire their patience and their flexibility with which they could compensate for my bad days.

I have found a competent and prompt technical support at the University in Delft personified in Jan Sterk and Jos van Driel. Especially Jan, a tender soul in the chassis of a giant, has always found the time and the drive to help me, and build for me the most minuscule pieces with his huge hands. An affectionate thank to both of them.

Equally competent, but in a completely different setting, was the friendly support found at the University Medical Center in Utrecht. I want to warmly thank Dr. Bleys for having responded to my appeal when I was looking for human specimens , and for his availability during the long days of experiment. My innocent cry of triumph "Ca-

davers have been found in Utrecht!" inadvertently put in one of my progress reports (and promptly removed) will make Ester and I laugh forever. With the same amount of gratitude I mention Willem van Wolferen and Simon Plomp, who were always willing to indulge us and comradely well-disposed towards our sometimes weird requests. For the experiment sessions on embalmed specimens, in the early phase of this research, I want to thank Gert-Jan Kleinrensink for having arranged the specimens, and Gilbert Hoek van Dijke for letting us use his infrared camera system.

My sincere thanks of course also to the members of the Doctoral Examination Committee, for having agreed to perform as critics and opponents for my dissertation.

Unrivalled, I want to thank our secretary Corinne du Burck, who has been a friend in personal matters and an assistant in administrative matters. She's the only one who can make the undiscussed Prof. Rixen look (and I'm sure feel) like a naughty boy being reprimanded.

Dismissing for a moment my apparel as PhD candidate, and treading the stage just as myself, I want to transmit my personal gratitude to the many who, in these years, have helped me *be*, and *become*, beyond the scope of this dissertation, even if some of them will never be reading these pages.

To the members of the organization committee of the International Modal Analysis Conference Katherine Ramsay, Shari Matthews, Jennifer Proulx, Joni Normandin, Tom Proulx and Al Wicks, for having become like a family to me during my three years of attendance.

To the chief editor of the journal "Experimental Techniques" Kristin Zimmerman for having inspired and assisted me in the preparation and publication of the series "Engineering Issues in Experimental Biomedicine".

One layer deeper, a sad quiet thank to Jens, for forcing me to grow and understand even if it cost me more than I could afford. I do wish things were different for both of us. Also somewhat battered is my gratitude to Alessandro, who has kept listening to me without realizing the toll it would take. A warm thank to Michaela, whose friendship is showing me that I can be my fallible human self and still be loved, and to her baby girl Valentina, my sweet goddaughter, for bringing me close to a dear dream, closer than I might ever be. And still, merry for a moment despite all this seriousness, a tender thank to Moca, for making me burst in laughter when I actually felt like crying.

My deepest gratitude and affection, again, to Ester, this time for her exceptional friendship, for having been here when I couldn't see nor think nor imagine any further, for her caring wisdom and her unceasing support. If it hadn't been for her willingness to catch me in my private free falls, I probably wouldn't have completed this disserta-

tion. For this and many other reasons, I feel that my graduation is also hers, and so my doctoral degree.

Finally, my unconditional love and gratitude to my family. To my mother Irma, my father Marco, and my sister Deborah for having supported me, each in their own personal way. And to my sister Pascale, who, by dying so young, has taught me how hopelessly precious and fragile life is.

Delft, Fall 2006

About me

I was born on July 5, 1972, in Sorengo, a town near Lugano in the Italian side of Switzerland.

In 1991 I obtained my college degree in the scientific curriculum at the Liceo cantonale in Lugano. In the same year I started my academic studies at the faculty of Mechanical Engineering of the ETH in Zurich (Switzerland), where I specialized in Biomedical Technologies and Energy Systems. Between 1996 and 1997 I worked at my master thesis at the NASA Johnson Space Center in Houston (USA). The study investigated the carbon dioxide concentration inside the Launch and Entry Suits helmet during a simulated Space Shuttle emergency landing, and the astronauts performance during a simulated emergency egress. It was awarded the Georg Fischer Price for the best master thesis at the ETH of that year.

In 1998 I decided to deepen my knowledge in biology and collaborated to a project at the Cantonal institute of bacteriology in Lugano, studying the population genetics of a bacterium called *Vibrio vulnificus*.

In 1999 the European Space Agency sponsored me for a one-year Young Graduate Traineeship at ESTEC (the ESA technology center in Noordwijk, The Netherlands), during which I investigated the accommodation of biological experiments onboard Biolab (the European biology lab on the International Space Station).

Between 2000 and 2002 I worked at the Space Biology Group of the ETH in Zurich, researching and preparing biological experiments for spaceflight, among which the experiment Codi, which investigated the cytoskeleton and the genetic expression in porcine chondrocytes during a sounding rocket flight, and the experiment Leukin, whose goal was to assess the immunological response of human leukocytes in microgravity, and which was unfortunately lost in the Columbia Space Shuttle accident in February 2003. In the same period I followed a two-year post-graduate course in Medical Physics, also at the ETH, during which I specialized in Robotics and Biomechanics, and which I concluded in summer 2002 with a thesis at the Department of Cybernetics of the University of Reading (UK) on the modeling of the three-dimensional motion of fingers and wrist of prosthetic and normal hands.

I started my PhD program at the Faculty of Mechanical, Maritime and Materials Engineering of the Delft University of Technology in November 2002.

Publications

P.A. Bishop, S.M. Lee, N.E. Conza, L.L. Clapp, A.D. Moore Jr, W.J. Williams, M.E. Guilliams, M.C. Greenisen. Carbon dioxide accumulation, walking performance, and metabolic cost in the NASA launch and entry suit. *Aviation, Space and Environmental Medicine*, 70(7): 656-665, 1999.

S.M. Lee, P.A. Bishop, S.M. Schneider, L.L. Clapp, W.J. Williams, N. Conza, M.C. Greenisen. Simulated shuttle egress: role of helmet visor position during approach and landing. *Aviation, Space and Environmental Medicine*, 72(5): 484-489, 2001.

N. Conza, P. Mainil-Varlet, F. Rieser, J. Kraemer, P. Bittmann, R. Huijser, L. van den Bergh, A. Cogoli. Tissue engineering in space. *Journal of Gravitational Physiology*, 8(1): P17-20, 2001.

M. Gutacker, N.E. Conza, C. Benagli, A. Pedroli, M.V. Bernasconi, L. Permin, R. Aznar, J.C. Piffaretti. Population genetics of Vibrio vulnificus: identification of two divisions and a distinct eel-pathogenic clone. *Applied and Environmental Microbiology*, 69(6): 3203-3212, 2003.

N.E. Conza, D.J. Rixen. Dynamic response of an embalmed human pelvis - a pilot study. In *World Congress in Medical Physics and Biomedical Engineering*, Sydney, Australia, August 24-29 2003.

N.E. Conza, D.J. Rixen. Dynamic Model of the human pelvis - Parameters Identification. In *22nd International Modal Analysis Conference (IMAC XXII)*, Dearborn, Michigan, USA, January 26-29 2004.

N.E. Conza, E. Vlaanderen. Engineering Issues in Experimental Biomedicine Series: Part 1: Introduction. *Experimental Techniques*, 28(6): 50-51, 2004.

N.E. Conza, A. Cogoli. Engineering Issues in Experimental Biomedicine Series: Part 2: Space biology. *Experimental Techniques*, 29(1): 43-46, 2005.

E. Vlaanderen, N.E. Conza, C.J. Snijders, A. Bouakaz , N. de Jong. Low back pain, the stiffness of the sacroiliac joint: A new method using ultrasound. *Ultrasound in Medicine and Biology*, 31(1): 39-44, 2005.

N.E. Conza, D.J. Rixen. Biomechanical Parameter Estimation using Frequency Domain Updating. In *23rd International Modal Analysis Conference (IMAC XXIII)*, Orlando, Florida, USA, January 31 - February 2 2005.

N.E. Conza, D.J. Rixen. Experiments on Human Pelvises: Challenges and Preliminary Results. In *23rd International Modal Analysis Conference (IMAC XXIII)*, Orlando, Florida, USA, January 31 - February 2 2005.

N.E. Conza. Engineering Issues in Experimental Biomedicine Series: Part 3: Tissue preconditioning. *Experimental Techniques*, 29(2): 43-66, 2005.

N.E. Conza. Engineering Issues in Experimental Biomedicine Series: Part 4: Tissue water content. *Experimental Techniques*, 29(3): 69-72, 2005.

N.E. Conza. Engineering Issues in Experimental Biomedicine Series: Part 5: Measuring and imaging what's inside. *Experimental Techniques*, 29(4): 46-51, 2005.

N.E. Conza. Engineering Issues in Experimental Biomedicine Series: Part 6: Statistics in medical research. *Experimental Techniques*, 29(5): 39-43, 2005.

N.E. Conza. Engineering Issues in Experimental Biomedicine Series: Part 7: Ultrasound detection system for musculoskeletal disorders. *Experimental Techniques*, 29(6): 54-57, 2005.

N.E. Conza, D.J. Rixen. Frequency Dependent Properties and Pelvis Parameter Identification. In *24th International Modal Analysis Conference (IMAC XXIV)*, St. Louis, Missouri, USA, January 30 - February 2 2006.

N.E. Conza, B. Soethoudt, E. Vlaanderen, D.J. Rixen. In vivo Bone Vibration Measurement by Ultrasound. In *24th International Modal Analysis Conference (IMAC XXIV)*, St. Louis, Missouri, January 30 - February 2 2006.

N.E. Conza, D.J. Rixen, S. Plomp. Vibration testing of a fresh-frozen human pelvis: the role of the pelvic ligaments. *Journal of Biomechanics* Aug 29 2006 [Epub ahead of print].

N.E. Conza, D.J. Rixen, C.J. Snijders. Identification methodology of the human pelvis for Low Back Pain diagnosis. In *International Conference on Noise & Vibration Engineering (ISMA2006)*, Leuven, Belgium, September 18-20 2006.

N.E. Conza, D.J. Rixen. Experimental modal analysis on a human specimen: lessons learned. *Experimental Techniques*, 30(6), 2006 (to appear).

N.E. Conza, D.J. Rixen. Influence of Frequency Dependent Properties on System Identification: Simulation Study on a Human Pelvis Model. *Submitted to Journal of Sound and Vibration*, 2006.